

**BIOMOLECULES IN THE GAS PHASE.
HIGH RESOLUTION ULTRAVIOLET SPECTROSCOPY
OF DNA BASES AND BASE PAIR ANALOGS**

by

Joseph Robert Roscioli

University of Pittsburgh

April, 2003

FOREWORD

It would take more than a few pages to thank all of the people that have helped me along in my five years in this incredible laboratory. I would especially like to thank Dr. David Borst for his enthusiasm, reassuring words, constructive criticisms, and challenging discussions for four years. I would also like to thank Dr. Jason Ribblett and Dr. Timothy Korter for their helpful support and discussions while in the laboratory. Thanks to Alexei Nikolaev for keeping my feet on the ground when they needed to be, and to Kathleen Schaefer for keeping my head in the clouds when it needed to be. Katie's unique insight and perspective on so much of life has been invaluable. Many thanks to other current and past group members who have helped and guided me for the past five years, both in and out of the laboratory, and to the University of Pittsburgh machine, glass, and electronic shops for their professional skills. Special thanks to Mr. Charles Wood and Ms. Susan O'Toole, two people who invigorated my thoughts on physics, chemistry and life.

Finally, endless thanks to Dr. David Pratt for being an incredible mentor, scientist, and philosopher. His insight has continually challenged my mind for five straight years, and will continue to for many more. Thanks to my family, for reminding me why I got into this business and for being an unending source of encouragement. And finally to my grandfather, George Hewitt, whose support reminds me that my success rests in the past 22 years, not in the following pages.

TABLE OF CONTENTS

Foreword.....	2
List of Tables.....	5
List of Figures.....	6
1.0 Introduction.....	9
1.1 References.....	15
2.0 High resolution electronic spectra of 2-hydroxy and 2-aminopyridine. Perturbing effects of the nitrogen atom in the aromatic ring	16
2.1 Introduction.....	19
2.2 Experimental.....	19
2.3 Results.....	21
2.4 Discussion.....	25
2.5 Acknowledgements.....	38
2.6 References.....	39
3.0 Hydrogen bonding and tunneling in the 2-pyridone-2- hydroxypyridine dimer. Effect of electronic excitation.....	41
3.1 Introduction.....	43
3.2 Experimental.....	46
3.3 Results.....	49
3.3.1 Ground state fluorescence-dip infrared spectra.....	51
3.3.2 Excited state fluorescence-dip infrared spectra.....	55
3.3.3 High resolution electronic spectroscopy of the S_1-S_0 origin.....	55
3.3.4 Calculated structure of <i>2PY·2HP</i> in the ground state.....	62
3.4 Discussion.....	62
3.4.1 Changes in H-bonding from the infrared spectra.....	66
3.4.2 Tunneling.....	69
3.5 Conclusions.....	75
3.6 Acknowledgements.....	76
3.7 References.....	77
4.0 Tunneling in the 2-hydroxypyridine/2-pyridone dimer. Effects of deuterium substitution on tunneling frequencies.....	79
4.1 Introduction.....	80
4.2 Results.....	80
4.3 Discussion.....	84

4.4	Conclusions.....	86
5.0	Base pair analogs in the gas phase.....	87
5.1	Introduction.....	89
5.2	Experimental.....	90
5.3	Results and Discussion.....	91
5.4	References and Notes.....	102
	Conclusions.....	105
	Appendix.....	107
7.1	Energy level structure theory.....	107
7.2	Rigid rotor Hamiltonian.....	109
7.3	Experimental setup.....	110
7.4	Data Analysis.....	113

LIST OF TABLES

Table 2.1.	Inertial parameters of 2-hydroxypyridine (2HP) and 2-aminopyridine (2AP) in their ground (S_0) and electronically excited (S_1) states.....	26
Table 2.2.	Inertial parameters of phenol and aniline in their ground (S_0) and electronically excited (S_1) states.....	27
Table 2.3.	CIS expansion coefficients squared of the principal one-electron excitations contributing to the S_1 - S_0 transitions of 2-hydroxypyridine (2HP), 2-aminopyridine (2AP), phenol, and aniline. (6-31G* basis set).....	32
Table 3.1.	Approximate rotational constants (in MHz) of the 2PY·2HP dimer of 2-hydroxypyridine in its S_0 and S_1 electronic states, compared to Hartree–Fock and density functional theoretical values.....	60
Table 5.1.	Inertial parameters of the zero-point vibrational levels of the ground (S_0) and first excited (S_1) singlet states of the A/T base pair mimic 2AP/2PY, based on a fit of its fluorescence excitation spectrum at ~ 330 nm (the band origin is at $30266.83 \pm 0.02 \text{ cm}^{-1}$). A, B, C, ΔI and κ are the rotational constants, inertial defect, and asymmetry parameter, respectively.....	94
Table 5.2.	Hydrogen bond lengths in 2AP/2PY and related systems (Å).....	97

LIST OF FIGURES

Figure 2.1.	The rovibronic S_1 - S_0 spectrum of 2-hydroxypyridine at ~ 277 nm. The inset shows a portion of the experimental spectrum at full resolution, together with two simulations, with and without superimposed lineshape functions. 173 lines were included in the fit, resulting in an OMC of 5.5 MHz. The single rovibronic linewidth is 170 ± 10 MHz. $T = 4.8$ K.....	22
Figure 2.2.	The rovibronic S_1 - S_0 spectrum of 2-aminopyridine at ~ 299 nm. The inset shows a portion of the experimental spectrum at full resolution, together with two simulations, with and without superimposed lineshape functions. 74 lines were included in the fit, resulting in an OMC of 6.5 MHz. The single rovibronic linewidth is 120 ± 10 MHz. $T = 5.0$ K.....	24
Figure 2.3.	Inertial axes, transition moment, and axis tilt orientations in 2-hydroxypyridine (top) and 2-aminopyridine (bottom). The θ -sign convention is that used for the axis tilt.....	30
Figure 2.4.	Calculated molecular orbitals of 2-hydroxypyridine (left) and 2-aminopyridine (right).....	34
Figure 2.5.	Transition densities of a) 2-hydroxypyridine, b) 2-aminopyridine, c) phenol and d) aniline.....	35
Figure 3.1.	Low resolution fluorescence excitation spectrum in the region of the 2PY·2HP S_1 - S_0 origin: (a) protonated sample; (b) spectrum obtained with a 1:1 H:D mixture in the labile N-H and O-H positions.....	50
Figure 3.2.	Ground state fluorescence-dip infrared spectra of (a) $(2PY)_2$ and (b) 2PY·2HP dimers in the hydride stretch region of the infrared.....	52
Figure 3.3.	Fluorescence-dip infrared spectra of the electronically excited dimers: (a) spectrum of $(2PY)_2$ recorded while monitoring fluorescence from its S_2 electronic origin at $30\,776\text{ cm}^{-1}$; (b) spectrum of 2PY·2HP recorded while monitoring fluorescence from its S_1 electronic origin at $30\,656\text{ cm}^{-1}$. The delay between	

	UV excitation laser and IR depletion laser is 19 ns in (a) and 24 ns in (b).....	56
Figure 3.4.	High resolution fluorescence excitation spectrum of the 2PY·2HP dimer at its S_1 – S_0 origin ($30\,656\text{ cm}^{-1}$).....	57
Figure 3.5.	Autocorrelation spectrum of the band in Fig. 4. The side bands at $\pm 520\text{ MHz}$ indicate the presence of two bands in the spectrum, split by 520 MHz	61
Figure 3.6.	Intermolecular normal mode eigenvectors for the ν_3 'cogwheel' and ν_6 'intermolecular stretch' vibrations, taken from the DFT B3LYP/6-311++G(d,p) calculation.....	65
Figure 3.7.	A direct comparison of the (a) S_0 and (b) S_1 state FDIR spectra of the 2PY·2HP dimer. Note the dramatic shift of the intense absorption to higher frequency in the electronically excited state. Proposed assignments are given on the absorptions.....	67
Figure 3.8.	B3LYP/6-311++G(d,p) calculated: (a) equilibrium structure (GS) with the vibrational eigenvector of the $\nu_{57}=3061\text{ cm}^{-1}$ normal mode, which correlates most closely with a pure double proton transfer motion, and (b) transition structure (TS) for double proton transfer with the eigenvector corresponding to the imaginary frequency $i1311\text{ cm}^{-1}$	70
Figure 3.9.	Calculated model potential for double proton transfer in the ground and electronically excited states of the 2PY·2HP dimer. (a) The barrier height in the ground state is the vibrationally adiabatic barrier of 2681 cm^{-1} calculated from the electronic and vibrational zero-point energies of GS and TS. The distance from GS to TS is in mass-weighted Cartesian coordinates. Tunneling splittings for $v=0-5$ are not visible on the scale of the figure. (b) The excited state double proton transfer potential was constructed by arbitrarily assuming the same $R(\text{TS-GS})$ distance as for the S_0 state; the barrier was lowered to 610 cm^{-1} so as to yield the observed tunneling splitting of 520 MHz (0.0173 cm^{-1}), also not visible in the figure.....	73
Figure 4.1	The fit, high resolution electronic spectrum of the 2HP/2PY dimer. A 527 MHz splitting is observed in the spectrum (see Figure 3.5, p. 60).....	81
Figure 4.2	Frequency and intensity fits of the a) 2HPd/2PY, b) 2HP/2PYd, and c) 2HPd/2PYd spectra. In the 2HPd/2PY spectrum, a 62 MHz tunneling splitting is observed.....	83

Figure 5.1.	The central $\sim 2 \text{ cm}^{-1}$ portion of the rotationally resolved fluorescence excitation spectrum of the origin band in the S_1 - S_0 electronic spectrum of the 2AP/2PY dimer at $\sim 330 \text{ nm}$, recorded in the collision-free environment of a molecular beam using a high resolution laser. Three scale expansions below illustrate a simulated spectrum at full resolution (1 MHz), and fits of the experimental spectrum at the experimental resolution of 18 MHz.....	92
Figure 5.2.	Model structure of the 2AP/2PY dimer illustrating the Watson-Crick configuration found experimentally and geometrical parameters derived from the fit of the spectrum in Fig. 5.1. r_1 and r_2 are the hydrogen bond distances $\text{N}\cdots\text{H-N}$ and $\text{N-H}\cdots\text{O}$, and ϕ is the (nonzero) dihedral angle.....	96
Figure 5.3.	Molecular orbitals of 2AP/2PY that participate in the S_1 - S_0 transition, which exhibit some delocalization owing to the partially covalent character of the two hydrogen bonds that link the two halves of the base pair mimic together.....	101
Figure 7.1	Energy level scheme used in high resolution electronic spectroscopy.....	108
Figure 7.2.	The experimental setup of the ultra high resolution UV spectrometer at the University of Pittsburgh.....	111
Figure 7.3	Side view of molecular source (on left), set of skimmers (center), and collection optics (right). The molecular beam is aligned by monitoring an argon signal from the molecular source.....	112
Figure 7.4	The process of fitting a spectrum, a) using the initial rotational constants, the simulated spectrum barely resembles the experimental. b) After fitting several transitions, general trends begin to appear. c) The final fit of the spectrum, after several hundred lines have been fit.....	114

1.0 INTRODUCTION

In April 1953, the field of biochemistry was launched to the forefront of scientific knowledge with the discovery of the double-helical structure of deoxyribonucleic acid (DNA). The magnitude of this discovery far outweighed that of any previous discovery in biochemistry simply because this structure and its implications impacted a large range of fields, from cryptographic theory to genetic sciences.

Since 1953, huge amounts of effort have been directed towards understanding the chemistry of the body. Most of these studies have utilized a *top-down* approach, in which empirical observations are made of the system, from which general conclusions can be drawn. While successful thus far, this approach lacks a fundamental underpinning so crucial to many other sciences. That is, while biochemistry has advanced, it has understood systems on a local level, rather than a global level that would allow for a unified physical understanding of many systems. One of the more significant reasons for this is that the field of chemical physics has lacked, until recently, the technology to perform physically based experiments on molecules of biological interest. The purpose of this set of experiments is to understand from a *bottom-up* approach the underlying laws that drive the activity and structure of molecules of biological interest, specifically analogs of DNA bases and base pairs. Such studies illustrate that not only is the field of chemical physics now capable of performing such experiments, but that it is also capable of making an impact in biochemistry.

It has often been said that two properties determine the activity of a molecule. First, its structure plays a crucial role. Francis Crick once said, “If you want to understand function, study structure,” and nowhere is this truer than in biochemistry. Second, the electron distribution of the molecule plays a critical role. The activity of a molecule can be determined by studying the transfer of electronic charge within a molecule or from one molecule to another. In addition, the electric dipole and quadrupole moments, both solely dependent upon electron distribution, play a critical role in the way molecules interact with other entities, such as surfaces and chains.

In recent years, high resolution electronic spectroscopy has made possible an improved understanding of both of these properties from a physical standpoint. In all of these experiments, the objective is the same: to understand the molecule’s structure and electronic distribution and the fundamental forces that induce them. Many forces influence the overall structure of biomolecules, including hydrogen bonding, π -orbital stacking, van der Waals interactions, and covalent interactions. The only way to truly understand these forces is to probe the molecules when they are in the absence of any external force fields. Consequently, all of these studies are performed in the gas phase, in which there are no forces acting upon the molecule except those from the molecule itself.

In such an experiment, the molecules of interest are vaporized and entrained in helium, formed into a molecular beam under ultrahigh vacuum conditions, then probed by a high resolution ultraviolet (UV) laser that scans its photon energy through a small range. Because of the high resolution of the laser and way in which it probes the molecular beam, this experiment allows for the ability to induce transitions within the molecules from a specific rotational energy level in the ground electronic state to a

specific rotational energy level in the excited electronic state. Such a process can be detected by the emission of light from the molecule as it relaxes back to the ground electronic state. As the energy of the laser is scanned, the resulting spectrum contains crucial information about the molecule's rotational energy levels in both electronic states, from which a detailed structure of the molecule can be determined with the aid of theory. In addition, by studying the intensity distribution of peaks within the spectrum, the shapes of the molecular orbitals involved in the transition can be determined. These two properties allow us to understand the physical mechanisms that underlie the chemical activity of the molecule.

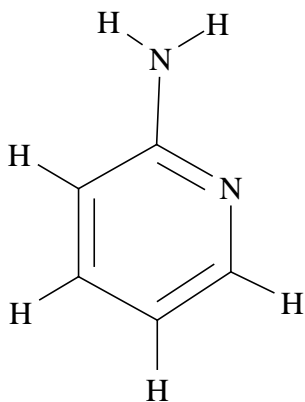
In this series of experiments, several different molecules were studied within the framework of high resolution electronic spectroscopy. All of them are classified as DNA base analogs or base pair analogs, molecules whose active regions are identical to those found in DNA bases and base pairs. These analogs are studied rather than the bases themselves for several reasons. First, the excited state lifetime of the DNA bases is believed to be on the order of picoseconds [1]. The resolution of the experiment (how well we are able to pick out rotational levels), ΔE , is dependent upon the excited state lifetime, Δt , of the molecule by the time-energy Heisenberg uncertainty relation:

$$\Delta E = \frac{\hbar}{2 \Delta t} \quad (1)$$

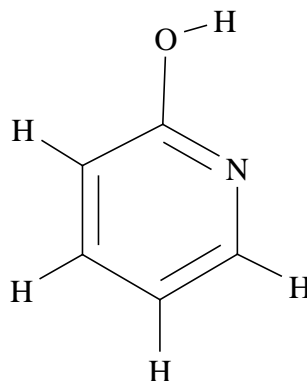
A picosecond lifetime corresponds to a resolution on the order of 10,000 MHz, which is not sufficient to resolve individual rotational transitions, thus not providing us with any structural information. Base pair analogs, however, typically have a lifetime on the order of tens of nanoseconds, providing a resolution of about 100 MHz. Second, the molecules

themselves tend to emit very little light after being excited in the gas phase, making it very difficult to detect when a transition has occurred. Third, in all of these experiments the molecules of interest must be in vapor phase to be a part of the molecular beam. All four DNA bases decompose below their melting point, making them very difficult to vaporize. However, the analogs vaporize below their decomposition point, making them more suitable for this experiment. Finally, it has been observed by DeVries *et al* [2] that the base pairs tend to orient themselves in the gas phase in many ways, only one of them being the classic Watson-Crick orientation that we are trying to understand. By using base pair analogs, we are able to create only this Watson-Crick pairing in the absence of external forces, allowing us to analyze the isolated hydrogen bond forces from base stacking and phosphate backbone forces.

The first two molecules, discussed in chapter 2, are 2-aminopyridine (2AP) and 2-hydroxypyridine (2HP), analogs of adenine (A) and enolized thymine (T-*enol*), respectively.



2-Aminopyridine

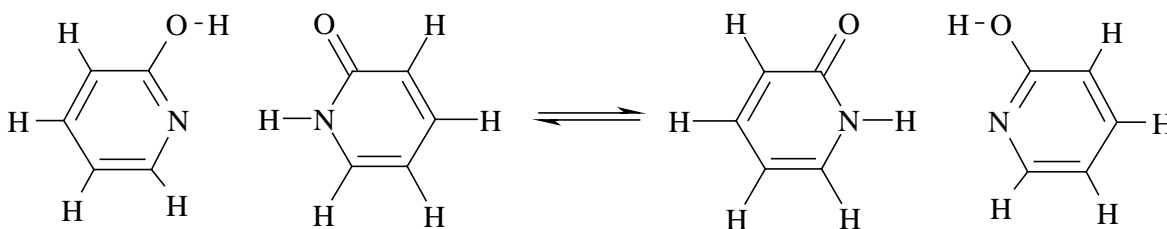


2-Hydroxypyridine

In both of these molecules, the force of interest is the *intra*-molecular hydrogen bond between the in-ring nitrogen and the amine-hydrogen (in the case of 2AP) or the

hydroxy-hydrogen (in the case of 2HP). For both of these molecules, a structure was determined which agreed well with theory, and the electron distribution within the molecule indicated that the in-ring nitrogen played a role in transferring a significant amount of charge density onto the amino or hydroxy group.

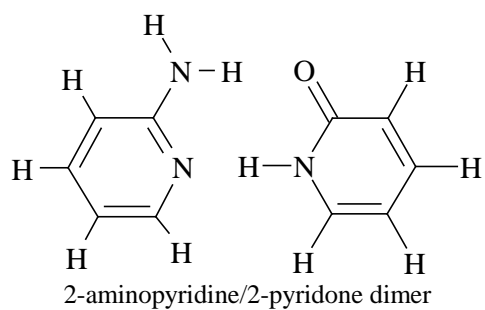
The second system, investigated in chapters 3 and 4, is the 2-hydroxypyridine/2-pyridone (2HP/2PY) mixed dimer. This system is particularly interesting because it is an analog of the thymine/thymine-*enol* dimer, in which both active protons can tunnel across the double hydrogen bonds:



Enol-keto tautomerism in the 2-hydroxypyridine/2-pyridone dimer

It is thought that this proton transfer may represent a mechanism by which base mutation can occur and propagate in DNA; thus, understanding the driving forces behind this motion could provide insight into ways to prevent or enhance the transfer. The interpretation of the spectrum of this dimer indicates that the transfer does indeed occur, but only in one of the two electronic states probed.

The final chapter is devoted to the 2-aminopyridine/2-pyridone (2AP/2PY) dimer, a direct analog of the adenine/thymine dimer. A study of the 2-aminopyridine monomer (chapter 2) indicates that the -NH_2 group is non-planar. Since the -NH_2 group is involved in the double-hydrogen bond, its non-planarity may be propagated through the



entire dimer, making the two rings non-coplanar. This would imply an inherent chirality in the dimer that may manifest itself in the overall helical nature of the DNA molecule. In addition to this property, investigation of the intermolecular distances would provide us with knowledge of hydrogen bond length and stability in both electronic states, in the absence of other forces such as π -orbital interactions and phosphate backbone stresses.

1.1 References

1. Kang, Hyuk; Lee, Kang Taek; Jung, Boyong; Ko, Yeon Jae; Kim, Seong Keun. School of Chemistry, Seoul National University, Seoul, S. Korea. *Journal of the American Chemical Society* (2002), 124(44), 12958-12959
2. Eyal Nir, Karl Kleinermanns, and Mattanjah S. de Vries. *NATURE* 408, 949-951 (2000)

**2.0 High Resolution Electronic Spectra of 2-Hydroxy and 2-Aminopyridine.
Perturbing Effects of the Nitrogen Atom in the Aromatic Ring.**

David R. Borst, Joseph R. Roscioli, and David W. Pratt
Department of Chemistry, University of Pittsburgh
Pittsburgh, PA 15260 USA.

Published in the *Journal of Physical Chemistry: A*, **106**, pp 4022-4027 (2002)

ABSTRACT

High resolution, rotationally resolved electronic spectra of 2-hydroxypyridine (2HP) and 2-aminopyridine (2AP) (at ~277 and ~299 nm, respectively) have been observed and fit using rigid-rotor Hamiltonians to within lifetime-limited resolutions of 170 and 120 MHz, respectively. The derived values of the rotational constants are very similar to those of phenol and aniline. However, 2HP and 2AP each exhibit inertial axis tilting, large rotations of their S_1 - S_0 electronic transition moments, and intramolecular hydrogen bonds, making them very different from their hydrocarbon analogs. Possible reasons for this behavior are discussed.

2.1 INTRODUCTION

Understanding the active structures within biological molecules is integral to understanding the function and interactions of such molecules within living organisms. Ring structures containing nitrogen atoms are quite common in biological systems, and provide an excellent forum for discussion of lone-pair electron effects. Such effects may play an important role in noncovalent interactions of heteratomic rings with one another, and with other hydrocarbon aromatic rings in larger macromolecules [1].

Examples of such structures include 2-hydroxypyridine (2HP) and 2-aminopyridine (2AP). Both contain in-ring nitrogen atoms, along with either *ortho* hydroxy or amino groups. 2HP, the enol tautomer of 2-pyridone (2PY), contains three potential hydrogen bonding (HB) sites; the in-ring nitrogen, the -OH group, and the π cloud of the aromatic ring. The corresponding active sites within 2AP are identical to those within adenine.

Both molecules have been extensively studied using a variety of high resolution gas phase techniques. Microwave spectra of both 2HP and 2PY have been observed and assigned [2]. Only the Z-isomer of 2HP was detected; the absence of the E-isomer suggests that an intramolecular HB preferentially stabilizes the former [3,4]. Kydd and Mills [5] measured the microwave spectrum of 2AP and found that, while the -NH₂ group is out-of-plane (31.6°), one hydrogen is 0.7 Å closer to the plane containing the ring. Electronic spectra of 2HP and 2PY also have been observed and assigned [6], the latter at high resolution [7]. In 1970, Hollas, *et al.* [8] described the rotational band contours in the electronic spectra of three isotopomers of 2AP. Additionally, later SVL fluorescence

studies of 2AP and some of its deuterated isotopomers [9] provided strong evidence for the existence of appreciable hydrogen bonding between the ring nitrogen and a hydrogen atom of the NH_2 group.

Described herein are the fully resolved electronic spectra of 2HP and 2AP, from which is derived new structural information about their S_0 and S_1 electronic states, from the determined values of their moments of inertia. New information also is obtained about the electronic distributions in the two states, from the observed S_1-S_0 transition moment orientations. The results show that 2HP and 2AP are quite different from their hydrocarbon analogs, phenol and aniline, and suggest that these differences may be relevant to their biological behavior.

2.2 EXPERIMENTAL

2HP and 2AP were purchased from Aldrich and used as received. Experiments at low resolution were performed as described previously [10]. Briefly, the sample was heated to 150°C , entrained in 60 psi of helium, and expanded into a vacuum chamber (10^{-5} Torr) through a 1 mm diameter pulsed valve (General Valve Series 9) operating at 10 Hz. The expansion was crossed by the frequency doubled output of a dye laser (Quanta Ray PDL-1), pumped by the second harmonic of a Nd^{3+} : YAG laser (Quanta Ray DCR-1A), also operating at 10 Hz. Fluorescein 548 laser dye was used to perform the 2HP experiment, and kiton red was used to perform the 2AP experiment. The resulting fluorescence was collected by a PMT, processed by a boxcar integrator, and digitally recorded by a data acquisition computer.

High resolution spectra were obtained using a CW molecular beam spectrometer described in detail elsewhere [11]. The present conditions were as follows. A ~1g sample of 2HP or 2AP was heated to 185° C and entrained in ~850 torr He. The mixture was expanded through a 280 μ m quartz nozzle held at 15-20° C into a vacuum chamber, skimmed about 2 cm downstream of the nozzle before entering a second differentially pumped chamber, and probed 10 cm downstream of the nozzle with a CW laser. The excitation source was an Ar⁺ pumped CW single frequency (FWHM ~ 1 MHz) tunable ring dye laser operating with rhodamine 110 dye (for 2HP) or rhodamine 6G dye (for 2AP) and frequency-doubled by an intracavity BBO (2HP) or LiIO₃ (2AP) crystal. Typical powers used were 300 μ W in the UV. The spectra were recorded at an acquisition rate of 50 Hz over a 2000 second scan. Four signals were collected. The PMT signal was collected with spatially selective optics using photon counting and stored on date acquisition computer. A signal from a near-confocal interferometer having a mode-matched free spectral range of 599.5040 \pm 0.005 MHz in the UV was collected to perform relative frequency calibration. The absorption spectrum of I₂ was collected to determine the absolute transition frequencies, which are accurate to \pm 30 MHz. Finally, the power signal was collected to normalize the PMT signal. Under these conditions, typical single rovibronic linewidths are ~ 30 MHz, principally limited by the Doppler effect.

Supplementing the experimental work, we also performed *ab initio* calculations using density functional theory. Geometry optimizations of the ground state were accomplished using B3LYP/6-31G* and S₁-S₀ transition moment orientations were determined using CIS/6-31G* methods. All calculations were performed using the

Gaussian 98 [12] suite of electronic structure programs on Indigo workstations, or using G98W on personal computers.

2.3 RESULTS

Figure 2.1 shows the first 5 cm^{-1} in the high resolution spectrum of the 0_0^0 band in the S_1 - S_0 electronic transition of 2HP, at 36117 cm^{-1} ($\sim 277\text{ nm}$) [6]. (The entire spectrum spans about $\sim 7\text{ cm}^{-1}$ under our experimental conditions.) Immediately apparent is the fact that this band is an *ab*-hybrid band since the spectrum contains both parallel and perpendicular transitions. Thus, to fit the spectrum, we independently simulated *a*-type and *b*-type bands, and varied their relative intensities until they matched those that were experimentally observed. Both simulations utilized the same sets of rotational constants for the S_0 and S_1 electronic states. We used the microwave values of these constants [2] for the ground states; these were not varied in the fit. We used estimates of these constants for the excited state, based on the known values for the closely related molecule phenol [13]. These were varied in a least-squares fashion in the fit, until the difference between the observed and calculated line positions was minimized.

An additional challenge emerged as the fit of the 0_0^0 band of 2HP was nearing completion. Despite our best efforts, certain experimental line intensities were not well reproduced in several simulations of the hybrid band spectrum, using a large variety of possible TM orientations and rotational temperatures. This challenge was met by assuming that the inertial axes of 2HP in the two electronic states are not coincident. This effect, termed “axis tilting” [14], was also encountered in an analysis of the

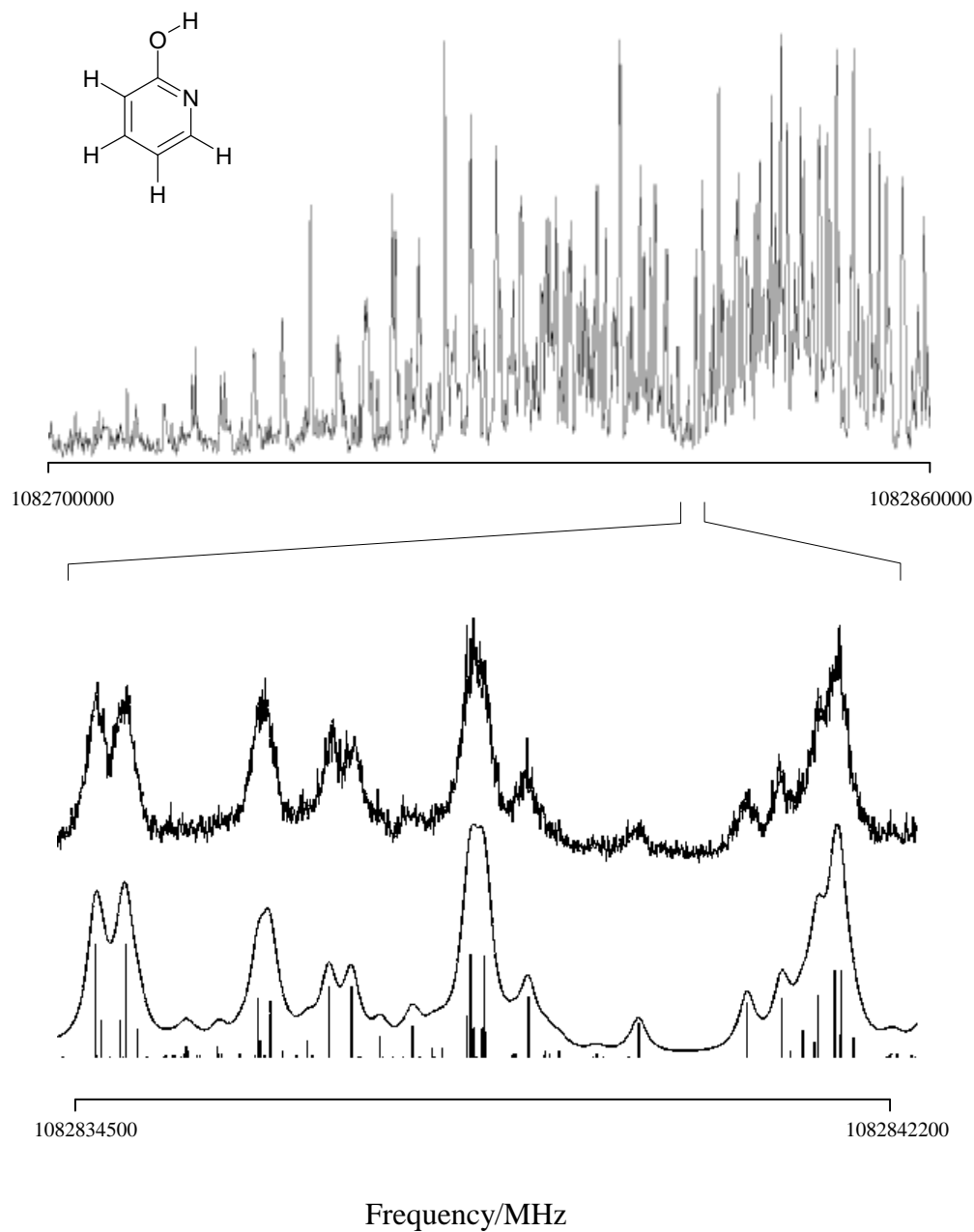


Figure 2.1. The rovibronic S_1 - S_0 spectrum of 2-hydroxypyridine at ~ 277 nm. The inset shows a portion of the experimental spectrum at full resolution, together with two simulations, with and without superimposed lineshape functions. 173 lines were included in the fit, resulting in an OMC of 5.5 MHz. The single rovibronic linewidth is 170 ± 10 MHz. $T = 4.8$ K.

corresponding spectrum of the 2HP tautomer, 2PY [7]. As discussed there, axis tilting leads to anomalous line intensities in a fully resolved spectrum, and may be accounted for by adding additional, off-diagonal terms in the excited state Hamiltonian. Following this procedure in the present case leads to the conclusions that the S_1 - S_0 TM in 2HP makes an angle of $\theta = \pm 53 \pm 3^\circ$ with respect to a , and that the inertial axes tilt in the opposite direction by $\phi = \mp 1.3 \pm 0.10$ when the photon is absorbed.

The quality of our fit is revealed by comparisons of portions of the experimental and computed spectra. An example is also shown in Fig. 2.1. Illustrated there is an ~ 8 GHz portion of the R branch at full experimental resolution, and two simulations, with and without convoluted lineshape functions. While congested, individual transitions could be identified in the spectra, and analyses of these with Voigt lineshape functions yielded Gaussian and Lorentzian linewidths of ~ 30 and ~ 170 MHz, respectively. The Lorentzian width corresponds to a lifetime of ~ 1 ns.

A similar procedure was followed for 2AP. Its S_1 - S_0 origin band is at 33471 cm^{-1} ($\sim 299 \text{ nm}$) [8], red shifted by 2646 cm^{-1} from the corresponding band in 2HP. Figure 2.2 shows the high resolution spectrum of this band in 2AP. It is also an ab -hybrid band and exhibits a small axis tilt, as well. Fits of this spectrum yielded a TM orientation of $\theta = \pm 58 \pm 3^\circ$ and a tilt angle of $\phi = \mp 1.4 \pm 0.2^\circ$. The value of θ in 2AP is significantly different from that in 2HP (53°). Individual rovibronic lines also could be identified (cf. Fig. 2.2) and fit to lineshape functions, yielding Gaussian and Lorentzian widths of ~ 30 and ~ 120 MHz, respectively. The Lorentzian width corresponds to a lifetime of ~ 1.5 ns, slightly longer than that in 2HP.

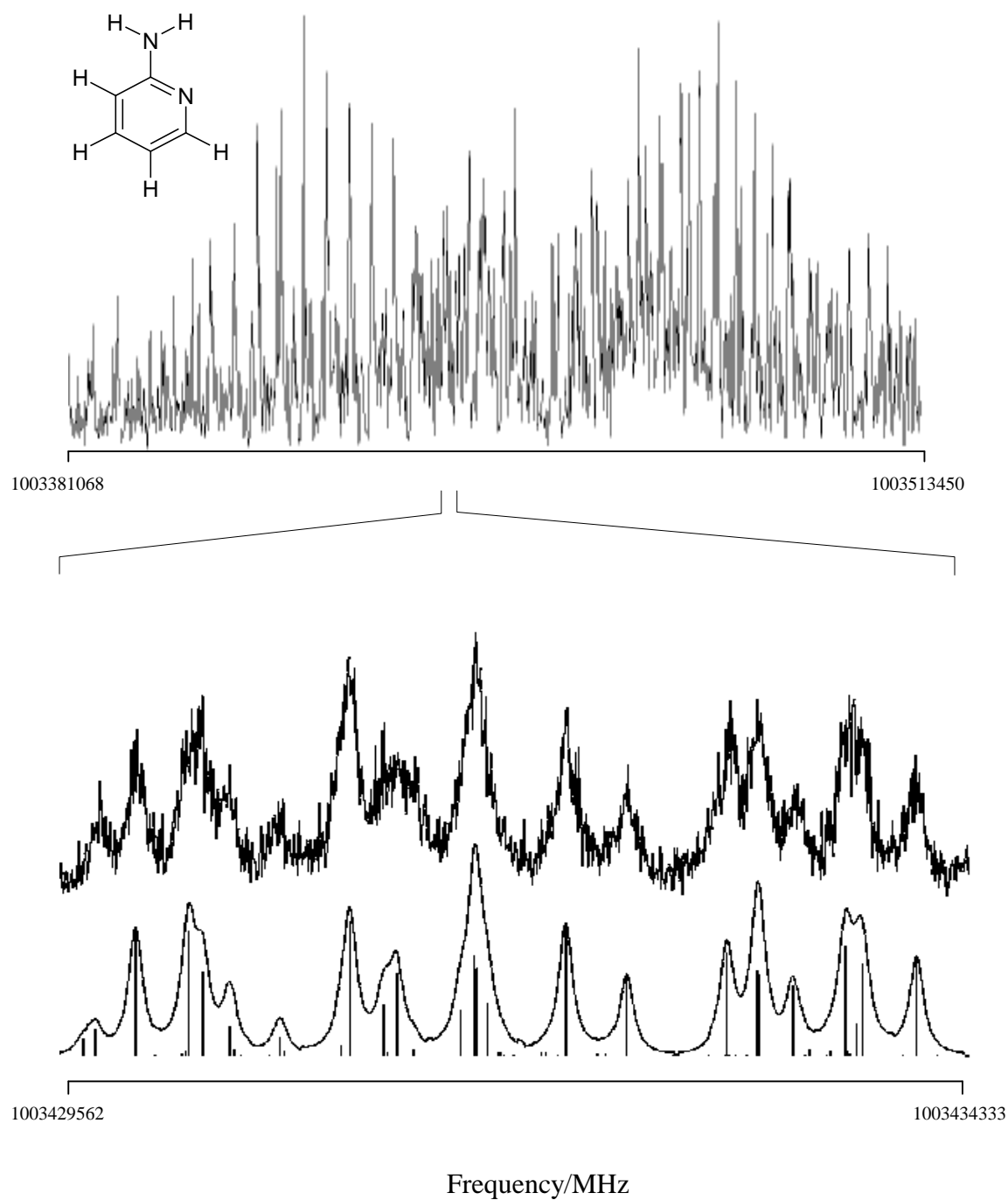


Figure 2.2. The rovibronic S_1 - S_0 spectrum of 2-aminopyridine at ~ 299 nm. The inset shows a portion of the experimental spectrum at full resolution, together with two simulations, with and without superimposed lineshape functions. 74 lines were included in the fit, resulting in an OMC of 6.5 MHz. The single rovibronic linewidth is 120 ± 10 MHz. $T = 5.0$ K.

Table 2.1 lists the inertial parameters derived from the fits of the origin bands in the high resolution S_1 - S_0 electronic spectra of 2HP and 2AP. As noted, the values shown for the S_0 state are from microwave studies; those for the S_1 state were derived from least squares fits of the spectra in Figs. 2.1 and 2.2. Comparing the rotational constants for the two states, of the two molecules, we see that they are remarkably similar, as expected. 2AP has slightly smaller values of A, B, and C, as a consequence of its slightly larger moments of inertia about the three principal axes, in both states. And the values of ΔA , ΔB , and ΔC for the two molecules, also are very similar. ΔA is large and negative whereas ΔB and ΔC are both relatively small, with different signs. These trends reflect, of course, the fact that the photon-induced changes in the geometries of 2HP and 2AP are qualitatively the same.

Comparing these results to those obtained previously, we note that our ΔA , ΔB , and ΔC values for 2AP agree very well with the earlier contour studies of Hollas, *et al.* [9]. We also note that significant discussion has been given, elsewhere, of the increasing tendency for ΔB to be positive in substituted benzenes, as one goes from increasingly double C-F to C-O to C-N bonds in the S_1 state [15]. 2AP fits within this trend.

2.4 DISCUSSION

2HP and 2AP are N-heterocyclic analogs of phenol and aniline, respectively. Therefore, it is interesting to compare the properties of the four molecules in their two

Table 2.1. Inertial parameters of 2-hydroxypyridine (2HP) and 2-aminopyridine (2AP) in their ground (S_0) and electronically excited (S_1) states.

Parameter	S_0^a	S_1	S_1-S_0
2HP			$\nu_0 = 36118.69(2) \text{ cm}^{-1}$
A,MHz	5824.95	5467.1(1)	-357.9
B,MHz	2767.53	2780.5(1)	13.0
C,MHz	1876.16	1844.6(1)	-31.6
$\Delta I, \mu\text{Å}^2$	-0.003	-0.212(23)	Band type $a:b=36:64$
κ	-0.548	-0.483	$\theta(a) = \pm 53 \pm 3^\circ$
2AP			$\nu_0 = 33471.39(2) \text{ cm}^{-1}$
A,MHz	5780.34	5439.9(1)	-340.5
B,MHz	2733.57	2771.7(1)	38.2
C,MHz	1857.66	1837.7(1)	-20.0
$\Delta I, \mu\text{Å}^2$	-0.258	-0.231(23)	Band type $a:b=28:72$
κ	-0.553	-0.481	$\theta(a) = \pm 58 \pm 3^\circ$

^aMicrowave values. See Refs. 2 and 5.

Table 2.2. Inertial parameters of phenol and aniline in their ground (S_0) and electronically excited (S_1) states.

Parameter	S_0^a	$S_1^{b,c}$	S_1-S_0
Phenol			$\nu_0 = 36348.7 \text{ cm}^{-1}$
A,MHz	5650.515	5313.6	-336.9
B,MHz	2619.236	2620.5	1.3
C,MHz	1789.855	1756.1	-33.8
$\Delta I, \mu\text{\AA}^2$	-0.0309	-0.18	Band type b
κ	-0.540	-0.514	$\theta(a) = \pm 90^\circ$
Aniline			$\nu_0 = 34029.19 \text{ cm}^{-1}$
A,MHz	5617.40	5286.9	-330.5
B,MHz	2593.83	2633.8	39.9
C,MHz	1777.04	1759.4	-17.6
$\Delta I, \mu\text{\AA}^2$	-0.406	-0.232	Band type b
κ	-0.575	-0.504	$\theta(a) = \pm 90^\circ$

^aMicrowave values. See Refs. 16 and 17.

^bUV values for phenol. See Ref. 13.

^cUV values for aniline. See Ref. 18.

electronic states. Table 2.2 lists the band origin frequencies, S_1 - S_0 transition moment orientations, and rotational constants of phenol and aniline [13,14] for comparison with

The S_1 - S_0 band origins of the N-heterocyclics are each red shifted with respect to their hydrocarbon analogs, by relatively small amounts (230 and 558 cm^{-1} , respectively). Their rotational constants are also qualitatively the same, with the N-heterocyclics having slightly larger A, B, and C values (smaller moments of inertia). The changes in these constants that occur when the molecules absorb light (ΔA , ΔB , and ΔC) also are very similar. But the S_1 - S_0 transition moment orientations of 2HP and 2AP are very different from their hydrocarbon analogs. Phenol and aniline each exhibit S_1 - S_0 transitions that are pure *b*-type, with $\theta(a) = \pm 90^\circ$, whereas 2HP and 2AP each exhibit S_1 - S_0 transitions that are *ab*-hybrid-type, with $\theta(a) = \pm 53^\circ$ and $\pm 58^\circ$, respectively. Thus, the electron distributions in 2HP and 2AP, and how they change when the photon is absorbed, must be very different from those in phenol and aniline.

Before discussing the ways in which the S_1 - S_0 transitions of 2HP and 2AP are different from those of their hydrocarbon analogs, we note one important similarity; all are $\pi\pi^*$ transitions, because they are in-plane polarized. An $n\pi^*$ transition would be polarized perpendicular to the plane, as is the case for pyridine itself. An early band contour analysis [19] of the origin band of the S_1 - S_0 transition of pyridine-4- d_1 (at ~ 287 nm) showed clearly that it is a *c*-type band. This observation has been confirmed in the high resolution optothermal study of pyridine in its S_1 state by Becucci, *et al.* [20]. Therefore, since all four transitions considered here are in-plane polarized, all are $\pi\pi^*$ transitions.

Nonetheless, the S_1 - S_0 transitions of 2HP and 2AP are different, as noted before. The first issue we must address is the orientation of the TM in the molecular frame, since experiment gives only the absolute value of θ , and not its sign. (Under some conditions, the sign of θ *can* be determined by experiment [21], but those conditions do not exist here.) So, we turn to theory for some guidance on this issue. *Ab initio* calculations were performed using Gaussian 98 [12] on both 2HP and 2AP, using the B3LYP method for the S_0 state and the CIS method for the S_1 state. Energy optimized geometries of each state were determined, yielding rotational constants in excellent agreement with experiment ($\sim 0.2\%$ for the S_0 state, $\sim 2.5\%$ for the S_1 state). Additionally, S_1 - S_0 TM orientations also were calculated, yielding the angles $\theta = -58^\circ$ and $\theta = -60^\circ$ for 2HP and 2AP, respectively. This shows that the TM vector is rotated in a counterclockwise fashion with respect to a , as illustrated in Fig. 2.3. The magnitudes of the calculated angles are also in excellent agreement with experiment ($\pm 53^\circ$ and $\pm 58^\circ$, respectively). The *ab initio* transition moments that agree best with experiment cross the ring, nearly “perpendicular” to the in-ring nitrogen.

A second approach may be taken to address this issue, an approach that is also rooted in theory. Recall that 2HP and 2AP both exhibit axis tilting; the inertial axes of their S_0 and S_1 states are not coincident. Also recall that a principal consequence of axis tilting in a fully resolved spectrum are “anomalous” line intensities, arising from interferences between different excitation channels [7,14]. Which transitions gain intensity, and which transitions lose intensity, is determined by the *relative* orientations of the TM vector (θ) and the direction of axis tilt, or reorientation (ϕ). Experimentally, in

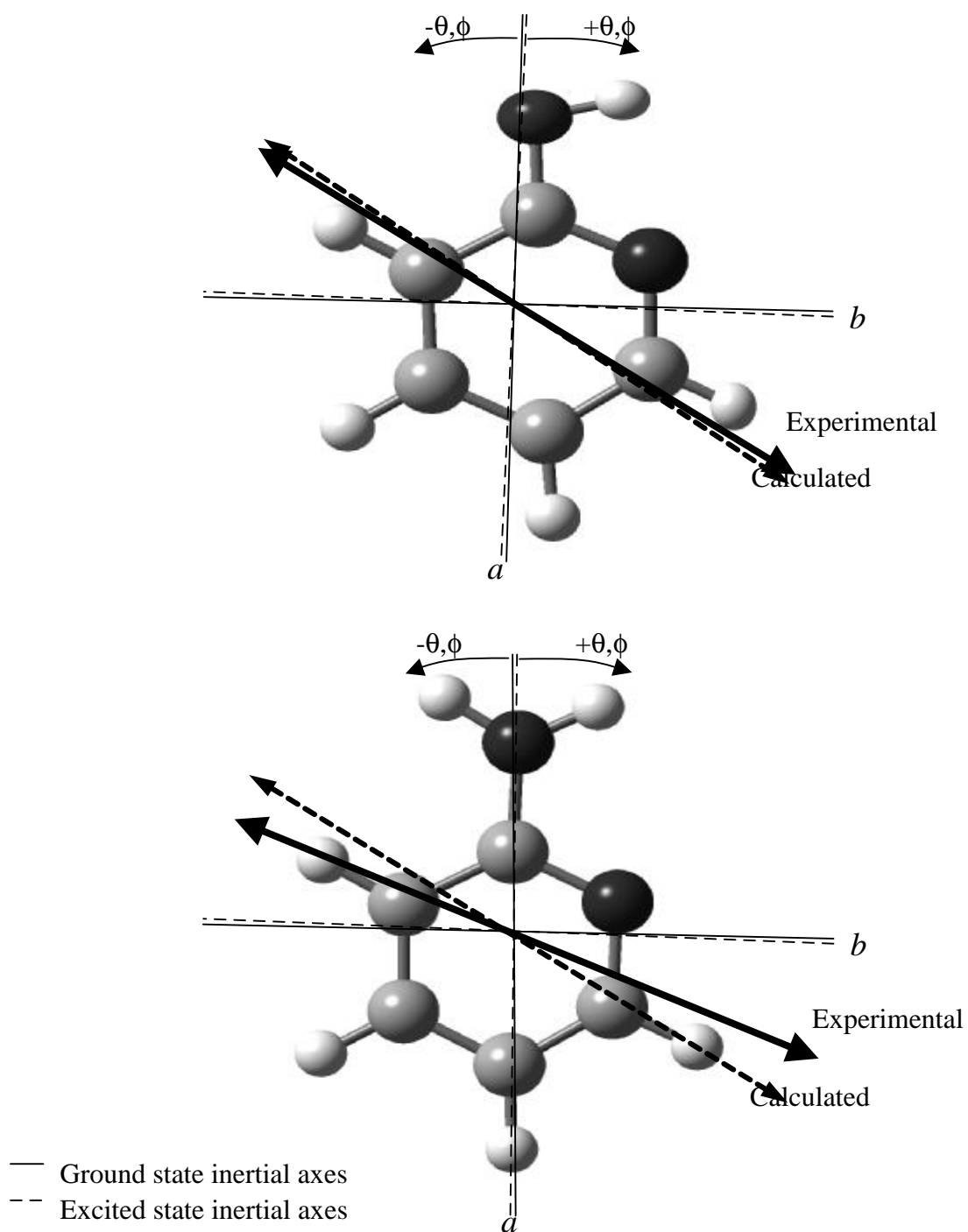


Figure 2.3. Inertial axes, transition moment, and axis tilt orientations in 2-hydroxypyridine (top) and 2-aminopyridine (bottom). The θ -sign convention is that used for the axis tilt.

the case of 2HP and 2AP, we know that θ and ϕ have opposite signs. Therefore, the sign of θ can be determined if the sign of ϕ is known.

Information about the sign of ϕ is contained in the results of the *ab initio* calculations on the two electronic states of 2HP and 2AP. Using the atomic positions determined from the energy-optimized structures, we constructed a Z-matrix for each molecule, in each state. These matrices were then diagonalized, to determine the location of the principal axes of inertia, and of each of the component atoms in this coordinate system. The results for each state were then compared, to determine the direction of the axis tilt. S_1 - S_0 excitation produces a clockwise tilt of the inertial axis in both molecules, as also shown in Fig. 2.3. Therefore, the θ values of 2HP and 2AP are both negative, as concluded before, since ϕ is positive in both cases.

In electronic spectroscopy, the TM is the dipole moment of an oscillating charge density and, hence, is related to the wavefunctions of the electrons in the two states connected by the photon. Thus,

$$(m_z)_{12} = \int \Psi_2^* \hat{m}_z \Psi_1 dt \quad (1)$$

Typically, the total electronic wavefunctions Ψ_1 and Ψ_2^* may be expressed as products of the occupied and unoccupied molecular orbitals (MO's) of the system. Thus, the orientation of the electronic TM in the molecular frame is determined by the nodal patterns of the participating MO's [22].

Information about the MO's that participate in the S_1 - S_0 transitions of phenol and aniline, and their N-heterocyclic analogs, also is contained in the results of the *ab initio* calculations. Table 2.3 lists the principal one-electron excitations that contribute to the S_1 - S_0 transitions in all four molecules. Examining these data, we see that the dominant

Table 2.3. CIS expansion coefficients squared of the principal one-electron excitations contributing to the S_1 - S_0 transitions of 2-hydroxypyridine (2HP), 2-aminopyridine (2AP), phenol, and aniline. (6-31G* basis set).

Molecule	(HOMO \rightarrow LUMO) ²	(HOMO-1 \rightarrow LUMO+1) ²
2HP	0.8844	0.1156
2AP	0.9145	0.0855
Phenol	0.7550	0.2450
Aniline	0.8300	0.1700

excitations in all four molecules are HOMO \rightarrow LUMO in type, with the next most significant contribution coming from HOMO-1 \rightarrow LUMO+1 excitations. Thus, differences between the TM orientation in the N-heterocyclies and the corresponding aromatics cannot be attributed to state mixing, since all four transitions are clearly 1L_b in character. 1L_a states are derived from excitations of the HOMO-1 \rightarrow LUMO and HOMO \rightarrow LUMO+1 type [22,23].

The principal factors responsible for the differences in the TM orientations are the nodal properties of the wavefunctions themselves. Figure 2.4 shows plots of the four relevant MO's in 2HP and 2AP. The HOMO-1 and LUMO orbitals of phenol and aniline exhibit nodes at the *para* carbon atoms, C₁ and C₄. Hence, the contribution from these atoms to the product $\Psi_1 \Psi_2^*$ is negligible. In contrast, the corresponding orbitals in 2HP and 2AP do exhibit density on C₁ and C₄; the nodes in HOMO-1 and LUMO are shifted away from these atoms. Additionally, the electron density in these orbitals on the -OH group of phenol, and on the -NH₂ group of aniline, is greatly enhanced in 2HP and 2AP, compared to the hydrocarbons themselves. There are further, minor distortions of the HOMO and LUMO+1 orbitals in 2HP and 2AP. Thus, when one computes the transition densities $\Psi_1 \Psi_2^*$, one finds that the nodal planes of these oscillating charge distributions are rotated significantly in 2HP and 2AP, compared to phenol and aniline. This is shown in Fig. 2.5.

It is likely that these differences in transition densities also are responsible, in fact, for the (small) differences in the values of ΔA , ΔB , and ΔC in the four molecules (*cf.* Tables 2.1 and 2.2). These effects were not analyzed in detail. But it is clear even on a cursory examination of Fig. 2.5 that the asymmetries in the oscillating charge

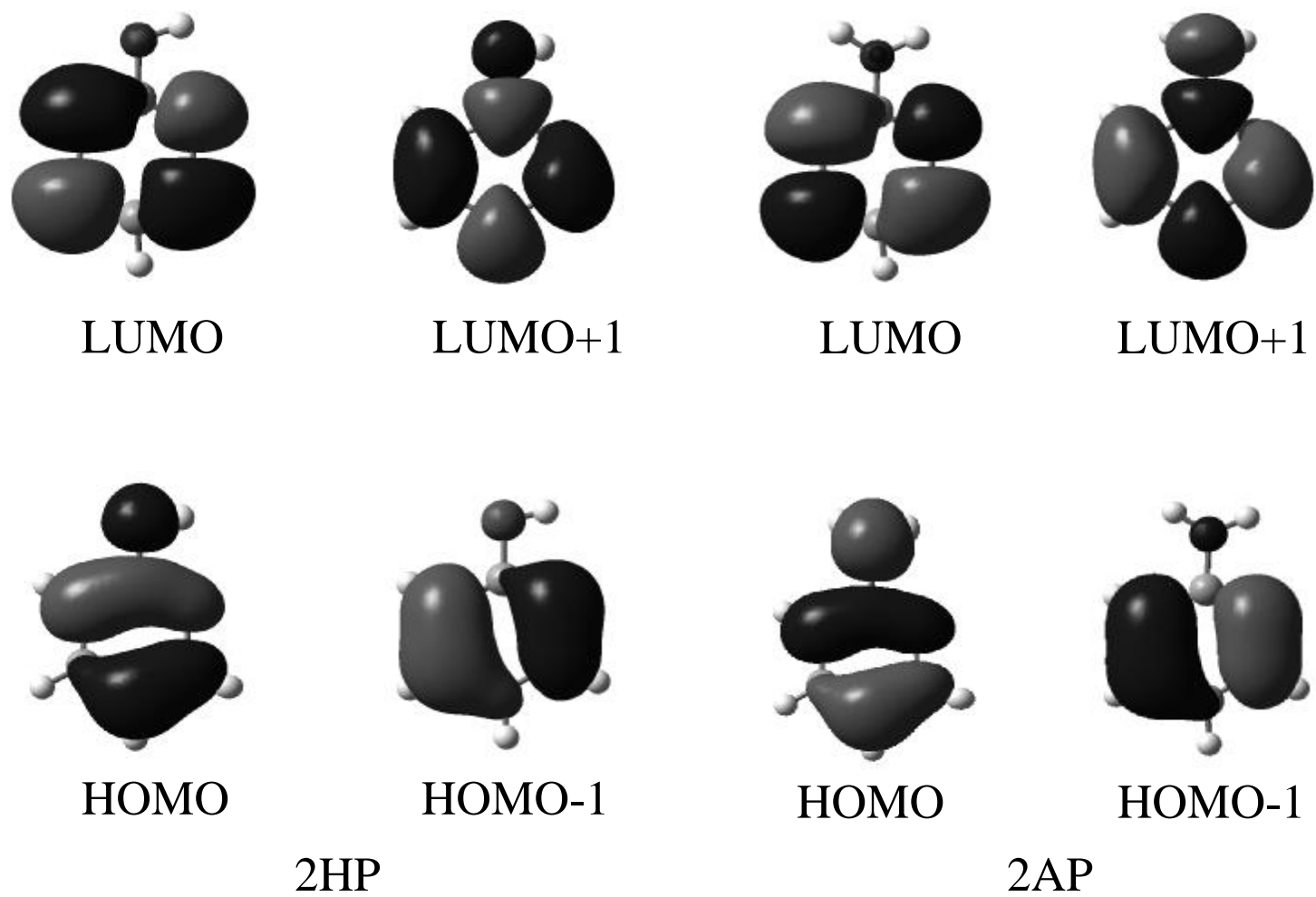


Figure 2.4. Calculated molecular orbitals of 2-hydroxypyridine (left) and 2-aminopyridine (right).

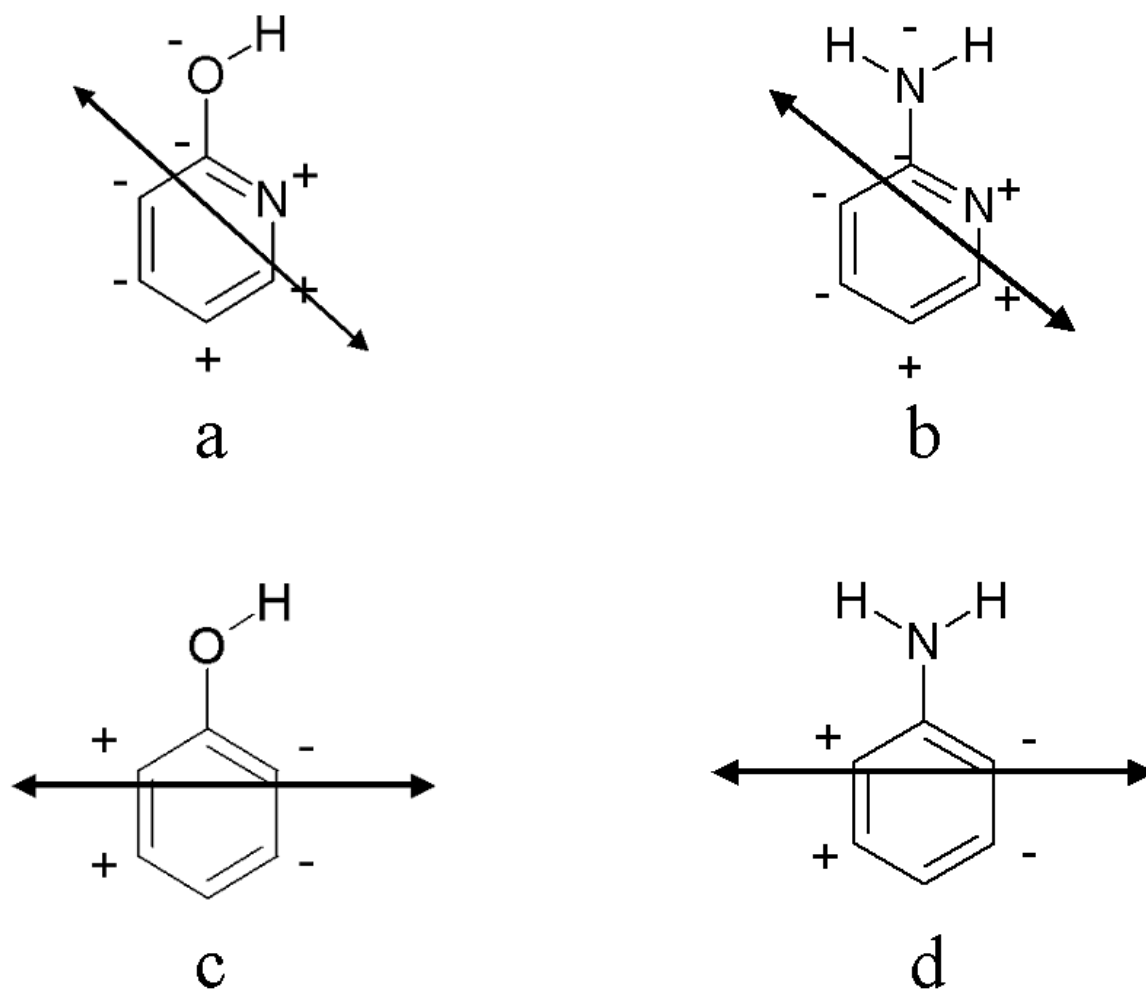


Figure 2.5. Transition densities of a) 2-hydroxypyridine, b) 2-aminopyridine, c) phenol and d) aniline.

distributions which are shown there are also responsible for the axis tilting that is observed in the spectra of 2HP and 2AP.

What causes the asymmetries in these charge distributions? The simple answer is, obviously, the in-ring nitrogen atom, which is electronically different from the C – H bond that it replaces. In particular, the aromatic nitrogen atom has a lone pair, whereas the carbon atom does not. We believe, however, that the nitrogen atom is only “indirectly” responsible for these differences, by virtue of an attractive interaction between its lone pair and the hydrogen atom(s) of the attached group; *i.e.*, an intramolecular hydrogen bond.

Positive evidence for the existence of such a bond is provided by the measured rotational constants of 2HP and 2AP, and especially in the values of the inertial defects derived from them (Tables 2.1 and 2.2). 2HP and phenol both have small negative values of ΔI , in their electronic ground states, indicating essentially planar structures. But the ΔI value of S_0 phenol ($-0.0309 \text{ amu } \text{\AA}^2$) is an order of magnitude larger than that of S_0 2HP ($-0.003 \text{ amu } \text{\AA}^2$). We suggest that the reason for this difference is that the OH group in phenol has much greater torsional amplitude than in 2HP, owing to the existence of an intramolecular HB in 2HP. Further, we know from theory that Z-2HP is considerably more stable than E-2HP. A similar effect has been observed in 2-hydroxyquinoline [24].

Ground state aniline is a non-planar molecule, owing to displacements along the out-of-plane amino inversion mode. Its inertial defect is $\Delta I = -0.406 \text{ amu } \text{\AA}^2$. This value also is reduced in magnitude significantly in 2AP, to $\Delta I = -0.258 \text{ amu } \text{\AA}^2$, again indicating an intramolecular HB. Both inertial defects decrease when the molecule is excited to the S_1 state (to the nearly identical values of -0.232 and $-0.231 \text{ amu } \text{\AA}^2$,

respectively). The S_1 state of aniline is known to be a *quasi* planar molecule [18]. Thus, we conclude that the S_0 state of 2AP also is planar, in the same sense, and that this is a consequence of an intramolecular HB.

The hydrogen bonding interaction is primarily electrostatic in nature. Thus, motion of electrons either towards or away from a HB site will have a significant effect on the HB itself. The nodal plane of the LUMO+1 orbital passes through the in-ring nitrogen (Fig. 2.4). Therefore, this atom loses electron density in the S_1 state, and the intramolecular HB in this state is significantly weaker, compared to the S_0 state. Consequently, torsion of the OH group in 2HP has a significantly higher amplitude, and ΔI increases in magnitude to $\Delta I = -0.34 \text{ amu } \text{\AA}^2$, providing a quantitative measure of this effect.

Summarizing, high resolution studies of the electronic spectra of 2-hydroxypyridine (2HP) and 2-aminopyridine (2AP) have made possible accurate measurements of the rotational constants of both molecules in their ground (S_0) and excited (S_1) electronic states. These constants are qualitatively similar to the two aromatic hydrocarbon analogs of 2HP and 2AP, phenol and aniline, showing that the geometries of the four molecules are largely the same. However, the electronic distributions in the two N-heterocyclics are significantly different from their hydrocarbon analogs. This is evidenced primarily by small inertial axis reorientations on S_1 excitation, significantly larger rotations of their electronic transition moment vectors in the molecular plane, and intramolecular hydrogen bonds between the in-plane nitrogen and a hydrogen atom of the attached -OH or -NH₂ group. Significant differences in the noncovalent interactions involving N-heterocyclic rings, compared to hydrocarbon

aromatic units, are possible biological consequences of these effects, which remain to be explored.

2.5 ACKNOWLEDGEMENTS

This work has been supported by NSF (CHE – 9987048). We thank Michael Hollas, Tim Korter, and Jason Ribblett for helpful discussions.

2.6 REFERENCES

1. See, for example, S. L. McKay, B. Haptonstall, and S. H. Gellman, *J. Amer. Chem. Soc.* **123**, 1244 (2001).
2. L. D. Hatherley, R. D. Brown, P. D. Godfrey, A. P. Pierlot, W. Caminati, D. Damiani, S. Melandri, and L. B. Favero, *J. Phys. Chem.* **97**, 46 (1993).
3. E (*entgegen*) denotes that the substituents of highest CIP priority [4], here the -OH and -N groups, at each end of the double bond are *trans* to one another; if the substituents are *cis*, the description is Z (*zusammen*).
4. E. L. Eliel, S. H. Wilen, and L. N. Mander, *Stereochemistry of Organic Compounds*, Wiley-Interscience, New York, 1994.
5. R. A. Kydd and I. M. Mills, *J. Mol. Spectrosc.* **42**, 320 (1972).
6. M. R. Nimlos, D. F. Kelley, and E. R. Bernstein, *J. Phys. Chem.* **93**, 643 (1989).
7. A. Held, B. B. Champagne, and D. W. Pratt, *J. Chem. Phys.* **95**, 8732 (1991).
8. J. M. Hollas, G. H. Kirby, and R. A. Wright, *Mol. Phys.* **18**, 327 (1970).
9. J. M. Hollas, H. Musa, and T. Ridley, *J. Mol. Spectrosc.* **104**, 107 (1984).
10. J. R. Johnson, K. D. Jordan, D. F. Plusquellic, and D. W. Pratt, *J. Chem. Phys.* **93**, 2258 (1990).
11. W. A. Majewski, D. F. Plusquellic and D. W. Pratt, *J. Chem. Phys.* **90**, 1362 (1989).
12. *Gaussian 98* (Revision A.9), M. J. Frisch, G. W. Trucks, H. B. Schlegel, G. E. Scuseria, M. A. Robb, J. R. Cheeseman, V. G. Zakrzewski, J. A. Montgomery, R. E. Stratmann, J. C. Burant, S. Dapprich, J. M. Millam, A. D. Daniels, K. N. Kudin, M. C. Strain, O. Farkas, J. Tomasi, V. Barone, M. Cossi, R. Cammi, B. Mennucci, C. Pomelli, C. Adamo, S. Clifford, J. Ochterski, G. A. Petersson, P. Y. Ayala, Q. Cui, K. Morokuma, D. K. Malick, A. D. Rabuck, K. Raghavachari, J. B. Foresman, J. Cioslowski, J. V. Ortiz, A. G. Baboul, B. B. Stefanov, G. Liu, A. Liashenko, P. Piskorz, I. Komaromi, R. Gomperts, R. L. Martin, D. J. Fox, T. Keith, M. A. Al-Laham, C. Y. Peng, A. Nanayakkara, M. Challacombe, P. M. W. Gill, B. G. Johnson, W. Chen, M. W. Wong, J. L. Andres, C. Gonzalez, M. Head-Gordon, E. S. Replogle and J. A. Pople, Gaussian, Inc., Pittsburgh PA, 1998.

13. G. Berden, W. L. Meerts, M. Schmitt, and K. Kleinermanns, *J. Chem. Phys.* **104**, 972 (1996).
14. J. T. Hougen and J. K. G. Watson, *Can. J. Phys.* **43**, 298 (1965).
15. T. Cvitas, J. M. Hollas, and G. H. Kirby, *Mol. Phys.* **19**, 305 (1970).
16. E. Mathier, D. Welti, A. Bauder, and Hs. H. Günthard, *J. Mol. Spectrosc.* **37**, 63 (1971).
17. D. G. Lister, J. K. Tyler, J. H. Høg, and N. W. Larsen, *J. Mol. Struct.* **23**, 253 (1976).
18. W. E. Sinclair and D. W. Pratt, *J. Chem. Phys.* **105**, 7942 (1996).
19. F. W. Birss, S. D. Colson, and D. A. Ramsay, *Can. J. Phys.* **51**, 1031 (1973).
20. M. Becucci, N. M. Lakin, G. Pietraperzia, P. R. Salvi, E. Castellucci, and E. R. Kerstel, *J. Chem. Phys.* **107**, 10399 (1997).
21. D. F. Plusquellic and D. W. Pratt, *J. Chem. Phys.* **97**, 8970 (1992).
22. L. Salem, *The Molecular Orbital Theory of Conjugated Systems*, W. A. Benjamin, Inc.; Reading, Massachusetts, 1966.
23. R. T. Kroemer, K. R. Liedl, J. A. Dickinson, E. G. Robertson, J. P. Simons, D. R. Borst, and D. W. Pratt, *J. Amer. Chem. Soc.* **120**, 12573 (1998).
24. A. Held, D. F. Plusquellic, J. L. Tomer, and D. W. Pratt, *J. Phys. Chem.* **95**, 2877 (1991).

3.0 Hydrogen bonding and tunneling in the 2-pyridone-2-hydroxypyridine dimer. Effect of electronic excitation

David R. Borst^a, Joseph R. Roscioli^a, David W. Pratt^a, Gina M. Florio^b, Timothy S. Zwier^b, Andreas Müller^c and Samuel Leutwyler^c

^a Department of Chemistry, University of Pittsburgh, 605 Chevron Science Center, Pittsburgh, PA 15260, USA

^b Department of Chemistry, Purdue University, West Lafayette, IN 47907-1393, USA

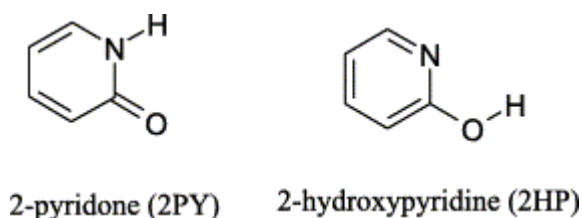
^c Departement für Chemie und Biochemie, Universität Bern, Freiestrasse 3, CH-3000, Bern 9, Switzerland

ABSTRACT

The 2-pyridone·2-hydroxypyridine (2PY·2HP) mixed dimer has been studied using high resolution ultraviolet spectroscopy in the region of the 2PY S_1 – S_0 origin, and fluorescence-dip infrared spectroscopy in the region of the hydride stretch fundamentals. The dense rotational structure of the electronic spectrum is characteristic of a *b*-type transition with a transition moment at $8^\circ \pm 3^\circ$ to the *b*-axis, consistent with excitation of the 2PY half of the dimer. A tunneling splitting of 520 ± 10 MHz appears in the spectrum, due to a double proton transfer in 2PY·2HP. The double proton transfer exchanges the chemical identity of the two monomer units, thereby leading to a double tautomerization. Theoretical calculations suggest that the barrier to such motion is about 8 kcal/mol in the ground state; hence, the observed tautomerization apparently occurs in the excited state. An approximate fit of the high resolution spectrum gives rotational constants that are consistent with an excited state structure in which only the OH...O hydrogen bond in the dimer is lengthened substantially. The infrared spectrum out of the pair of ground state zero-point tunneling levels in the XH stretch region is reminiscent of that in the pure (2PY)₂ dimer. Its peak absorption frequency is at 2700 cm^{-1} , but the infrared band is spread over about 500 cm^{-1} , with reproducible sub-structure due to strong, anharmonic coupling. The excited state spectrum, in contrast, is dominated by a transition at 3135 cm^{-1} . This band is assigned to the OH fundamental, which is shifted to higher frequency by the weakening of the OH...O hydrogen bond upon electronic excitation.

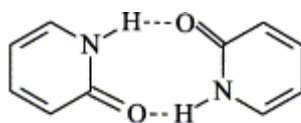
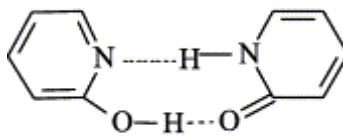
3.1 INTRODUCTION

2-Pyridone (2PY) and 2-hydroxypyridine (2HP) are *keto-enol* tautomers of one another. This tautomeric pair has received much attention in the past largely because the two tautomers are very similar in energy, with both present in substantial concentrations at room temperature, facilitating their study under a wide range of conditions [1-5]. The barrier to tautomerization is large in the monomers, because H-atom tunneling must occur over a large distance with substantial heavy atom rearrangement. Theoretical values of this barrier fall in the range of 35–38 kcal/mol [6].

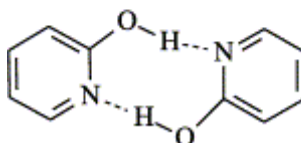


A substantial reduction in the barrier to tautomerization is predicted on complex formation [6]. The two tautomers have complementary H-bonding sites that are adjacent to one another; the NH donor and C=O acceptor sites in 2PY become pyridinal nitrogen acceptor and OH donor sites in 2HP. As a result, the tautomers can form stable complexes with many other species, including H₂O and NH₃ [1, 4, 5, 7 and 8].

The two tautomers also can form three chemically distinct and strongly bound dimers; the (2PY)₂ and (2HP)₂ homodimers, and the 2PY·2HP mixed dimer [9-12].

(2PY)₂

2PY·2HP

(2HP)₂

The recent calculations of Müller, *et al.* [12] predict D_0 values for the (2PY)₂, 2PY·2HP, and (2HP)₂ dimers of 17.6, 13.6, and 14.1 kcal/mol, respectively. In the symmetric dimers, tautomerization involves a double H-atom transfer in a distinctly asymmetric double well that interconverts the two dimers:



As a result, no tunneling splitting is anticipated in these dimers. Indeed, the (2PY)₂ dimer, whose S_2 – S_0 origin transition has been fully rotationally resolved and analyzed [9 and 10], exhibits no tunneling splitting.

The 2PY·2HP mixed dimer, which contains both the *keto* and *enol* tautomers, can undergo a double H-atom transfer that exchanges the two monomers' chemical identities in a symmetric double well:



Here, a tunneling splitting is anticipated, and will reflect the rate of exchange between the two wells. Resolution of such tunneling splittings is anticipated to require high resolution

spectroscopy, as recently demonstrated by Remmers, *et al.* [13], who resolved a tunneling splitting for double H-atom transfer of ~ 1100 MHz (~ 0.04 cm $^{-1}$) in the benzoic acid dimer.

The mechanism of excited state double proton transfer after photoexcitation of canonical base pairs has attracted a great deal of experimental and theoretical interest. Given the close chemical similarity of 2PY to uracil and of 2HP to *isoguanine*, the rate of tunneling in dimers such as 2PY·2HP is of fundamental importance because of its implication in radiation-induced mutations resulting from the formation of the rare *enol* tautomeric form of the nucleobases during DNA replication [14].

A second motivation for the present study is to probe the cooperatively strengthened hydrogen bonds in the 2PY·2HP dimer by comparison to those in the symmetric (2PY) $_2$ dimer. The infrared spectrum of (2PY) $_2$ in the hydride stretch region has recently been studied by Matsuda, *et al.* [4]. It shows a broad, intense NH stretch absorption shifted down almost 700 cm $^{-1}$ in frequency, as is characteristic of strongly H-bonded dimers. In that case, the spectrum reflects the presence of two equivalent NH \cdots O hydrogen bonds, which are strongly coupled to one another. We seek here to probe changes in the hydride stretch infrared spectrum induced by the somewhat weaker binding energy of the 2PY·2HP dimer by comparison to (2PY) $_2$, and its inclusion of two different H-bonds (one NH \cdots N and one OH \cdots O).

Finally, by recording the hydride stretch infrared spectrum in the S $_1$ excited state, we will probe the effect of electronic excitation of the 2PY tautomer on H-bonding in the 2PY·2HP dimer. This dimer is a model system in which to study the effects of electronic excitation on hydrogen bonding, because both tautomers, 2PY and 2HP, have accessible

electronically excited states. The S_1 state of the 2PY monomer is about 5000 cm^{-1} below that of 2HP, so it is anticipated that electronic excitation will be localized on one or the other of the tautomers. The recent studies of Müller, *et al.* [12] have identified transitions in the vicinity of the $(2\text{PY})_2 S_2-S_0$ transition that they assign to the S_1-S_0 transition of the 2PY·2HP dimer involving localized excitation of the 2PY tautomer in the dimer, $(2\text{PY})^*\cdot 2\text{HP}$. That work concentrated on the vibronic spectroscopy of 2PY·2HP and its deuterated isotopomers, with particular attention focused on intermolecular vibrations.

The present study builds on that work with two complementary experiments that shed new light on the effect of electronic excitation on the H-bonding and tunneling in the 2PY·2HP dimer. A high resolution study of the 2PY·2HP S_1-S_0 origin is used to identify tunneling splitting ascribable to the double proton transfer, and to measure the qualitative structural changes which accompany electronic excitation. Fluorescence-dip infrared spectra in the S_0 and S_1 states are then used to probe the effects of H-bonding on the hydride stretch vibrations in both states. We shall see that these data lead to a picture of the effects of electronic excitation which confirms and sharpens the deductions of Müller, *et al.* [12], based on their vibronic spectroscopy. The primary effect of electronic excitation in the 2PY·2HP dimer is to weaken, and thus elongate the $\text{OH}\cdots\text{O}$ hydrogen bond, while producing a much smaller effect on the $\text{NH}\cdots\text{N}$ hydrogen bond.

3.2 EXPERIMENTAL

Ultraviolet (UV) experiments with vibronic resolution were performed at both the University of Pittsburgh and Purdue University. The Pittsburgh apparatus has been

described previously [15]. Briefly, the sample of 2HP was heated to 420 K, entrained in 5 bar of helium, and expanded into a vacuum chamber using a 1 mm diameter pulsed valve (General Valve Series 9) operating at 10 Hz. The expansion was crossed by the frequency doubled output of a dye laser (Quanta Ray PDL-1) operating with DCM and pumped by the second harmonic of a Nd^{3+} :YAG laser (Quanta Ray DCR-1A), also operating at 10 Hz. The resulting fluorescence was collected by a photomultiplier tube, processed by a boxcar integrator, and digitally recorded by a data acquisition computer.

The Purdue apparatus and methods have also been described previously [16]. In this case, the jet-cooled dimers were prepared by flowing a 70% neon/30% helium mixture at a backing pressure of 2–3 bar over a sample of 2HP heated to 370 K. The mixture was expanded from a pulsed valve (0.8 mm dia) into a chamber pumped by a Roots blower. Fluorescence excitation spectra were recorded by crossing the expansion 5 mm downstream from the nozzle with the doubled output of a Nd^{3+} :YAG-pumped dye laser operating with DCM dye in methanol. Unfocused pulse energies of about 300 $\mu\text{J}/\text{pulse}$ were typically used. The fluorescence was collected by an f/1 lens and imaged onto a UV-enhanced photomultiplier tube.

Infrared (IR) spectra were recorded at Purdue using the fluorescence-dip infrared (FDIR) technique [16]. In this method, the fluorescence intensity of a selected transition in the excitation spectrum is monitored with an ultraviolet laser. Every other UV laser pulse was preceded by 150 ns with a counter-propagating, spatially overlapped IR pulse from an infrared parametric converter (LaserVision, 1–2 mJ/pulse, 0.25 cm^{-1} resolution). When the IR laser pulse is resonant with an infrared transition out of the level being monitored in LIF, the population of that level is decreased. This decrease in population is

detected as a dip in the UV fluorescence signal. The difference in the fluorescence signal obtained without and with the IR laser present is recorded as a function of IR frequency using the active baseline subtraction mode of a gated integrator, which is interfaced to a personal computer.

A similar technique was used to measure the IR spectrum of the electronically excited state. In this case, the IR pulse was delayed so as to occur during the lifetime of the excited state level probed by the UV laser. The S_1 origin lifetime of the 2PY·2HP dimer was measured to be 14 ± 2 ns. When the IR light is resonant with a transition out of the S_1 zero-point level, it transfers population to vibrational levels 3100 cm^{-1} or more above the zero-point level. Fast non-radiative processes quench the fluorescence of these levels, leading to a dip in the fluorescence. Careful control of the time delay of the IR parametric converter from the UV laser (~ 20 ns in this case) was required in order to completely remove contributions to the spectrum from the ground state level, yet retain sufficient excited state population to record the S_1 FDIR spectrum with a good signal-to-noise ratio. A second gated integrator, gated on the rising edge of the fluorescence signal, was used to correct for shot-to-shot fluctuations in the fluorescence signal.

Finally, fluorescence excitation spectra at high resolution were obtained in Pittsburgh using the CW molecular beam spectrometer described in detail elsewhere [17]. The present conditions were as follows. The sample containing 2HP was heated to 450 K and entrained in 1–2 bar He. The mixture was expanded through a $280\text{ }\mu\text{m}$ quartz nozzle held at 470 K into a vacuum chamber. The resulting molecular beam was skimmed about 2 cm downstream of the nozzle before entering a second differentially pumped chamber where it was probed 10 cm downstream of the nozzle. The excitation source was an Ar^+

pumped CW single frequency tunable ring laser operating with DCM dye and frequency doubled by an intracavity LiIO_3 crystal. Typical powers used were 500 μW in the UV. The spectra were acquired at a rate of 50 Hz over a 2000 s scan. Four signals were collected. The PMT signal was collected with spatially selective optics using photon counting and stored on data acquisition computer. A signal from a near-confocal interferometer having a mode-matched free spectral range of 599.504 ± 0.005 MHz in the UV was collected to perform relative frequency calibration. The absorption spectrum of I_2 was collected to determine the absolute transition frequencies, which are accurate to ± 3 MHz. Finally, the power signal was collected to normalize the PMT signal.

Supplementing the experimental work, we also performed density functional theory calculations using the BLYP/6-31+G* and B3LYP/6-311++G(d,p) methods [12 and 18]. Full geometry optimizations were carried out, followed by harmonic vibrational frequency calculations.

2-Hydroxypyridine (2HP) was commercially available (Aldrich) and used as received. Deuteration of the sample was accomplished by exchange with CH_3OD .

3.3 RESULTS

Fig. 3.1 shows the low resolution fluorescence excitation spectrum of 2PY in the vicinity of the $\text{S}_2\text{--S}_0$ origin band of the 2PY dimer, $(2\text{PY})_2$, which appears at $30\,776\text{ cm}^{-1}$ [9, 10]. Approximately 120 cm^{-1} to the red of this band, at $30\,656\text{ cm}^{-1}$, is a single band that has recently been identified by Müller, *et al.* [12] as the $\text{S}_1\text{--S}_0$ origin band of the 2PY·2HP dimer. When the experiment was repeated using a sample containing a 1:1

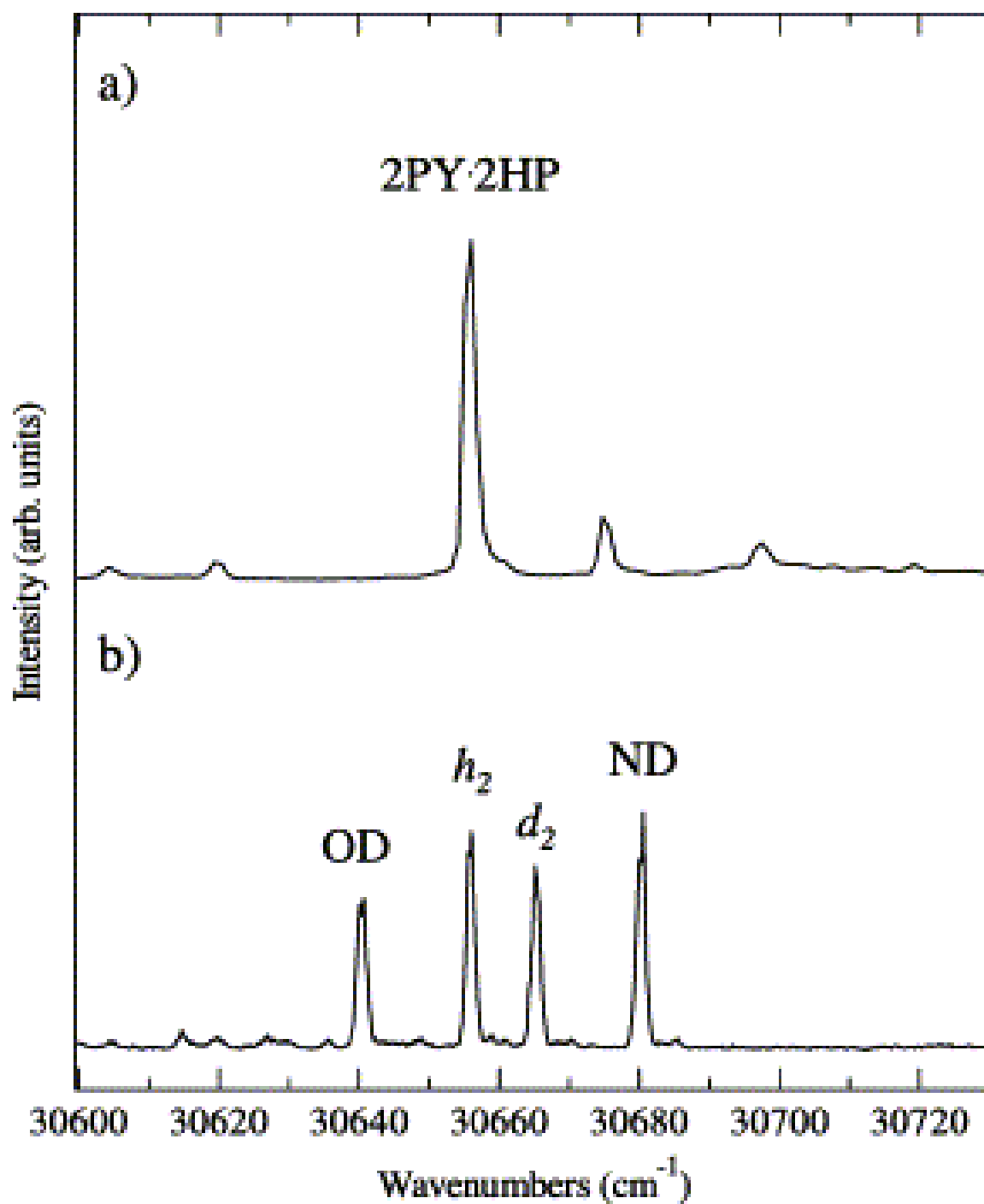


Figure 3.1. Low resolution fluorescence excitation spectrum in the region of the 2PY·2HP S_1 – S_0 origin: (a) protonated sample; (b) spectrum obtained with a 1:1 H:D mixture in the labile N–H and O–H positions.

mixture of protonated and deuterated 2HP, three new bands appear in the vicinity of 30656 cm^{-1} , one to the red and two to the blue. Using mass-resolved REMPI spectroscopy, Müller, *et al.* [12] have assigned the band at $30\,665\text{ cm}^{-1}$ to the doubly deuterated $\text{d}_2(\text{N-D/O-D})$ dimer and the bands at $30\,681$ and $30\,640\text{ cm}^{-1}$ to the two partially deuterated $\text{d}_1(\text{N-D})$ and $\text{d}_1(\text{O-D})$ dimers. The latter two bands are resolved because the two positions of deuterium substitution are inequivalent in the mixed dimer, as we have confirmed in independent low resolution experiments. Furthermore, as Müller, *et al.* [12] surmised, the close proximity of the $2\text{PY}\cdot 2\text{HP}$ origin transition ($30\,656\text{ cm}^{-1}$) to that of the $\text{h}_2(2\text{PY})_2$ ($30\,776\text{ cm}^{-1}$) suggests that the electronic excitation is localized on the 2PY molecule in the mixed dimer. This was confirmed by the high resolution experiments (*vide infra*).

3.3.1 Ground state fluorescence-dip infrared spectra

Figs. 3.2(a) and (b) show the ground state IR spectra of the $(2\text{PY})_2$ and $2\text{PY}\cdot 2\text{HP}$ dimers in the hydride stretching region ($2400\text{--}3550\text{ cm}^{-1}$), respectively, as obtained by the FDIR technique. The spectrum of $(2\text{PY})_2$ was obtained with the UV laser fixed at the $\text{S}_2\text{--S}_0$ origin ($30\,776\text{ cm}^{-1}$) and is identical to that described previously by Matsuda, *et al.* [4]. The spectrum is reproduced here for comparison with the corresponding spectrum of the $2\text{PY}\cdot 2\text{HP}$ dimer shown below it. The latter spectrum was obtained with the UV laser fixed at the $2\text{PY}\cdot 2\text{HP}$ $\text{S}_1\text{--S}_0$ origin ($30\,656\text{ cm}^{-1}$). Besides the weak transitions above 3000 cm^{-1} (due to the aromatic CH stretch fundamentals), the entire absorption shown in Fig. 3.2 derives its oscillator strength from the XH stretch fundamentals involved in the strong H-bonds that hold the dimer together (NH/NH in $(2\text{PY})_2$ and NH/OH in the

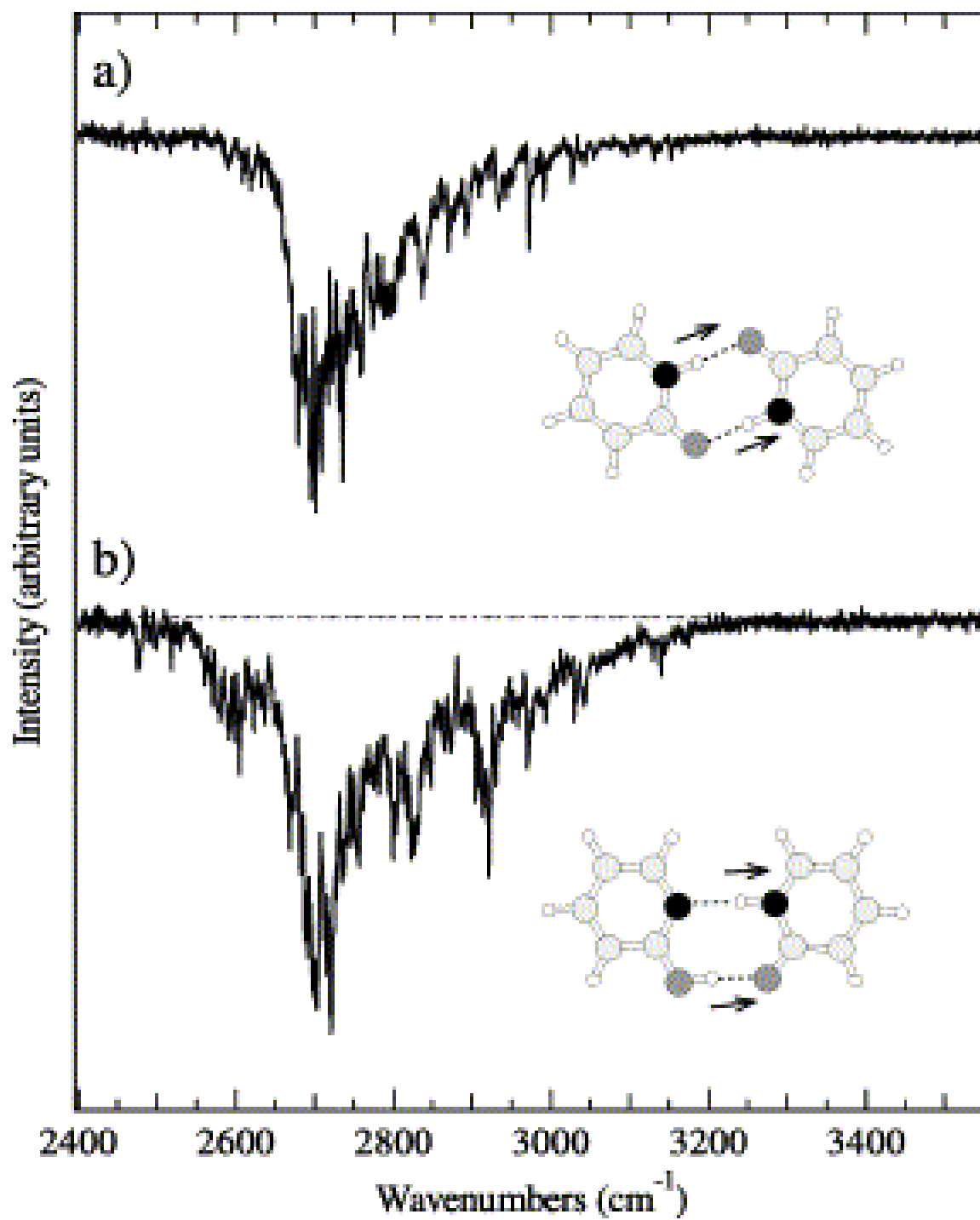


Figure 3.2. Ground state fluorescence-dip infrared spectra of (a) $(2\text{PY})_2$ and (b) $2\text{PY}\cdot 2\text{HP}$ dimers in the hydride stretch region of the infrared.

2PY·2HP dimer).

Not surprisingly, several of the most obvious features of the spectrum of the 2PY·2HP dimer (Fig. 3.2(b)) closely resemble those of the 2PY dimer above it (Fig. 3.2(a)). First, the spectrum is extremely broad, with absorption intensity spread over almost 500 cm^{-1} . Second, the band maximum of Fig. 3.2(b) occurs at about 2700 cm^{-1} , corresponding to frequency shifts of about 750 cm^{-1} from the NH stretch fundamental of the 2PY monomer (3448 cm^{-1}) and 900 cm^{-1} from the OH stretch fundamental of the 2HP monomer (3598 cm^{-1}). Third, the XH stretch band exhibits dense, reproducible sub-structure with an average spacing of some $5\text{--}10\text{ cm}^{-1}$. Finally, the transition is unusually intense, with integrated absorption intensity that is easily a factor of 50 greater than that of either monomer's XH stretch fundamental.

All these shared features in the infrared spectra of Fig. 3.2 reflect the strong, cooperatively strengthened hydrogen bonds present in both dimers. In the $(2\text{PY})_2$ dimer, a single NH stretch infrared fundamental carries the oscillator strength of the entire band. The two equivalent NH bonds are coupled to one another, forming NH stretch normal modes of a_g and b_u symmetry. In the former, the two NH bonds stretch in-phase with one another (*i.e.*, both bonds stretch simultaneously) while in the latter, one NH bond stretches while the other contracts, as shown in the inset of Fig. 3.2(a). The b_u symmetry fundamental is IR allowed, while the lower frequency a_g mode is forbidden. The splitting between the b_u and a_g fundamentals is calculated to be 59 cm^{-1} . Matsuda, *et al.* [4] observed the a_g fundamental at 2600 cm^{-1} in the Raman spectrum, about 100 cm^{-1} below the IR maximum in Fig. 3.2(a).

In contrast, in the 2PY·2HP mixed dimer, the NH and OH groups are

inequivalent, although they are still strongly coupled to one another. Thus, the calculated harmonic vibrational frequencies and infrared intensities for the mixed dimer show an intense band due to the out-of-phase oscillation of the two XH groups, but also show weak intensity in the lower frequency 'in-phase' band. A closer comparison of the spectra of Fig. 3.2(a) and (b) shows that there is a weak band on the low frequency side of the main band in the mixed dimer's spectrum at $\sim 2600\text{ cm}^{-1}$ (Fig. 3.2(b)) that is not present in the 2PY dimer spectrum above it. We tentatively assign this sideband to the weakly allowed in-phase XH stretch fundamental.

The breadth and sub-structure of the spectrum results from the strong, anharmonic coupling of the XH stretch vibration(s) with background states that spreads the XH stretch oscillator strength over a host of bands spanning more than 500 cm^{-1} . Recent theoretical analyses of the IR spectra of benzoic acid [19] and formic acid dimers [20] indicates that, in these cases, the dominant anharmonic term is a 2:1 Fermi resonance of the XH stretch(es) with the overtones and combinations of the XH bend(s). However, there is no 'pure' XH bending vibration in these dimers. Some 15–20 combination bands spread over the $2500\text{--}3000\text{ cm}^{-1}$ region possess some degree of XH bend character, and thereby gain intensity through the 2:1 Fermi resonance. The large cubic anharmonic constant ($\sim 370\text{ cm}^{-1}$) spreads the intensity over almost 500 cm^{-1} . Second tier couplings split the bands still further, leading to the observed, dense sub-structure. A similar behavior has been observed in other molecules containing H-bonded bridges across *cis*-amide groups [21].

3.3.2 Excited state fluorescence-dip infrared spectra

The S_2 state FDIR spectrum of $(2PY)_2$ and the S_1 state FDIR spectrum of the $2PY \cdot 2HP$ dimer are shown in Fig. 3.3(a) and (b), respectively. The two spectra are very different from each other, and from the corresponding ground state spectra. That for the $2PY$ dimer was recorded with the UV pulse (at $30\,776\text{ cm}^{-1}$) preceding the IR pulse by 19 ns and is similar in appearance to that reported by Matsuda, *et al.* [4]. In the excited state spectrum, the XH stretch absorption maximum is shifted to higher frequency by $\sim 260\text{ cm}^{-1}$ relative to the ground state maximum at $\sim 2700\text{ cm}^{-1}$. At the same time, the width of the band decreases from more than 500 cm^{-1} in S_0 to less than 300 cm^{-1} in S_2 .

The corresponding spectrum of the S_1 state of the $2PY \cdot 2HP$ dimer, recorded with the UV pulse preceding the IR by 24 ns, shows an even larger change upon electronic excitation. The dominant peak in the spectrum is shifted about 440 cm^{-1} to higher frequency in the excited state (3135 cm^{-1}) than it is in the ground state (2700 cm^{-1}). At the same time, the band sharpens still further to only 40 cm^{-1} full width at half maximum. Both these features point to a substantial weakening of one or both hydrogen bonds upon electronic excitation. A further interpretation of the spectrum of Fig. 3.3(b) will be taken up after the high resolution spectrum of the mixed dimer has been considered.

3.3.3 High resolution electronic spectroscopy of the S_1-S_0 origin

Fig. 3.4 shows the S_1-S_0 fluorescence excitation spectrum of the mixed $(2PY \cdot 2HP)$ dimer band (at $30\,656\text{ cm}^{-1}$) at high resolution. The band spans $\sim 3\text{ cm}^{-1}$ and contains thousands of lines, each exhibiting widths of order 100 MHz or less. (The homogeneous width expected from the measured fluorescence lifetime is $\sim 12\text{ MHz}$.) The

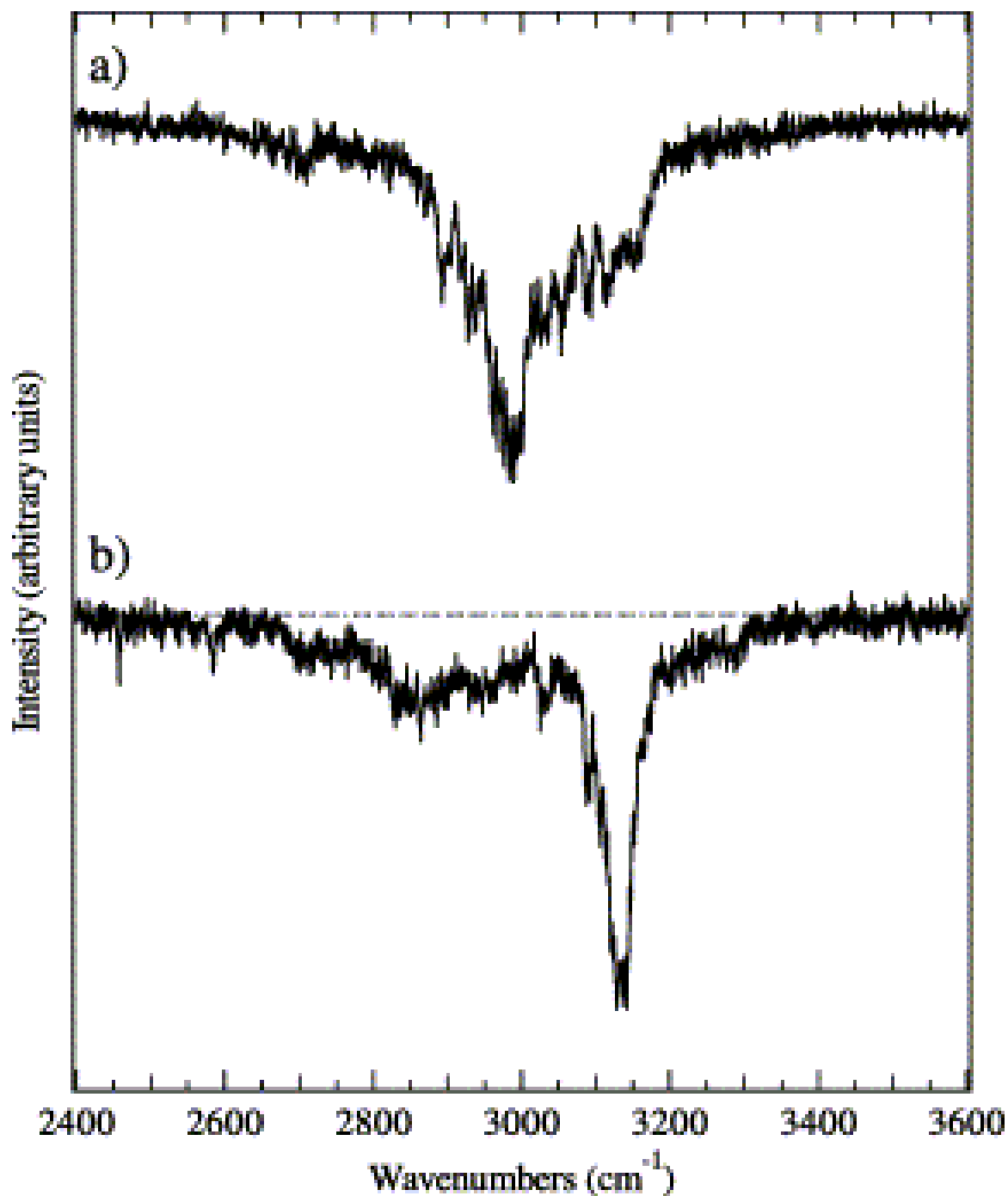


Figure 3.3. Fluorescence-dip infrared spectra of the electronically excited dimers: (a) spectrum of $(2PY)_2$ recorded while monitoring fluorescence from its S_2 electronic origin at $30\,776\text{ cm}^{-1}$; (b) spectrum of $2PY\cdot 2HP$ recorded while monitoring fluorescence from its S_1 electronic origin at $30\,656\text{ cm}^{-1}$. The delay between the UV excitation laser and the IR depletion laser is 19 ns in (a) and 24 ns in (b).

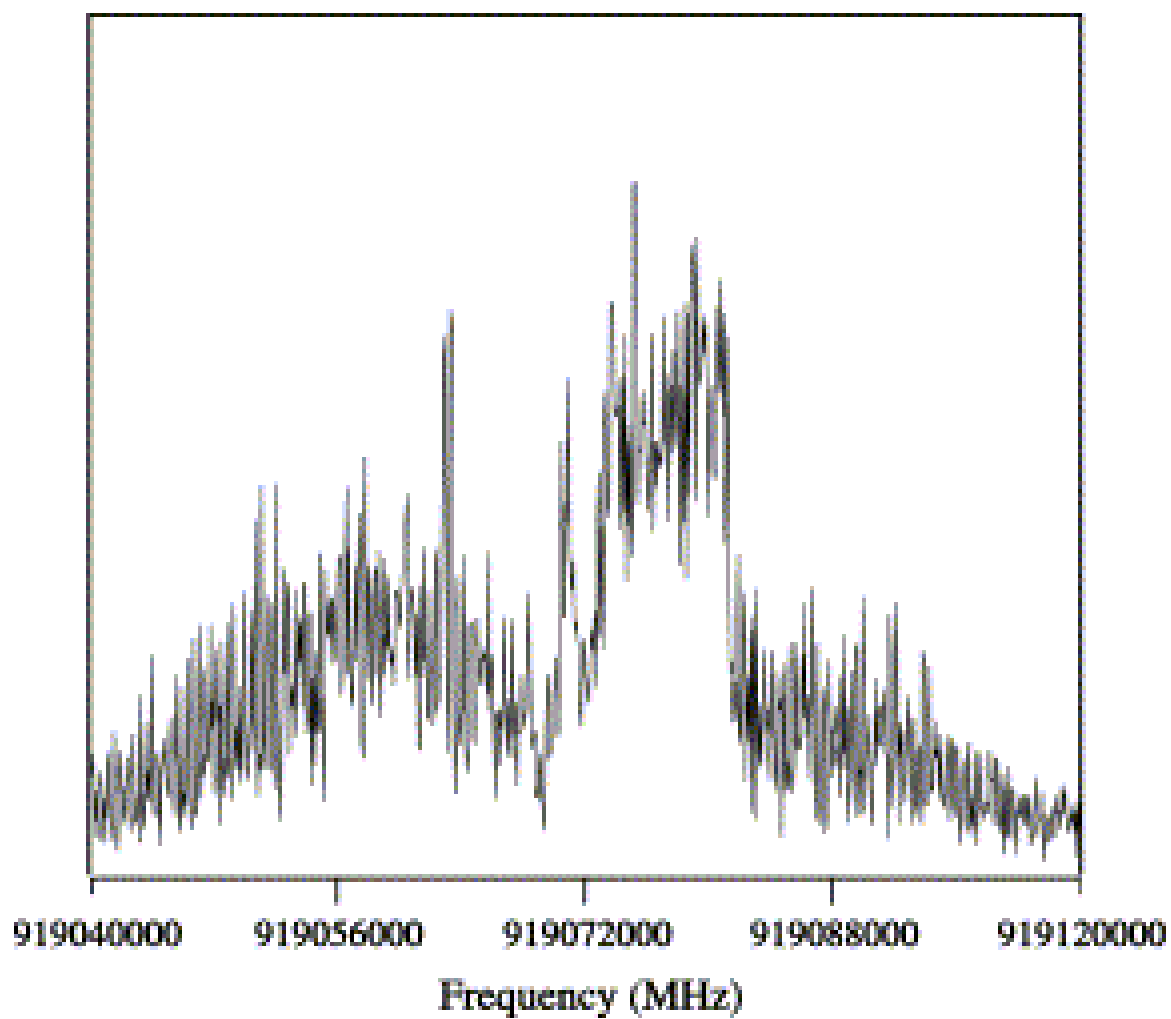
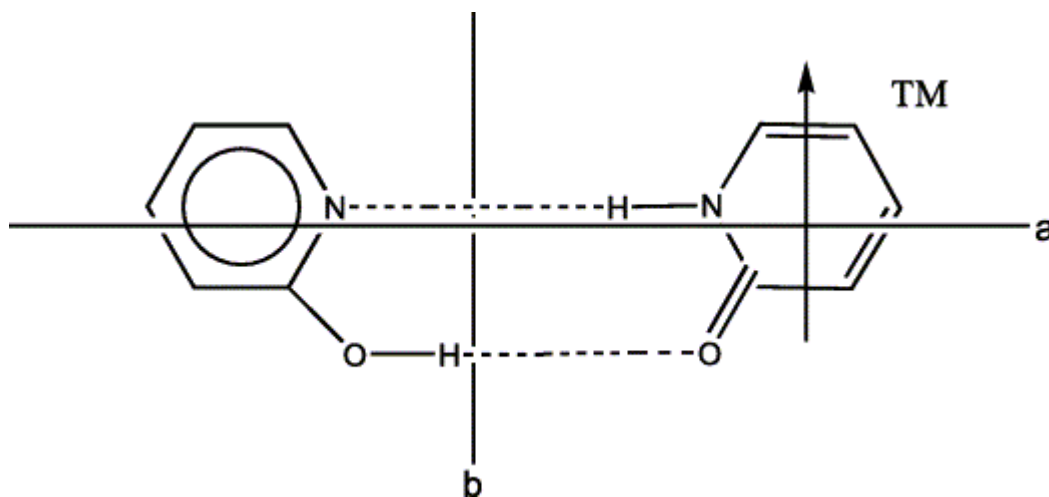


Figure 3.4. High resolution fluorescence excitation spectrum of the 2PY·2HP dimer at its S_1 - S_0 origin ($30\,656\text{ cm}^{-1}$).

severe congestion of the spectrum has so far precluded a conventional fit. Individual lines have not been assigned to unique transitions between lower and upper state rovibronic levels because they could not be identified. However, valuable information has been extracted from an approximate analysis of the spectrum.

The spectrum in Fig. 3.4 exhibits primarily *b*-type transitions. It also exhibits a small amount of *a*-type character in the strong, central Q-branch region of the spectrum. The relative intensities of these two types of transitions give an estimate of the angle between the optical transition moment and the *b* inertial axis of $\theta_{\text{TM}} = 8^\circ \pm 3^\circ$. Now, the S_1 - S_0 TM in 2PY itself makes an angle of -51° with respect to its *a* axis [2]. The corresponding TM in 2HP makes an angle of $\pm 60^\circ$ with respect to its *a* axis [22]. If the S_1 - S_0 excitation in the mixed 2PY·2HP dimer is largely localized on the 2PY fragment, as we anticipate from the close proximity of the band to the S_1 - S_0 origin of 2PY monomer, then we would expect its TM to lie near the dimer *b* axis, as observed. This observation provides independent confirmation of the assignment of this band to the 2PY·2HP mixed dimer.



An approximate fit of the spectrum in Fig. 3.4 was obtained using a procedure

developed by Remmers, *et al.* [13] in their analysis of the incompletely resolved electronic spectrum of the benzoic acid dimer. First, theoretical values of rotational constants of the ground state of the 2PY·2HP dimer were calculated using DFT methods (*vide infra*). These are listed in Table 3.1. Then, a simulated spectrum was generated using the determined value of θ_{TM} , assuming identical constants for the S_1 state. Next, these constants were adjusted to provide the best match with the overall appearance of the experimental spectrum, using derivatives calculated with the aid of the Hellman–Feynman theorem. Finally, the ground state constants were adjusted, while keeping the differences in these constants between the two states fixed, in order to determine an approximate range of values for which a reasonable match to the spectrum could be made. These results are also listed in Table 3.1.

Finally, a further examination of the spectrum in Fig. 3.4 revealed that all of the stronger transitions are accompanied by a second transition at regular intervals. This suggests that the 2PY·2HP dimer band at $30\,656\text{ cm}^{-1}$ consists of two sub-bands. An autocorrelation analysis [23] was performed to measure the separation of the two sub-bands. This analysis is shown in Fig. 3.5. The distinct features on either side of the maximum at the origin indicate that two sub-spectra are present in Fig. 3.4, displaced by $520 \pm 10\text{ MHz}$. As will be seen, this splitting has its origin in a tunneling motion, in either the ground state or the excited state of 2PY·2HP. A potential candidate for the tunneling motion is the double proton transfer associated with the $2\text{PY}\cdot 2\text{HP} \rightleftharpoons 2\text{HP}\cdot 2\text{PY}$ tautomerization.

Table 3.1. Approximate rotational constants (in MHz) of the 2PY·2HP dimer of 2-hydroxypyridine in its S_0 and S_1 electronic states, compared to Hartree–Fock and density functional theoretical values

State	A	B	C
S_0 (exp.)	1707 (15) ^a	327 (5)	274 (5)
S_0 : SCF/6-31G(d,p)	[1717.35]	[328.55]	[275.68]
S_0 : B3LYP/6-311++G(d,p)	[1671.09]	[341.66]	[283.66]
S_1 (exp.) ^b	1662 (5)	327 (3)	374 (3)
S_1 : CIS/6-31G(d,p)	[1718.66]	[322.31]	[271.61]
S_1 - S_0	-45 (5)	0 (3)	0 (3)
CIS-SCF	[+5.3]	[-6.2]	[-4.1]

^a Uncertainties in parentheses.

^b Origin at 30657.08(2) cm^{-1} .

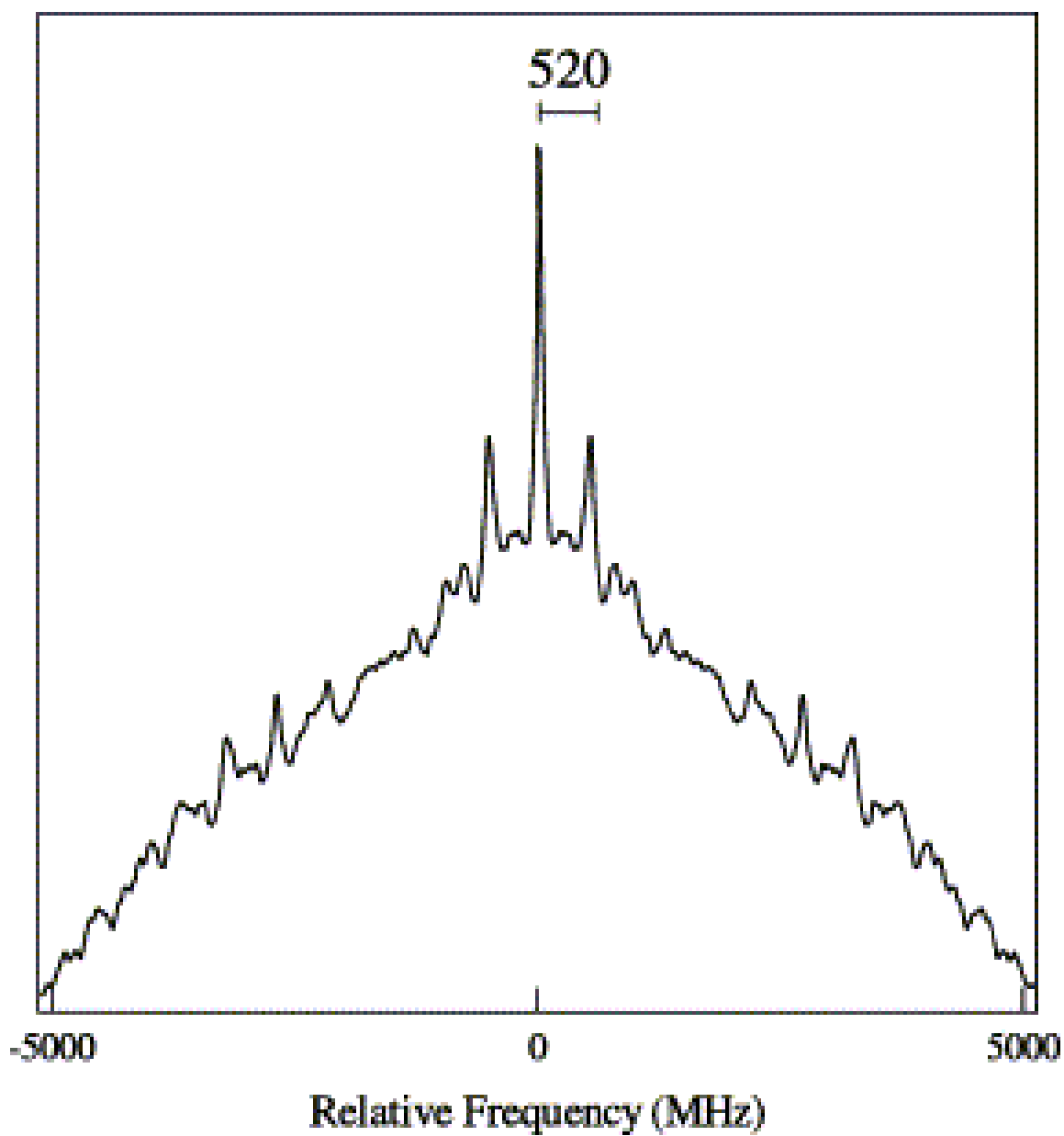


Figure 3.5. Autocorrelation spectrum of the band in Fig. 3.4. The side bands at ± 520 MHz indicate the presence of two bands in the spectrum, split by 520 MHz.

3.3.4 Calculated structure of 2PY·2HP in the ground state

The DFT B3LYP/6-311++G(d,p) calculations predict a ground state structure for the 2PY·2HP dimer that is planar, with rotational constants that are in good agreement with experiment (cf. Table 3.1). According to theory, the 2PY·2HP dimer has heavy atom separations of 2.646 Å (OH...O) and 2.915 Å (NH...N). The corresponding NH...O separations in the (2PY)₂ dimer are 2.78 Å, in very good agreement with the experimental value of 2.77 ± 0.03 Å [10]. Thus, the principal difference between the structures of the 2PY·2HP and (2PY)₂ dimers is that the OH...O and NH...N bonds in 2PY·2HP are about 0.12 Å shorter and 0.15 Å longer, respectively, than the NH...O bonds in (2PY)₂.

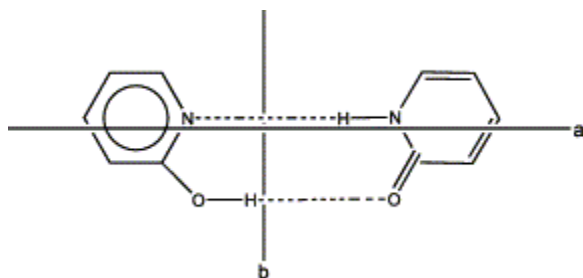
3.4 DISCUSSION

The experimental data presented in the previous section provide two complementary views of the effect of electronic excitation on the hydrogen bonding and tunneling in the 2PY·2HP mixed dimer. The high resolution spectrum of the S₁–S₀ origin transition provides new information about the structural changes that accompany electronic excitation and the hydrogen atom tunneling process. On the other hand, the S₀ and S₁ state FDIR data probe the hydrogen bonding in the two states *via* the response of the hydride stretch vibrations to electronic excitation.

The most obvious effect of electronic excitation is a decrease in the binding energy of the dimer. The 0₀⁰ band of the S₁–S₀ transition of 2PY·2HP is blue-shifted by 825 cm⁻¹ from the "A" 0₀⁰ band of the 2PY monomer at 29 831 cm⁻¹ [1, 2]. This amounts

to a decrease in binding energy of 2.36 kcal/mol upon electronic excitation. Müller, *et al.* [12] have carried out DFT B3LYP calculations which predict a ground state binding energy of 13.6 kcal/mol. Thus electronic excitation weakens the total binding of the dimer by about 20%, but how this decrease is distributed between the $\text{NH}\cdots\text{N}$ and $\text{OH}\cdots\text{O}$ hydrogen bonds that hold the dimer together is not clear from the electronic frequency shift alone.

More information about the structure of the 2PY·2HP dimer in its S_1 state is provided by the change in its rotational constants upon electronic excitation. The A rotational constant decreases by ~ 45 MHz in going from S_0 to S_1 , whereas the B and C rotational constants remain approximately the same (*cf.* Table 3.1). As shown in the structure below,



the B rotational constant is most sensitive to mass displacements along the line joining the centers-of-mass of the two monomers, whereas the A rotational constant is most sensitive to displacements perpendicular to this axis. The observed photoinduced changes in rotational constants thus suggest that, while there is little change in the radial separation of the two centers-of-mass, there is a displacement of one unit with respect to the other along an in-plane angular coordinate.

More specific information about the magnitudes of these effects can be obtained

in the following way. Suppose we attribute the observed changes in the rotational constants to changes in only the intermolecular bond distances, ignoring possible changes in the geometries of the monomer units themselves. This leads to estimated heavy atom separations of 3.073 Å for the OH...O hydrogen bond and 3.081 Å for the NH...N hydrogen bond in the S_1 state. Comparing these distances to the theoretical values for the ground state, we see that the OH...O hydrogen bond length increases by ~ 0.3 Å when the photon is absorbed, whereas the NH...N hydrogen bond length increases by only ~ 0.1 Å. The two bonds weaken on electronic excitation. But the decrease in the OH...O bond strength is substantially larger than the decrease in the NH...N bond strength, thereby accounting for the angular displacement of one unit with respect to the other.

This model quite evidently overestimates the magnitude of the geometry change in the OH...O hydrogen bond. Nevertheless, its qualitative prediction is in excellent agreement with the calculations and the vibronic spectroscopy of Müller, *et al.* [12]. These authors have carried out CIS calculations on the mixed dimer which predict an increase in the OH...O heavy atom separation of 0.06 Å, but a negligible (0.01 Å) change in the NH...N separation on S_1 excitation.

The asymmetric motion of the two monomers upon electronic excitation, in which the OH...O hydrogen bond lengthens while the NH...N hydrogen bond does not, would seem most closely related to the ν_3 'cogwheel' or 'opening' intermolecular vibration, calculated at 87 cm^{-1} [12]. However, the vibronic spectrum shows a dominant Franck-Condon progression in a mode with 158 cm^{-1} frequency, assigned by Müller, *et al.* [12] to the intermolecular stretch, ν_6 , with a calculated value of 156 cm^{-1} . At the same time, there is no evidence for a progression in the cogwheel mode ν_3 . Fig. 3.6 shows the form of the

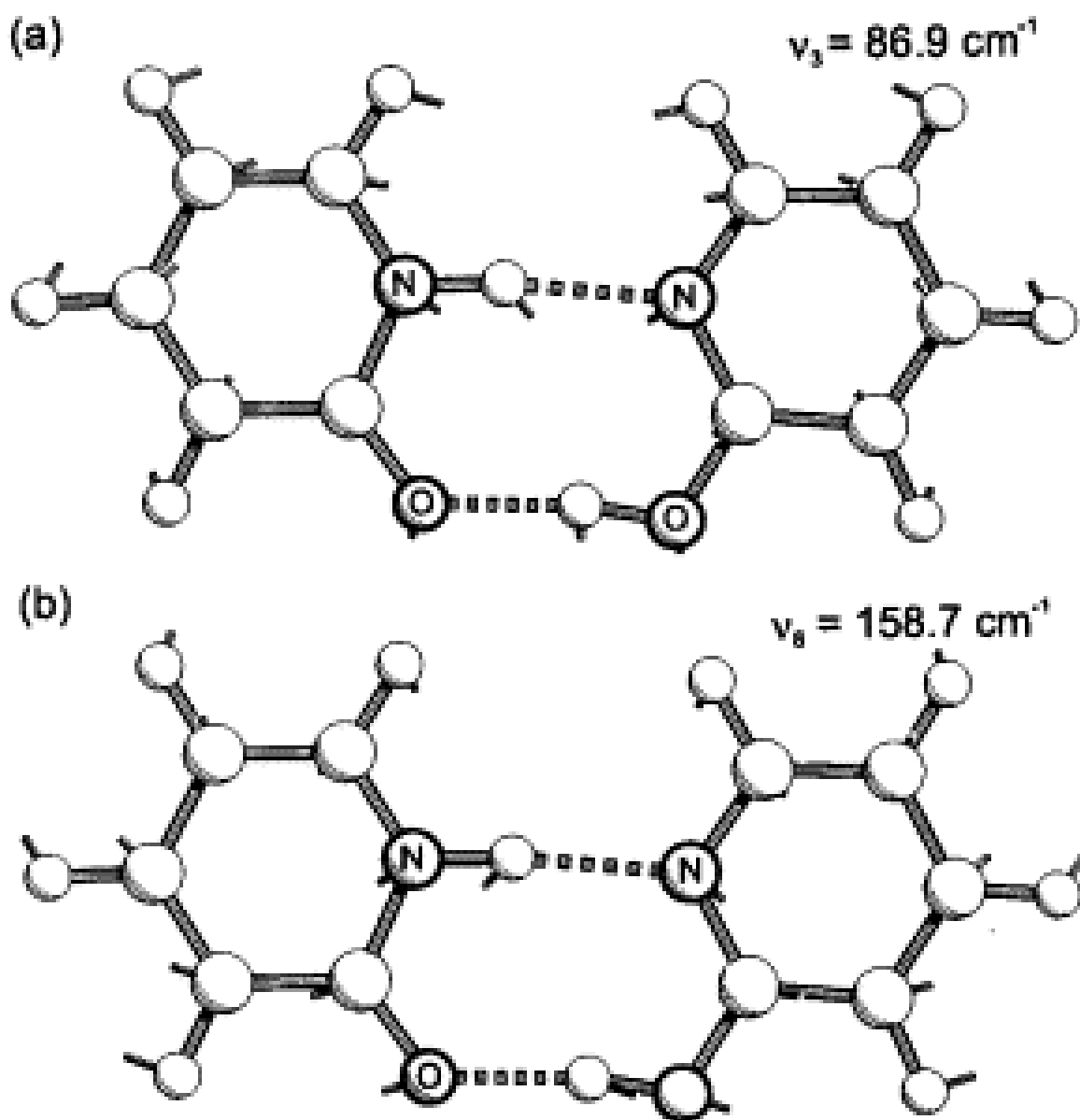


Figure 3.6. Intermolecular normal mode eigenvectors for the ν_3 'cogwheel' and ν_6 'intermolecular stretch' vibrations, taken from the DFT B3LYP/6-311++G(d,p) calculation.

`cogwheel' and `intermolecular stretch' normal modes from the DFT B3LYP calculation.

Close inspection of these normal modes reveals that they are both mixtures of stretch and cogwheel motions, as noted by Müller, *et al.* [12]. Furthermore, the OH...O separation is changed substantially by the intermolecular stretch motion, but hardly at all by the cogwheel mode. Thus, the nature of the geometry change deduced from the rotational analysis is at least qualitatively consistent with the Franck–Condon analysis based on the intermolecular motions from Müller, *et al.* [12].

3.4.1 Changes in H-bonding from the infrared spectra

These structural deductions provide a foundation for a proper interpretation of the S_1 state FDIR spectrum. Fig. 3.7 makes a direct comparison between the ground state and excited state infrared spectra of 2PY·2HP.

In the ground electronic state, the OH...O and NH...N hydrogen bonds are both strong, and the OH and NH oscillations are strongly coupled to one another, as shown schematically in Fig. 3.7(a). The higher frequency mode is similar to the corresponding b_u symmetry fundamental in $(2PY)_2$, shown in Fig. 3.2(a), and carries most of the oscillator strength of the entire band. The lower frequency band, which correlates with the a_g symmetry fundamental in $(2PY)_2$, gains some oscillator strength due to the asymmetry of the 2PY·2HP mixed dimer, producing the weak band near 2600 cm^{-1} .

In the S_1 state (Fig. 3.7(b)), the weakening of the OH...O hydrogen bond leads to a reduced coupling between the OH and NH bonds, making them more nearly local OH and NH stretches. The lengthening of the OH...O hydrogen bond upon electronic excitation then leads to an assignment of the intense band near 3140 cm^{-1} to the OH

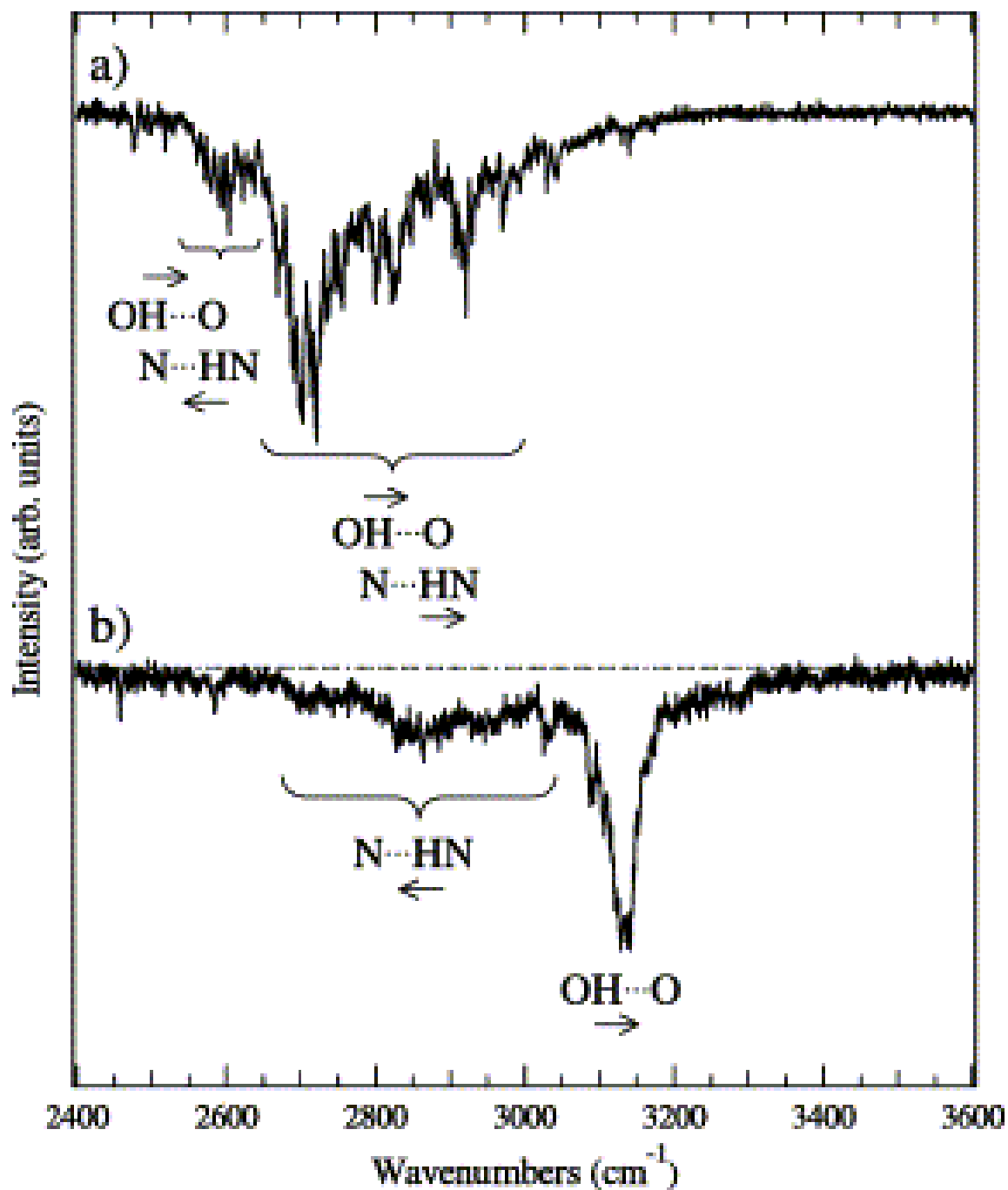


Figure 3.7. A direct comparison of the (a) S_0 and (b) S_1 state FDIR spectra of the 2PY·2HP dimer. Note the dramatic shift of the intense absorption to higher frequency in the electronically excited state. Proposed assignments are given on the absorptions.

stretch of the OH...O group, while the broad, less intense absorption over the 2800–3000 cm^{-1} region is assigned to the NH stretch of the NH...N group. If we estimate the frequencies of the uncoupled NH and OH groups in the ground state to be 2650 cm^{-1} (the average of the two observed frequencies at 2600 and 2700 cm^{-1}), then the S_1 state OH stretch is shifted to higher frequency by almost 500 cm^{-1} , while the NH stretch is also weakened, but by a much smaller amount ($\sim 250 \text{ cm}^{-1}$).

In point of fact, we do not know quantitatively the extent to which the coupling between OH and NH stretches is reduced by electronic excitation. However, the proposed assignment of the S_1 spectrum in terms of local mode NH and OH oscillators is consistent with a similar assignment of the S_1 state hydride stretch infrared spectrum of $2\text{PY}\cdot(\text{H}_2\text{O})_1$ and $2\text{PY}\cdot(\text{H}_2\text{O})_2$ by Matsuda, *et al.* [4] and Zwier [24]. There, too, it is the OH...O hydrogen bond that appears to be weakened by the electronic excitation, while the NH...O hydrogen bond is hardly changed in frequency upon electronic excitation.

Additional insight into the origin of these effects is provided by theory. As noted, excitation of $2\text{PY}\cdot 2\text{HP}$ by light is largely confined to the 2PY "side" of the dimer. Therefore, it is appropriate to consider the MO's of 2PY itself when thinking about the nature of the S_1 – S_0 electronic transition in the $2\text{PY}\cdot 2\text{HP}$ dimer. CIS calculations [18] show that the S_1 – S_0 transition of 2PY consists mainly of a HOMO to LUMO excitation, leading to (a) a partial reversal of the bond order alternation in the ring, (b) an increase in electron density in the N–H bond, and (c) a decrease in electron density in the C=O bond. A reduced electron density in the C=O bond will, by simple electrostatic arguments, make it less attractive to the hydrogen atom of the OH group, reducing the strength of the OH...O bond. In agreement with this, our SCF/CIS calculations show that the structure of

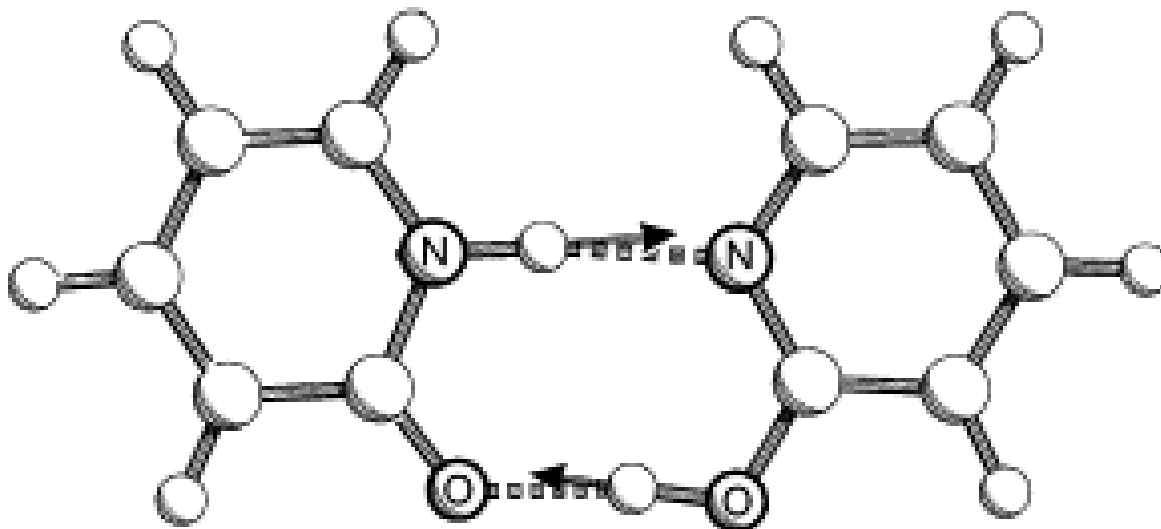
the 2HP side of the dimer is largely unaffected by S_1 excitation, except for a noticeable shortening of the OH bond. In contrast, the 2PY side of the dimer undergoes several structural changes, including changes in the ring bond lengths as large as 0.08 Å. Other calculations [25] support this view.

3.4.2 Tunneling

Having deduced the nature of the structural change accompanying electronic excitation, and the effect that this structural change has on the hydrogen bonding in the dimer, we return once again to the issue of the tunneling splitting observed in the electronic spectrum. The 2PY·2HP mixed dimer can undergo a double proton transfer in which the tautomeric state of the two monomers is interchanged. This results in a symmetric double minimum potential well and associated tunneling splitting in each electronic state. Unfortunately, the experimentally measured tunneling splitting supplies only the *difference* in tunneling splittings between ground and excited states, not the absolute magnitude of the tunneling splitting in either state.

In order to gain further insight to the anticipated magnitude of the tunneling splitting in the ground electronic state, *ab initio* calculations were carried out to determine the barrier height and structural changes associated with the ground state double proton transfer process. The doubly hydrogen bonded equilibrium structure (ground STATE=GS) was optimized at the Hartree–Fock/6-31G(d,p) level, and with the hybrid B3LYP DFT method using the 6-311++G(d,p) valence triple zeta basis set. With both methods, GS is planar (C_s symmetric), in agreement with experiment; the B3LYP GS structure is shown in Fig. 3.8(a). The SCF rotational constants are in excellent

(a) GS (C_s) $\nu_{57} = 3061 \text{ cm}^{-1}$



(b) TS (C_{2v}) $\nu_i = i1311 \text{ cm}^{-1}$

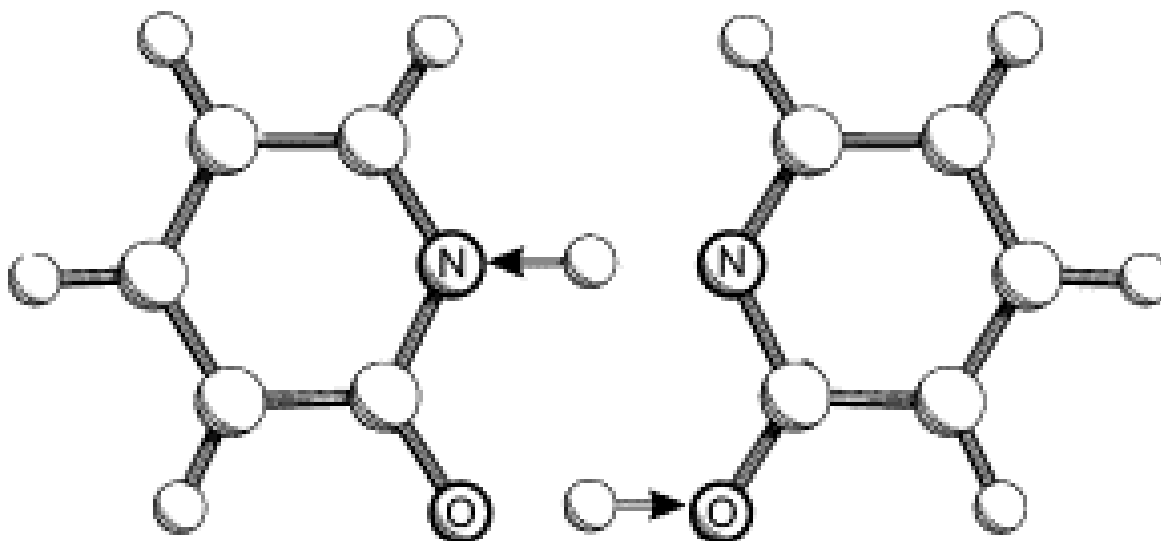


Figure 3.8. B3LYP/6-311++G(d,p) calculated (a) equilibrium structure (GS) with the vibrational eigenvector of the $\nu_{57}=3061 \text{ cm}^{-1}$ normal mode, which correlates most closely with a pure double proton transfer motion, and (b) transition structure (TS) for double proton transfer with the eigenvector corresponding to the imaginary frequency $i1311 \text{ cm}^{-1}$.

agreement with experiment, while those predicted by the B3LYP/6-311++G(d,p) method are slightly smaller for A and larger for B, C (*cf.* Table 3.1).

The suitability of different quantum chemical methods for calculating proton transfer potentials and surfaces has been widely discussed. Current evidence is that the HF method overestimates proton transfer barriers and that correlated methods such as MP2 or coupled cluster methods are necessary to obtain very accurate barriers [26, 27]. Relaxed MP2 calculations with large enough basis sets are prohibitive for a system with 14 second-row atoms. B3LYP calculations yield barriers of 60–80% of the MP2 barrier height with a substantially smaller computational effort [26–28]. Hence, we also used B3LYP/6-311++G(d,p) for the calculation of the double proton transfer transition state (=TS). We first displaced the 2PY N–H proton in steps of 0.05 Å towards the 2HP moiety, fully optimizing the 2PY·2HP geometry at each step. This leads to an asymmetric potential energy curve, since for large N–H distances the 2HP moiety is 'pushed away' from 2PY. The structure at the highest point of this PE curve was then further optimized to an index-1 saddle point by the QST2 procedure [18]. The TS structure is predicted to be planar and C_{2v} symmetric, as shown in Fig. 3.8(b). The finding of a single transition state for double proton transfer implies that the ground state proton transfer is *cooperative*.

During the proton transfer, both H bonds shorten considerably. The NH...N distance decreases by 0.33 Å from 2.91 to 2.58 Å and the OH...O distance decreases by 0.24 Å from 2.65 to 2.40 Å. Simultaneously, the N–H bond length increases from 1.04 to 1.29 Å and the O–H bond length increases from 1.00 to 1.20 Å.

The purely electronic barrier height, derived from the difference of B3LYP total

energies, is 8.334 kcal/mol (2915 cm⁻¹). More relevant is the *vibrationally adiabatic* barrier height, for which the zero-point vibrational energies of all normal modes except the double proton transfer mode are added to the electronic barrier height. For the TS, this mode is the single mode with imaginary frequency, i1311 cm⁻¹, shown in Fig. 3.8(b). For the GS, the choice of the double proton transfer mode as $\nu_{57}=3061$ cm⁻¹ was unequivocal, since this is the N–H/O–H stretching mode which is most similar to the TS proton transfer mode, as shown in Fig. 3.8(b). The other two N–H/O–H stretching modes (ν_{58} and ν_{59}) involve much smaller N–H/O–H and larger C–H displacements. The resulting vibrationally adiabatic barrier is 7.666 kcal/mol (2681 cm⁻¹).

The double proton transfer path length was calculated by first superimposing the centers of mass of the GS and TS structures and then minimizing the relative distances of the corresponding atoms of 2HP and 2PY in the GS and TS structures. The distance between GS and TS

$$R(\text{TS} - \text{GS}) = \left\{ \sum_{i=1}^{24} m_i \Delta r_i^2(\text{TS} - \text{GS}) \right\}^{1/2}$$

was calculated in mass-weighted Cartesian coordinates. Each individual distance, $\Delta r_i(\text{TS} - \text{GS})$ was approximated as a straight line, leading to a lower limit for the total mass-weighted distance, $R(\text{TS} - \text{GS}) = 2.21 \text{ u}^{1/2} \text{ \AA}$. It should be realized that the length of this path is determined by the motions of the 2HP and 2PY frames, since each C, N and O atom moves 0.2 to 0.35 Å during the double proton transfer, see above.

The resulting symmetric double minimum potential for the S₀ state is shown in Fig. 3.9.

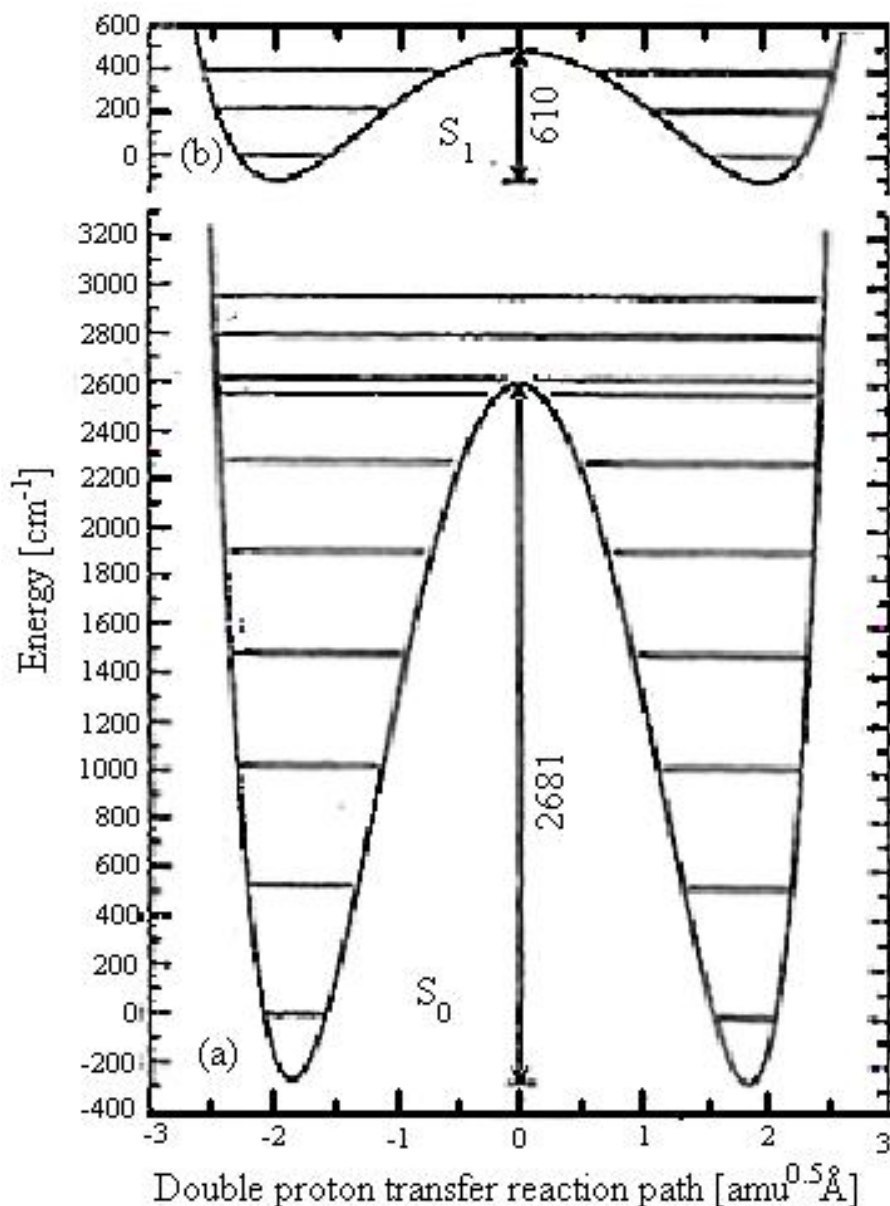


Figure 3.9. Calculated model potential for double proton transfer in the ground and electronically excited states of the 2PY·2HP dimer. (a) The barrier height in the ground state is the vibrationally adiabatic barrier of 2681 cm^{-1} calculated from the electronic and vibrational zero-point energies of GS and TS. The distance from GS to TS is in mass-weighted Cartesian coordinates. Tunneling splittings for $v=0-5$ are not visible on the scale of the figure. (b) The excited state double proton transfer potential was constructed by arbitrarily assuming the same $R(\text{TS-GS})$ distance as for the S_0 state; the barrier was lowered to 610 cm^{-1} so as to yield the observed tunneling splitting of 520 MHz (0.0173 cm^{-1}), also not visible in the figure.

The one-dimensional vibrational wave functions were calculated using a fourth-order Runge–Kutta method and are numerically precise to $<<10^{-6}$ cm $^{-1}$ (30 kHz). The calculated splitting between the symmetric and antisymmetric $0^+/0^-$ vibrational ground states is $<10^{-6}$ cm $^{-1}$, much smaller than the observed splitting of 0.017 cm $^{-1}$. A higher level electronic calculation (MP2) would probably raise the barrier by an estimated 20–40%. A more quantitative evaluation of the double proton transfer path length $R(\text{TS-GS})$ in curvilinear coordinates and including counter-rotations of the 2HP and 2PY sub-units would increase the distance between GS and TS even further. It follows that the model potential in Fig. 3.9(a) leads to an *upper limit* for the tunneling splitting. We conclude that, if the observed tunneling splitting arises from the double proton transfer reaction, it must be due to tunneling in the S_1 excited state rather than the ground electronic state.

How much lower must the S_1 state barrier be to yield the observed tunneling splitting? For simplicity, we fixed $R(\text{TS-GS})$ at the S_0 state value, although it must increase, as the rotational analysis (*vide supra*) and the Franck–Condon analysis [14] have shown. Simple scaling of the barrier height to 610 cm $^{-1}$ (1.74 kcal/mol) yielded the observed 520 MHz splitting. The resulting potential and the lowest three pairs of vibrations are shown in Fig. 3.9(b).

Before leaving the issue of tunneling, an alternative source of the tunneling splitting should be briefly considered. The CIS calculations of Müller, *et al.* [12] predict that the 2PY monomer in the mixed dimer is slightly non-planar (pyramidal) about the N atom, with a 10 cm $^{-1}$ barrier for interconversion between the two pyramidal structure. This gives rise to a double minimum potential well for interconversion between the two equivalent non-planar minima, with a tunneling splitting between 0^+ and 0^- levels.

However, the ground state dimer is planar, with a zero-point level which is symmetric about the planar configuration (0^+). Transitions from this level will be only to the 0^+ excited state level, and cannot explain the tunneling splitting observed.

3.5 CONCLUSIONS

Combined data from high resolution electronic spectroscopy and S_0 and S_1 state infrared spectroscopy experiments have led to a more complete picture of the changes in hydrogen bonding that accompany electronic excitation in the mixed 2PY·2HP dimer. The dominant change involves a significant weakening of the OH...O hydrogen bond in S_1 compared to S_0 , perhaps accompanied by a smaller weakening of the NH...N hydrogen bond. That the former bond strength, rather than the latter, is principally affected by the absorption of a photon may be traced to the localization of the optical excitation on the 2PY side of the molecule.

The 2PY·2HP dimer has also been shown to be a paradigm system for photoinduced double proton transfer in DNA base pairs. In the ground state, the double proton transfer, leading to cooperative tautomerization, is calculated to occur on a relaxed potential having a relatively high barrier of ≈ 8 kcal/mol, leading to a predicted tunneling splitting of $<10^{-6}$ cm $^{-1}$. Given the calculated ground state structure and the changes between the S_0 and S_1 states that can be inferred from experiment, the observed tunneling splitting of 520 ± 10 MHz can only be interpreted as a cooperative double proton transfer if the S_1 state has the relatively low barrier for double transfer of ≈ 1 kcal/mol. Such a tunneling process is intriguing because it involves both nuclear motion and simultaneous

hopping of the electronic excitation between the two molecules. High resolution scans of deuterated isotopomers ultimately will be needed to probe the excited state tunneling in greater detail. Such scans are currently being pursued.

3.6 ACKNOWLEDGEMENTS

G.M.F. wishes to thank her Pittsburgh hosts for their hospitality during her research visit. This work has been supported by NSF (CHE-9728636 and CHE-9987048) and the Schweiz. Nationalfonds (Project 2000-61890).

3.7 REFERENCES

1. M.R. Nimlos, D.F. Kelley, E.R. Bernstein, J. Chem. Phys. 93 (1989) 643.
2. A. Held, B.B. Champagne, D.W. Pratt, J. Chem. Phys. 95 (1991) 8372.
3. L.D. Hatherly, R.D. Brown, P.D. Godfrey, A.P. Pierlot, W. Caminati, D. Damiani, S. Melandri, L.B. Favero, J. Chem. Phys. 97 (1993) 46.
4. Y. Matsuda, T. Ebata, N. Mikami, J. Chem. Phys. 110 (1999) 8397.
5. G.M. Florio, C.J. Gruenloh, R.C. Quimpo, T.S. Zwier, J. Chem. Phys. 113 (2000) 11143.
6. V. Barone, C. Adamo, J. Chem. Phys. 99 (1995) 15062.
7. A. Held, D.W. Pratt, J. Am. Chem. Soc. 115 (1993) 9708.
8. A. Held, D.W. Pratt, J. Am. Chem. Soc. 115 (1993) 9718.
9. A. Held, D.W. Pratt, J. Am. Chem. Soc. 112 (1990) 8629.
10. A. Held, D.W. Pratt, J. Chem. Phys. 96 (1992) 4869.
11. A. Meuller, F. Talbot, S. Leutwyler, J. Chem. Phys. 112 (2000) 3717.
12. A. Meuller, F. Talbot, S. Leutwyler, J. Chem. Phys. 115 (2001) 5192.
13. K. Remmers, W.L. Meerts, I. Ozier, J. Chem. Phys. 112 (2000) 10890.
14. L. Stryer, in: Biochemistry, fourth ed., W.H. Freeman & Co, New York, 1995, p. 809.
15. J.R. Johnson, K.D. Jordan, D.F. Plusquellic, D.W. Pratt, J. Chem. Phys. 93 (1990) 2258.
16. T.S. Zwier, Annu. Rev. Phys. Chem. 47 (1996) 205.
17. W.A. Majewski, J.F. Pfanstiel, D.F. Plusquellic, D.W. Pratt, in: A.B. Myers, T.R. Rizzo (Eds.), *Laser Techniques in Chemistry*, Wiley, New York, 1995, p. 101.
18. M.J. Frisch *et al.*, Gaussian 98 (Revision A.7), Gaussian Inc, Pittsburgh, PA, 1998.
19. G.M. Florio, E.L. Sibert III, T.S. Zwier, Faraday Discuss. 118 (2001) 315.
20. E.L. Sibert III, K.D. Jordan, G.M. Florio, T.S. Zwier, in preparation.

21. J.R. Carney, A.V. Fedorov, J.R. Cable, T.S. Zwier, J. Phys. Chem. A 105 (2001) 3487.
22. D.R. Borst, J.R. Roscioli, D.W. Pratt, J. Phys. Chem. A 106 (2002) 4022.
23. R.M. Helm, H.-P. Vogel, H.J. Neusser, Chem. Phys. Lett. 270 (1997) 285.
24. T.S. Zwier, J. Phys. Chem. 105A (2001) 8827.
25. P.-T. Chou, C.-Y. Wei, F.-T. Hung, J. Phys. Chem. 101B (1997) 9119.
26. S. Sadukhan, D. Munoz, C. Adamo, G.E. Scuseria, Chem. Phys. Lett. 306 (1999) 83.
27. M. Meuwly, A. Bach, S. Leutwyler, J. Am. Chem. Soc. 123 (2001) 11446.
28. T. Loerting, K.R. Liedl, B.M. Rode, J. Chem. Phys. 109 (1998) 2672.

4.0 Tunneling in the 2-hydroxypyridine/2-pyridone dimer. Effects of deuterium substitution on tunneling frequencies.

Joseph R. Roscioli and David W. Pratt

Department of Chemistry, University of Pittsburgh
Pittsburgh, PA 15260 USA.

Work in progress.

4.1 INTRODUCTION

The following are results and discussions from recent data obtained by high-resolution electronic spectroscopy regarding the nature of the proton tunneling observed in the 2HP/2PY dimer. The dimer was deuterated at one or both of the active hydrogens and the high-resolution electronic spectrum was obtained. Preliminary conclusions are made regarding the meaning of such transfers, as they pertain to the data discussed in chapter 3.

4.2 RESULTS

The low-resolution vibronic spectrum of protonated 2HP/2PY is shown in figure 3.1, with an electronic origin of $30,656\text{cm}^{-1}$. Upon partial deuteration of the sample, the origin splits into 4 peaks, indicating that there are two exchangeable hydrogens in the species, representing 2HP/2PY, 2HPd/2PY, 2HP/2PYd, and 2HPd/2PYd. The high-resolution spectrum of the protonated species is shown in figure 4.1, exhibiting a 527 MHz tunneling splitting. Because of the low vapor pressure of the dimer, high temperatures were required to vaporize enough sample to obtain a spectrum. Consequently, the rotational temperature of this spectrum is ~ 10 K, creating over 20,000 observed transitions. In addition, because of the tunneling splitting, the number of transitions is exactly doubled, resulting in over 40,000 observed transitions.

The large number of transitions, along with the small width of the spectrum ($\sim 2\text{cm}^{-1}$) and a resolution of 38 MHz make most of the transitions overlap. This

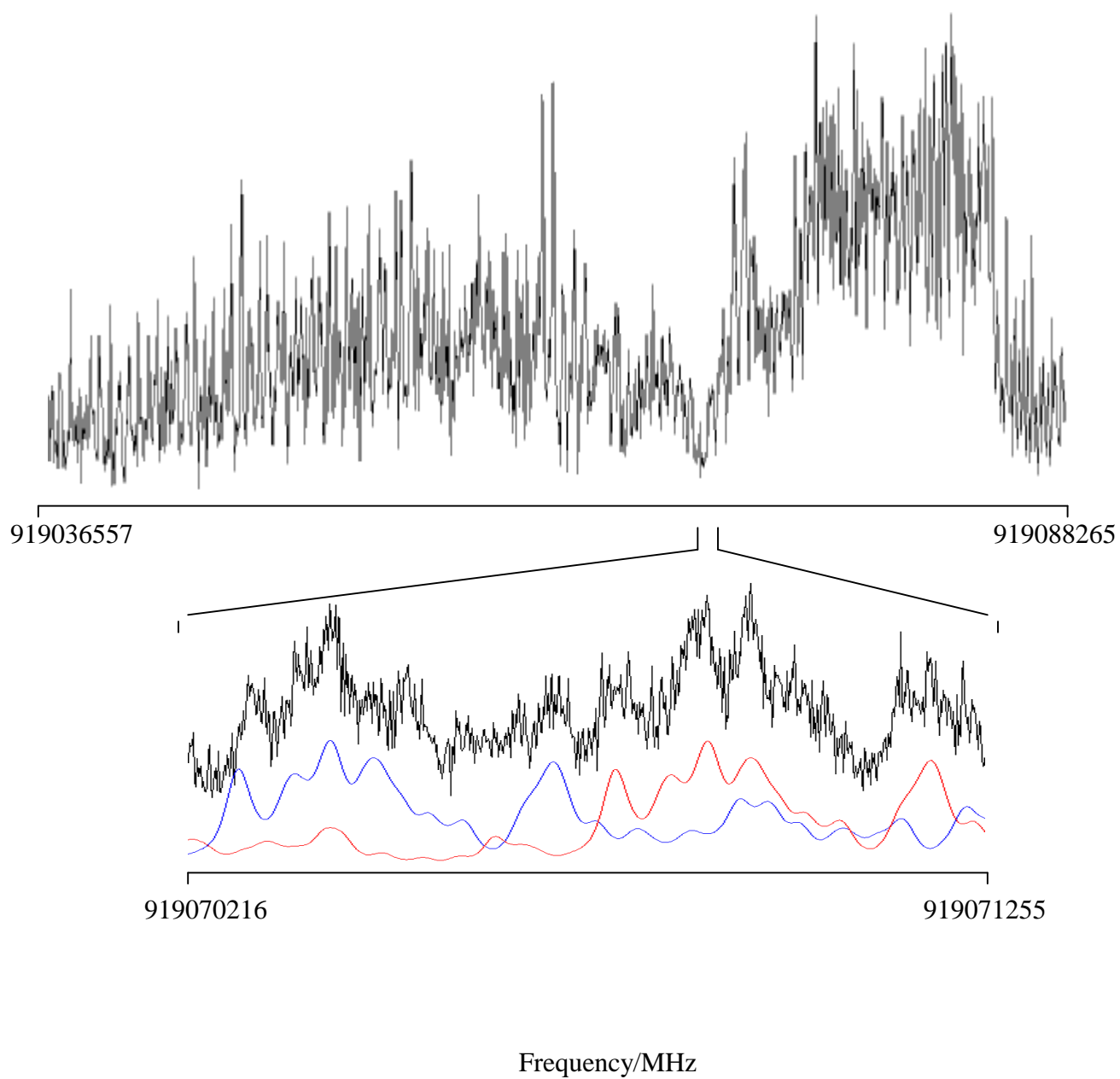


Figure 4.1. The fit, high resolution electronic spectrum of the 2HP/2PY dimer. The spectrum could only be fit by two simulations, shown below the experimental trace, split by 527 MHz. (see Figure 3.5, p. 60).

congestion made a traditional fit of the spectrum prohibitively difficult.

In an attempt to solve this problem, and also to shed light on the tunneling dynamics in the 2HP/2PY dimer, similar high resolution experiments were performed on the deuterated species: 2HPd/2PY, 2HP/2PYd, and 2HPd/2PYd. Typical results are shown in Fig. 4.2 a), b), and c), respectively. Examining these in detail, we see from Figs. 4.2 b) and c) that neither 2HP/2PYd nor 2HPd/2PYd exhibit a tunneling splitting at our resolution. Thus, their spectra are greatly simplified, making possible rigorous fits and determination of rotational constants of all four species. We also see, from Fig. 4.2 a), that 2HPd/2PY does exhibit a tunneling splitting, but this splitting is reduced to 62 ± 3 MHz. These changes provide new insight into the dynamics of the double-proton transfer in the 2HP/2PY dimer.

From the experimentally determined rotational constants, a dimer structure was determined, including approximate positions of the tunneling atoms. From these positions, the rotational constants of the doubly-protonated species were determined and used to fit the protonated spectrum. Upon excitation, both hydrogen bonds do slightly increase in size, most likely due to a weakening and lengthening of the N-H and O-H bonds. This weakening probably drops the barrier to tunneling enough to observe tunneling splitting in the rotationally resolved spectrum.

While the N-H...N bond appears to be similar to those found in the Cambridge Structural Database, the O...H-O bond is significantly shorter. This is indicative of two properties of the hydrogen bond. First, it implies that the hydrogen bond itself is quite strong, significantly stronger than other O...H-O bonds observed in other complexes of 2-

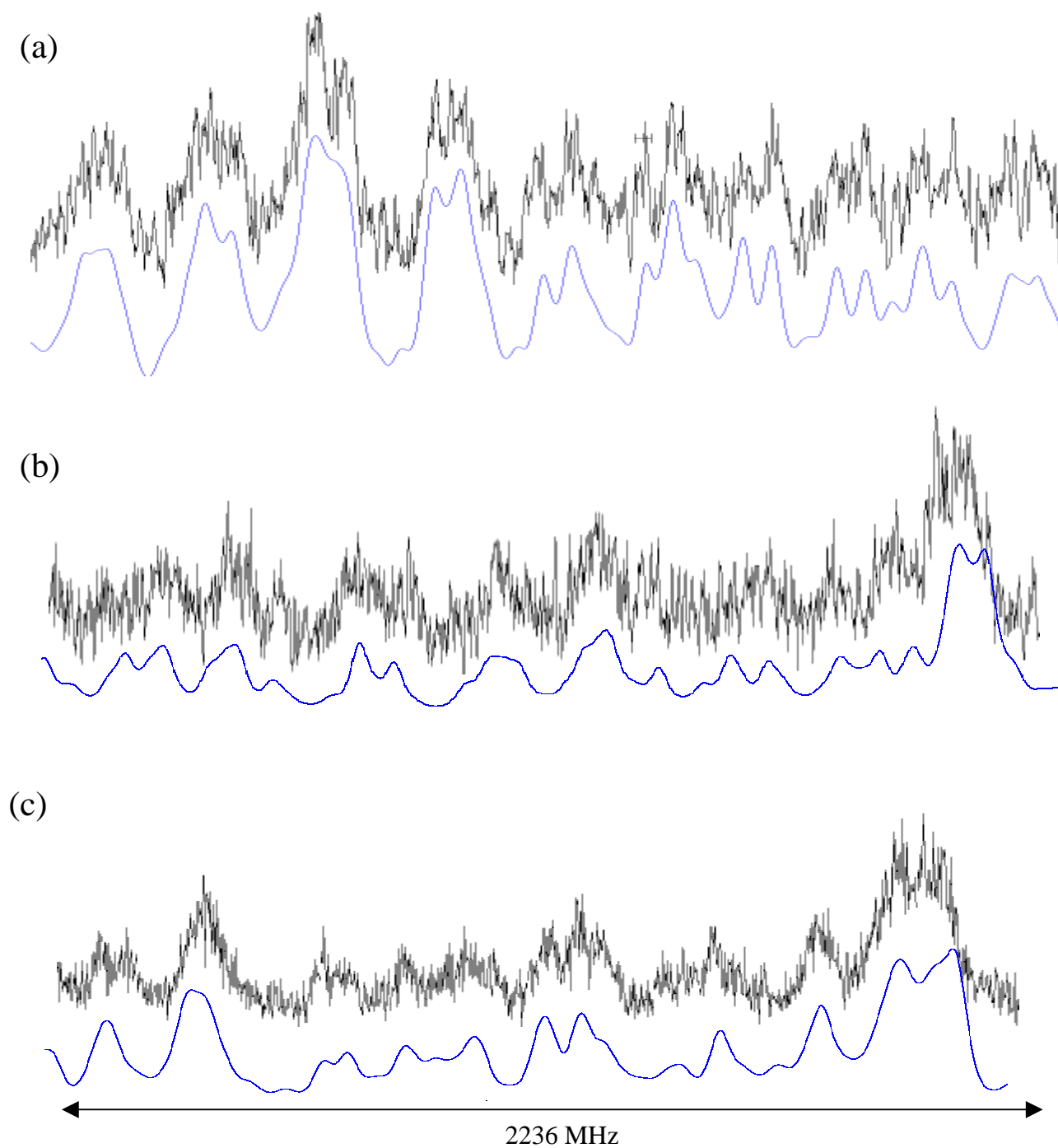


Figure 4.2. Frequency and intensity fits of the a) 2HPd/2PY, b) 2HP/2PYd, and c) 2HPd/2PYd spectra. In the 2HPd/2PY spectrum, a 62MHz tunneling splitting is observed.

pyridone [refs]. Second, this implies that the barrier to tunneling for the *enol* hydrogen is probably smaller than the corresponding barrier for the *keto* hydrogen.

Summarizing, the 2HP/2PY dimer exhibits a tunneling splitting of 527 MHz. Upon double-deuteration and *keto*-deuteration of the dimer, we see this tunneling quenched. However, the 2HPd/2PY dimer exhibits a tunneling splitting of 62 MHz. The observation of tunneling in one partial deuteration but not in the other implies a fundamental difference between the N-H and O-H stretches. Specifically, it indicates that the two atoms involved in the transfer are not identical, and play differing roles in the tunneling motion.

4.3 DISCUSSION

The frequency of a the proton transfer is found via the following relation [ref Bell]:

$$\nu_t = 4 \frac{\nu}{\pi} \exp \left(\frac{-\sqrt{2\mu}}{\hbar} \int_{-x_1}^{+x_1} (V - E_0)^{\frac{1}{2}} dx \right)$$

where ν is the classical oscillating frequency of the mode that facilitates the transfer, μ is the reduced mass of that mode, V is the potential barrier function, and E_0 is the energy of the vibrational mode. $+x_1$ and $-x_1$ are the two minima of the potential well. The integral is a quantity that is roughly independent of the deuterium substitution, and is therefore set as a constant χ . For the purely protonated case, since the normal mode frequency and reduced mass has been calculated in the past (section 3) and the tunneling splitting is well known, χ can be solved for from the protonated spectrum. Using this quantity, the

effective reduced mass in the 2HPD2PY case can be adjusted for to obtain a splitting of 62 MHz. Solving the above equation in this way yields a reduced mass of 1.48 a.m.u..

It was previously hypothesized (chapter 3) that the doubly-protonated and doubly-deuterated species both have a normal mode that facilitates the double proton transfer, in which both tunneling atoms are moving in concert. However, in the case of 2HPd/2PY the symmetry that allows a symmetric and anti-symmetric stretch no longer exists, implying that the two stretches (N-H and O-H) are effectively decoupled. Indeed, calculation (B3LYP/6-311G+**) indicates that such a normal mode does not exist, and are replaced by two modes, one in which the O-H stretch dominates, and one in which the N-H stretch dominates. Logically, then, the mode that facilitates the proton transfer will be a linear combination of these two modes, in which there is an effective reduced mass that accounts for the relative motion of the two nuclei. Within this conceptual framework, the experimentally determined reduced mass of 1.48 a.m.u., corresponds to a stretch that is 69% N-H and 31% O-H, by reduced mass.

The fact that the 2HPd/2PY spectrum exhibits a splitting, while the 2HP/2PYd spectrum does not, indicates that one stretch plays a larger role in the transfer than the other stretch. This is reinforced by the reduced mass percentages derived above. This hypothesis can be rationalized by considering the nature of the tunneling barrier. During the transfer, two separate bonds must be taken into account: the N-H bond and the O-H bond, as both of these are (classically) being broken and reformed. The overall barrier to tunneling is the sum of the two individual barriers associated with the breaking of these bonds. Because these two bonds are different, the barrier heights associated with them are likewise different. Thus, one of the bonds contributes more to the overall barrier than

the other, implying that the motion of one of the atoms is more important to the transfer than the other. Since deuteration of the *keto* hydrogen affects the spectrum more than deuteration of the *enol* hydrogen, the N-H bond is contributing more to the barrier than the O-H. This hypothesis is supported by the very small O...H-O distance observed in the dimer, which would effectively reduce the barrier to transfer as compared to the N-H...N barrier. However, the fact that deuteration of the *enol* hydrogen reduces the splitting by a factor of eight implies that it does nonetheless contribute significantly to the overall barrier. This is seen in the reduced mass percentages, in which the N-H stretch dominates, but the O-H stretch still plays an important role.

4.4 CONCLUSIONS

That a 62 MHz tunneling is observed in the one of the partially-deuterated dimers and not in the others is indicative that one stretch plays a larger role than the other stretch. Using the differences in splitting, we are able to determine the extent to which each stretch plays a role in the transfer. Further investigation will include refined determinations of the sizes and shapes of each barrier.

5.0 Base Pair Analogs in the Gas Phase

Joseph R. Roscioli and David W. Pratt

Department of Chemistry, University of Pittsburgh
Pittsburgh, PA 15260 USA.

Submitted for publication

ABSTRACT

A rotationally resolved electronic spectrum of the gas phase dimer 2-aminopyridine/2-pyridone (2AP/2PY), an analog of the adenine/thymine (A/T) base pair, has been observed and assigned, leading to precise measurements of its moments of inertia and preliminary determinations of its structure. A Watson-Crick configuration results, with N...H-N and N-H...O hydrogen bond lengths of 2.898 and 2.810 Å, respectively. The two bases are found not to be coplanar; a dihedral angle of 6.1° between the base planes is also estimated from the measured moments of inertia. Possible chemical and biological implications of these results are discussed.

5.1 INTRODUCTION

Fifty years have elapsed since X-ray diffraction photographs of fibers pulled from concentrated solutions of DNA revealed that its structure is a double-stranded helix held together by hydrogen bonds between the complementary base pairs adenine (A) and thymine (T), and guanine (G) and cytosine (C) (1-3), providing a molecular level explanation of heredity (4). Despite this passage of time, the structure of an *isolated* A/T or G/C base pair in the absence of solvent and/or a surrounding medium has yet to be determined. Only the average structure of the base pairs in the condensed phase can be determined from fiber diffraction patterns of DNA. To be sure, we now know that there are many different kinds of DNA and that, while they share many common features, they can differ significantly in detail. These differences include the number of residues per turn, the translation per residue, the angle between the base planes and the helix axis, and the dihedral angle between base planes (5). We also know that these features may be functionally important, both in gene expression as well as in the construction of the cell (6). But we do not know the extent to which the differences in DNA structures are a consequence of the condensed phase environment in which they are found. Gas phase studies are needed not only to provide benchmark structures but also to quantify the relative importance of *intra* and *intermolecular* interactions in molecular biology.

Towards this end, we report here a preliminary determination of the structure of the base pair *mimic* 2-aminopyridine/2-pyridone (2AP/2PY) using the technique of rotationally resolved electronic spectroscopy in the gas phase. 2AP/2PY is found to be held together by two N \cdots H-N and N-H \cdots O hydrogen bonds, identical to those found in

the A/T base pair itself. As will be seen, understanding the nature of these interactions provides new insight into the structure, stability, and electronic properties of the bonds that hold DNA together.

5.2 EXPERIMENTAL

Our experiments were performed in the collision-free environment of a molecular beam (7). Approximately 1 g of 2AP was placed in a quartz sample container at nearly 200° C and entrained in 6 psig of He for 20 minutes, after which approximately 2 g of 2PY was added to the sample container. 30 minutes later, an obtainable, constant electronic spectrum of the 2AP/2PY dimer was detected at ~ 330 nm for another 30 minutes. During this time, the mixture was expanded through a 280 μ m quartz nozzle held at 150° C into a vacuum chamber, skimmed about 2 cm downstream of the nozzle before entering a second differentially pumped chamber, and probed 10 cm downstream of the nozzle with a high resolution laser (FWHM ~ 1 MHz in the UV). The excitation source was an argon-ion pumped CW single frequency tunable ring dye laser operating with DCM and frequency-doubled by an intracavity LiIO₃ crystal. Typical powers used were 400 μ W in the UV. The spectra were acquired at an acquisition rate of 50 Hz over a 2000 second scan. Four signals were collected. The PMT detected fluorescence signal was collected with spatially selective optics using photon counting and stored on data acquisition computer. A signal from a near-confocal interferometer having a mode-matched free spectral range of 599.5040 \pm 0.005 MHz in the UV was collected to perform relative frequency calibration. The absorption spectrum of I₂ was collected to

determine the absolute transition frequencies, which are accurate to +/- 18 MHz. Finally, the power signal was collected to normalize the PMT signal.

Supplementing the experimental work, *ab initio* calculations at ground state B3LYP/6-31G+(d,p) and excited state CIS/6-31G levels were performed using the Gaussian 98 [8] suite of electronic structure programs on personal computers.

5.3 RESULTS AND DISCUSSION

Previous studies of this type on isolated nucleic acid bases, *albeit* at significantly lower resolution, have faced serious obstacles. The pyrimidine bases C and T exhibit broad absorption bands and a near-total absence of fluorescence, even at low temperature or in supersonic jets (9-11), apparently due to rapid nonradiative decay of the excited S_1 state (12). But vibrationally resolved UV spectra have recently been measured for A, G, and the G/G and G/C dimers in the gas phase, using R2PI detection techniques in supersonic jets (13-15). And Müller, *et al.* (16) have recently used both R2PI and fluorescence-based methods to detect S_1 - S_0 vibronic spectra of the 2AP/2PY base pair analog described here.

The high resolution fluorescence excitation spectrum of the presumed S_1 - S_0 electronic origin of the 2AP/2PY dimer is shown in Fig. 5.1. This spectrum was both frequency- and intensity-fit, with an observed-minus-calculated (OMC) standard deviation of 3.5 MHz. It was obtained at a relatively high temperature (~7 K), and therefore contains over 15,000 transitions. Due to this congestion, one peak corresponding to a single transition could not be identified within the spectrum.

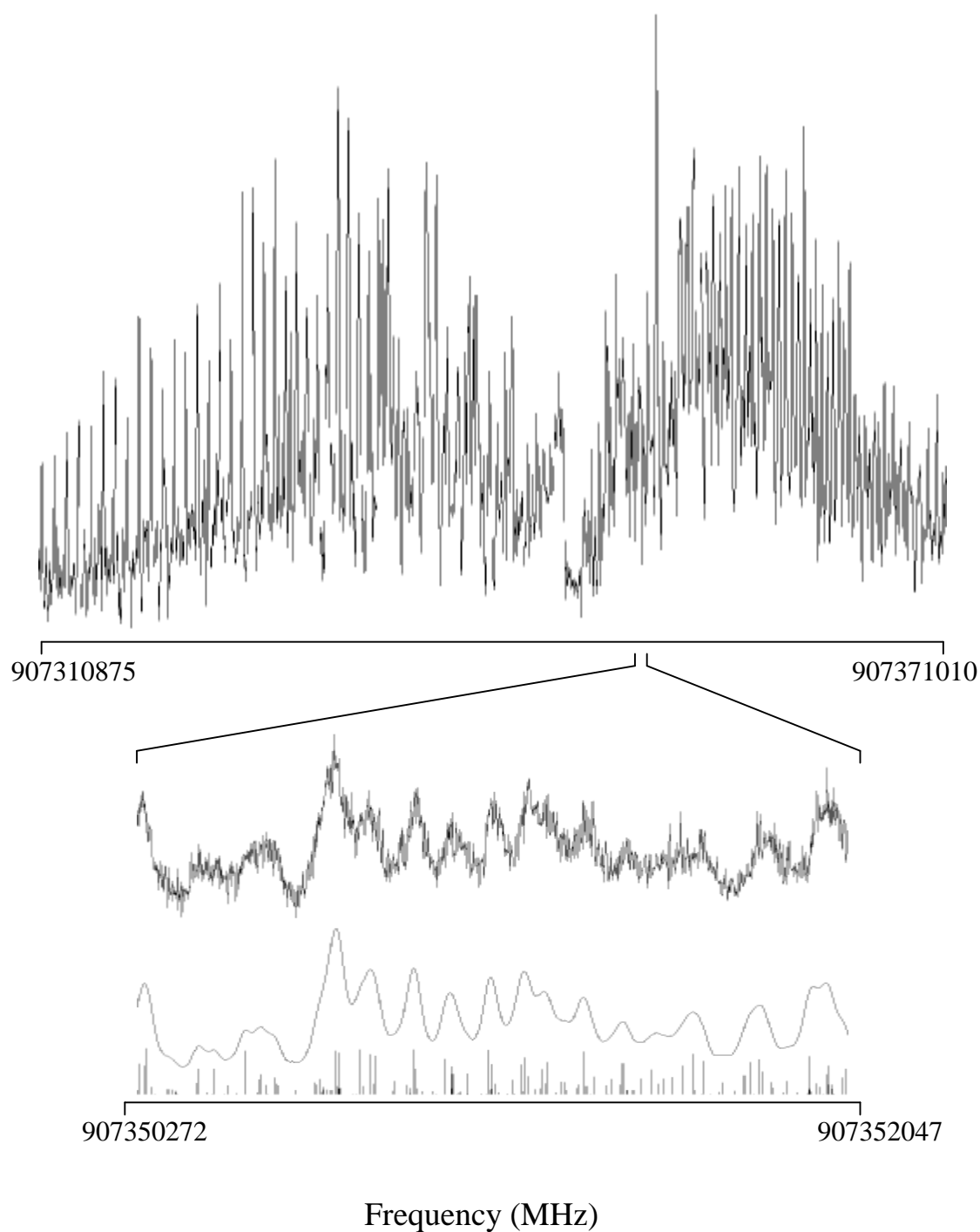


Figure 5.1. The central $\sim 2 \text{ cm}^{-1}$ portion of the rotationally resolved fluorescence excitation spectrum of the origin band in the S_1 - S_0 electronic spectrum of the 2AP/2PY dimer at $\sim 330 \text{ nm}$, recorded in the collision-free environment of a molecular beam using a high resolution laser. Three scale expansions below illustrate a simulated spectrum at full resolution (1 MHz), and fits of the experimental spectrum at the experimental resolution of 18 MHz.

However, the intensity fit reveals a Lorentzian linewidth of 38 ± 3 MHz, corresponding to an excitation lifetime of 4.2 ± 0.3 ns. The frequency fit of the spectrum yields rotational constants that are conservatively estimated to be accurate to one-tenth of this width, or 0.4 MHz. These constants are listed in Table 5.1, together with the calculated (B3LYP/6-31G+(d,p)) rotational constants of the 2AP/2PY dimer. The theoretical values of 2AP/2PY are all within 3% of the experimental ones, confirming its structure. 2AP/2PY has the Watson-Crick configuration, with two N...H-N and N-H...O hydrogen bonds joining the monomer units together, exactly as in the A/T base pair found in naturally occurring DNA.

The intensity fit of the spectrum in Fig. 5.1 also shows that the S_1 - S_0 electronic transition moment (TM) makes an angle of $\pm 62 \pm 3^\circ$ with the a axis of the dimer. Because the ratio of a -type intensity and b -type intensity depends upon the square of the TM, only its relative orientation can be determined experimentally. However, if the TM of the 2PY monomer (17) is placed within the inertial axis frame of the dimer, one of the two possible TM orientations is found to coincide to within 8° of that of the monomer. Thus, we conclude that TM orientation in the dimer is rotated by 62° in a counterclockwise direction, away from its a axis.

Three rotational constants are clearly inadequate to determine the structure of a large molecule like 2AP/2PY, in either electronic state. But these constants are primarily sensitive to the separation of the two monomer units, and to the dihedral angle between the two base planes, and only secondarily sensitive to the detailed geometry of the two rings. The rotational constants of the two monomer units have been determined by both microwave (18, 19) and high resolution UV methods (20), and these are well reproduced

Table 5.1. Inertial parameters of the zero-point vibrational levels of the ground (S_0) and first excited (S_1) singlet states of the A/T base pair mimic 2AP/2PY, based on a fit of its fluorescence excitation spectrum at ~ 330 nm (the band origin is at 30266.83 ± 0.02 cm^{-1}). A, B, C, ΔI and κ are the rotational constants, inertial defect, and asymmetry parameter, respectively.

Parameter	Experimental		Theoretical ^a
	S_0 State	S_1 State	S_0 State
A, MHz	1602.8(4)	1596.9(4)	1602.1
B, MHz	341.0(4)	336.9(4)	332.6
C, MHz	281.5(4)	278.5(4)	275.8
$\Delta I, \mu\text{\AA}^2$	-2.11	-2.19	
κ	-0.910	-0.911	

^a B3LYP/6-31G+(d,p) values.

by *ab initio* calculations. Therefore, we base our preliminary determination of the ground state geometry of 2AP/2PY on the (B3LYP/6-31G+(d,p)) theoretical structures of 2AP and 2PY, and on the further assumption that these are unchanged on complex formation. A coordinate system was then defined that represents the approach of the two monomer units along the N...H-N direction, as shown in Fig. 5.2. r_1 is the (heavy-atom) distance between the two nitrogen atoms, r_2 is the analogous distance between the amino nitrogen and oxygen atoms, and ϕ is the torsional (or C-N-N-C dihedral) angle between the two planes. Unique values of these three parameters were then obtained by varying them until the calculated values of A, B, and C matched the observed ones, within experimental error. This yields the hydrogen bond lengths r_1 (N...H-N) = 2.898 ± 0.002 Å, r_2 (N-H...O) = 2.810 ± 0.004 Å, and the dihedral angle $\phi = 6.1 \pm 0.2^\circ$.

Table 5.2 compares the experimental values of the hydrogen bond lengths in ground state 2AP/2PY with theoretical estimates (16) and with experimental values for the 2AP dimer (21), the 2PY dimer (22), and the Watson-Crick A/T base pair found in sodium adenylyl-3', 5'-uridine (SAU) by Seeman, *et al.* (23). The latter experimental values are based on X-ray diffraction studies of crystals. Theory gives a good account of the properties of the hydrogen bonds in 2AP/2PY. At the B3LYP/6-311++G (2d, 2p) level (16), the two (heavy-atom) distances are quite different, as observed in the gas phase. The theoretical values are 0.04 and 0.07 Å longer, respectively. [Symmetry (or the lack thereof) seems to play an important role in those interactions, as the “asymmetric” dimer 2HP/2PY also has N...H-N and O-H...O bonds of significantly different lengths (2.86 and 2.45 Å, respectively (24))]. Experimentally, the N...H-N bond in 2AP/2PY is found to be 0.17 Å shorter than that in 2AP/2AP, but 0.08 Å longer than

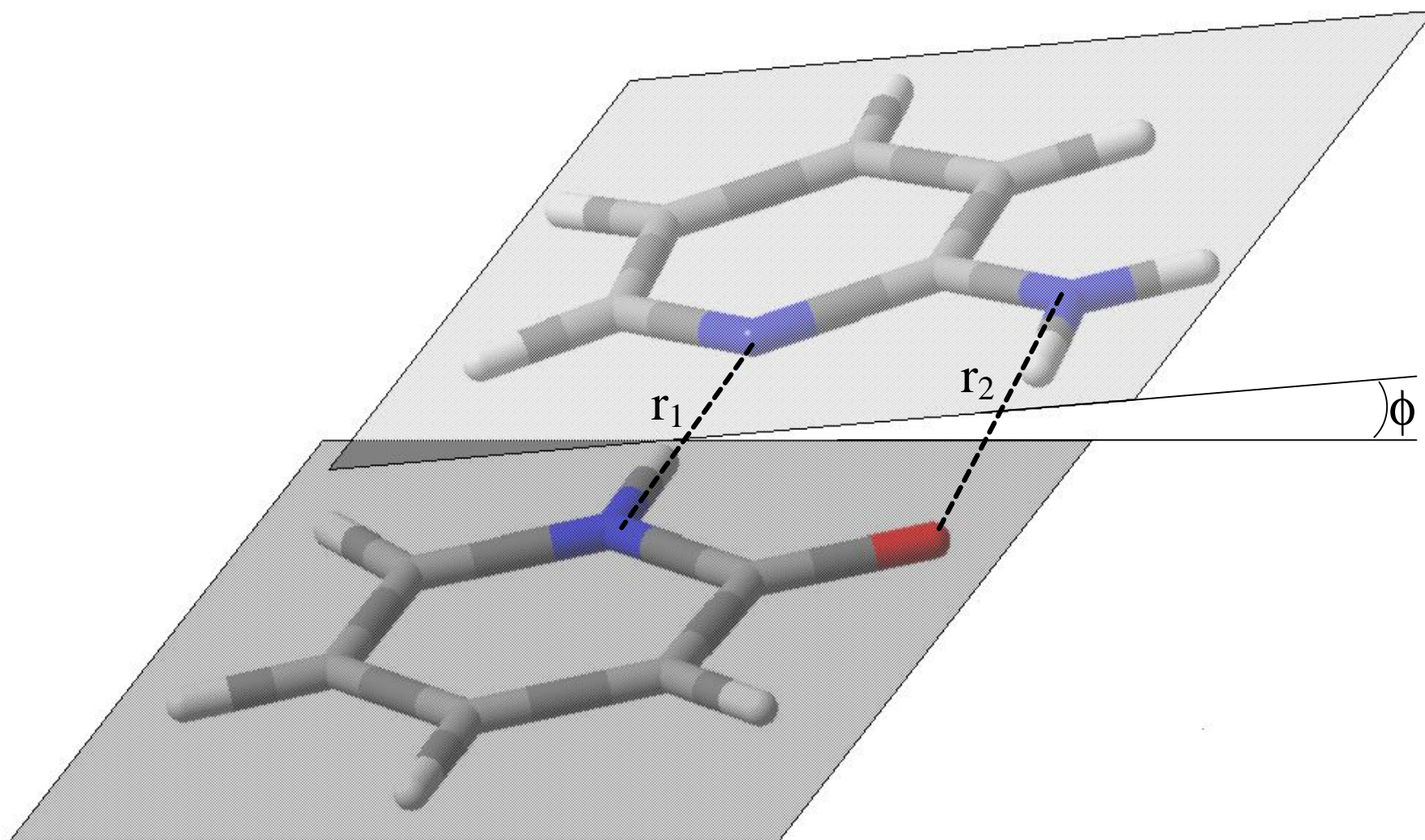


Figure 5.2. Model structure of the 2AP/2PY dimer illustrating the Watson-Crick configuration found experimentally and geometrical parameters derived from the fit of the spectrum in Fig. 1. r_1 and r_2 are the hydrogen bond distances N...H-N and N-H...O, and ϕ is the (nonzero) dihedral angle.

Table 5.2. Hydrogen bond lengths in 2AP/2PY and related systems (Å).

	2AP/2PY	2AP/2PY	2AP/2AP	2PY/2PY	SAU
Bond	Gas phase	Calc (16)	Cryst (21)	Cryst (22)	Cryst (23)
N...H-N	2.90	2.94	3.07	—	2.82
N-H...O	2.81	2.88	—	2.76	2.95

that in SAU. The N-H...O bond in 2AP/2PY is 0.05 Å longer than that in 2PY/2PY but 0.14 Å shorter than that in SAU. These data suggest that crystal packing effects on hydrogen bond lengths are significant.

A survey of 88 crystal structures with similar hydrogen bonding motifs in the CSD (25) reveals average bond lengths of r_1 (N...H-N) = 2.92 ± 0.10 Å and r_2 (N-H...O) = 3.00 ± 0.09 Å. The gas phase value of r_1 (=2.90 Å) lies well within the distribution of X-ray values, but the gas phase value of r_2 (=2.81 Å) lies well outside this distribution.

More surprising, perhaps, is the experimental finding (supported by theory (16)) that 2AP/2PY is not a planar molecule in either electronic state. Most models of DNA assume that the complementary base pairs occupy a common plane. But, in 2AP/2PY, at least, this is not the case, as is immediately apparent from the inertial defects ($\Delta I = I_a - I_b - I_c$) that are derived from the fit of its high resolution spectrum. Both electronic states of 2AP/2PY have ΔI values of order $-2 \mu\text{Å}^2$, indicating a significant deviation from planarity. (Values of $\Delta I \sim 0$ are expected for a planar molecule). The calculated ground state structure of 2AP/2PY has $\Delta I \sim -2.17 \mu\text{Å}^2$. Examination of this structure suggests that the source of the nonplanarity is the NH₂ group of 2AP. Ground state 2AP has $\Delta I \sim -0.26 \mu\text{Å}^2$ (20), supporting this view. Indeed, aniline itself is a nonplanar molecule (26). Recent measurements of the vibrational TM angles in adenine suggest that it, too, is nonplanar in the gas phase with the NH₂ group tilted $\sim 20^\circ$ out-of-plane (27). Thus, the statement that “clear, direct experimental evidence about the nonplanarity of isolated bases is still missing due to the (lack of) resolution of the available experimental techniques” (28) is now moot.

The biological consequences of this nonplanarity may be significant. Some interstrand amino-group contacts in B-DNA crystal structures appear to be stabilized by amino-group pyramidalization and interstrand bifurcated hydrogen bonds (28). In 2AP itself, Kydd and Mills (19) established that the angle between the plane made by the NH_2 group and the ring is nearly 32° in the gas phase. In the crystal structure (21), this angle is reduced to $\sim 15^\circ$. This difference indicates that the geometry of the amino group is highly dependent upon the local environment of the molecule. The flexibility offered by the NH_2 group is advantageous for the dimer, because the NH_2 group will most likely deform in such a way that the $\text{N-H}\cdots\text{O}$ bond is linear, creating an overall structure that is bound by two linear hydrogen bonds *via* an induced fit.

More globally, it is apparent that an incipient chirality is created when a planar base connects to a nonplanar one, giving the base pair a right- or left-handed sense, on its own. It is believed that helices form when a series of subunits bind to each other in a regular way, to take advantage of a π -stacking of the bases. Is it possible that the *direction* of the helix twist can be traced to the nonplanar character of the purine bases? Further experiments and/or calculations will be necessary to answer this intriguing question.

Finally, the present results also shed light on the current controversy regarding the nature of the hydrogen bond (29). At one extreme, hydrogen bonds are attributed to purely electrostatic, or electrostatic plus polarization interactions; at the other, covalent interactions are held to be extremely important. Figure 5.3 shows the calculated highest occupied molecular orbital (HOMO) and lowest unoccupied molecular orbital (LUMO) of the energy optimized ground state of 2AP/2PY, as determined by DFT methods.

According to theory, the one-electron HOMO \rightarrow LUMO excitation makes the major contribution to the S_1 - S_0 spectrum of 2AP/2PY. The transition is highly localized on the 2PY “side” of the molecule. The fact that the electronic origin of 2AP/2PY is shifted by only $\sim 400\text{ cm}^{-1}$ with respect to that of 2PY itself (17) is consistent with this result. But a closer examination of Fig. 5.3 shows that the two orbitals are partially delocalized into the 2AP portion of the molecule. In agreement with this, experiment shows that the S_1 - S_0 TM is not parallel to that of 2PY. Covalent interactions between the two monomer units are the only plausible explanation of this behavior. Both hydrogen bonds lengthen by $\sim 0.05\text{ \AA}$ on electronic excitation. However, as is also shown in Fig. 5.3, the covalent contributions to these bonds are bonding in the S_1 state and antibonding in the S_0 state. Thus, the hydrogen bonds in 2AP/2PY must also be significantly electrostatic in character (30).

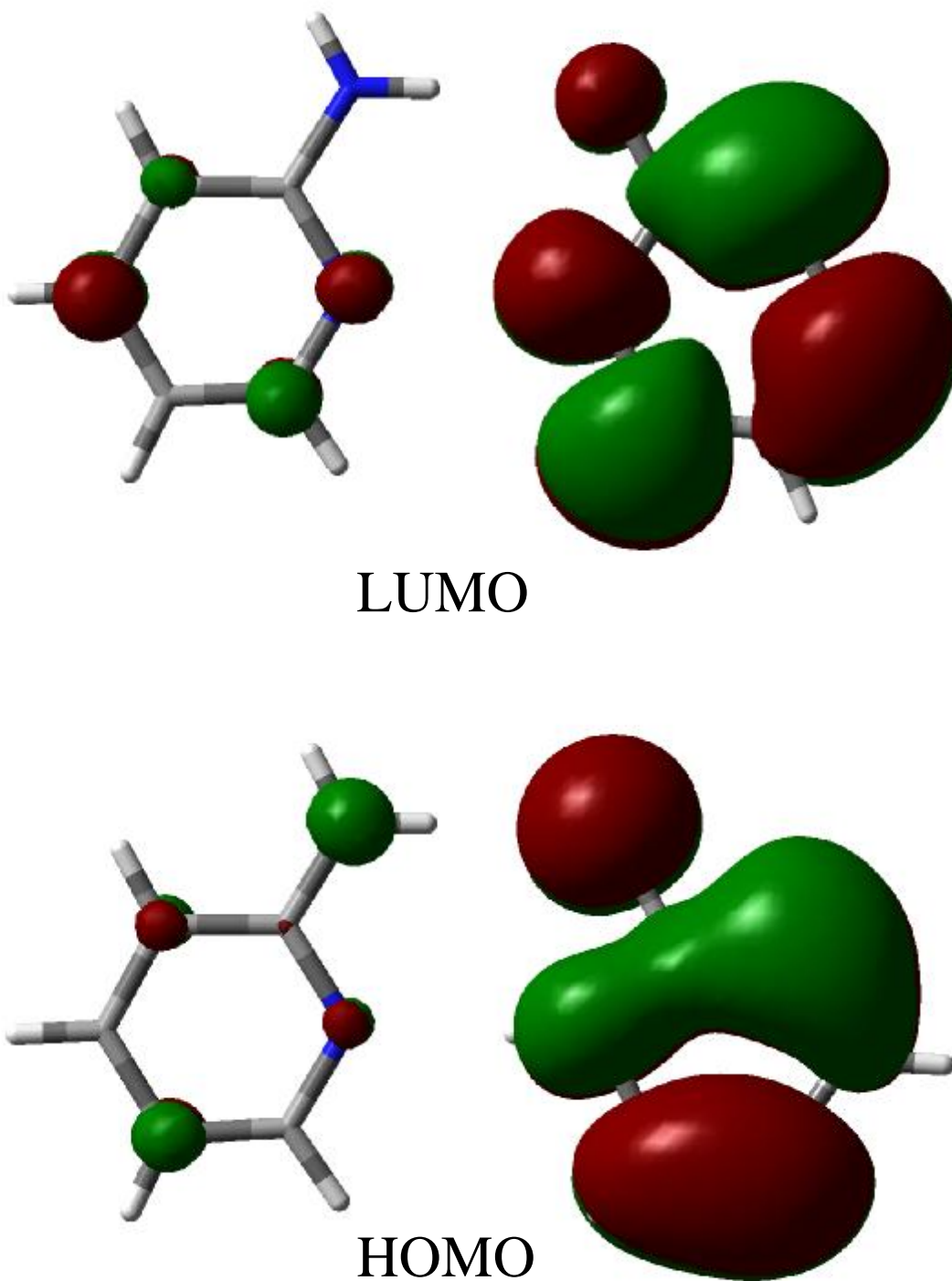


Figure 5.3. Molecular orbitals of 2AP/2PY that participate in the S_1 - S_0 transition, which exhibit some delocalization owing to the partially covalent character of the two hydrogen bonds that link the two halves of the base pair mimic together.

5.4 REFERENCES AND NOTES

1. J. D. Watson and F. H. C. Crick, "Molecular Structure of Nucleic Acids. A Structure for Deoxyribose Nucleic Acid", *Nature* **171**, 737-738 (1953).
2. M. H. F. Wilkins, A. R. Stokes, and H. R. Wilson, "Molecular Structure of Nucleic Acids. Molecular Structure of Deoxypentose Nucleic Acids", *Nature* **171**, 738-740 (1953).
3. R. E. Franklin and R. G. Gosling, "Molecular Structure of Nucleic Acids. Molecular Configuration in Sodium Thymonucleate", *Nature* **171**, 740-741 (1953).
4. J. D. Watson and F. H. C. Crick, "Genetic Implications of the Structure of Deoxyribonucleic Acid", *Nature* **171**, 964-967 (1953).
5. L. Stryer, *Biochemistry*, 4th Ed., W. H. Freeman, New York, 1995.
6. B. Alberts, D. Bray, J. Lewis, M. Raff, K. Roberts, and J. D. Watson, *Molecular Biology of the Cell*, Garland Publishing, New York, 1994.
7. W. A. Majewski, J. F. Pfanstiel, D. F. Plusquellic, and D. W. Pratt, "High Resolution Optical Spectroscopy in the Ultraviolet", *Laser Techniques in Chemistry*, ed. A. B. Myers and T. R. Rizzo, Wiley and Sons, New York, 1995, pp. 101-148.
8. Gaussian 98, Revision A.4, M. J. Frisch, G. W. Trucks, H. B. Schlegel, G. E. Scuseria, M. A. Robb, J. R. Cheeseman, V. G. Zakrzewski, J. A. Montgomery, Jr., R. E. Stratmann, J. C. Burant, S. Dapprich, J. M. Millam, A. D. Daniels, K. N. Kudin, M. C. Strain, O. Farkas, J. Tomasi, V. Barone, M. Cossi, R. Cammi, B. Mennucci, C. Pomelli, C. Adamo, S. Clifford, J. Ochterski, G. A. Petersson, P. Y. Ayala, Q. Cui, K. Morokuma, D. K. Malick, A. D. Rabuck, K. Raghavachari, J. B. Foresman, J. Cioslowski, J. V. Ortiz, B. B. Stefanov, G. Liu, A. Liashenko, P. Piskorz, I. Komaromi, R. Gomperts, R. L. Martin, D. J. Fox, T. Keith, M. A. Al-Laham, C. Y. Peng, A. Nanayakkara, C. Gonzalez, M. Challacombe, P. M. W. Gill, B. Johnson, W. Chen, M. W. Wong, J. L. Andres, C. Gonzalez, M. Head-Gordon, E. S. Replogle, and J. A. Pople, Gaussian, Inc., Pittsburgh, PA, 1998.
9. M. Fujii, T. Tamura, N. Mikami, and M. Ito, "Electronic Spectra of Uracil in a Supersonic Jet", *Chem. Phys. Lett.* **126**, 583-587 (1986).
10. Y. Tsuchiya, T. Tamura, M. Fujii, and M. Ito, "Keto-enol Tautomer of Uracil and Thymine", *J. Phys. Chem.* **92**, 1760-1765 (1988).

11. B.B.Brady, L. A. Peteanu, and D. H. Levy, "The Electronic Spectra of the Pyrimidine Bases Uracil and Thymine in a Supersonic Jet", *Chem. Phys. Lett.* **147**, 538-543 (1988).
12. H. Kang, K. T. Lee, B. Jung, Y. J. Ko, and S. K. Kim, "Intrinsic Lifetimes of the Excited State of DNA and RNA Bases", *J. Amer. Chem. Soc.* **124**, 12958-12959 (2002).
13. E. Nir, L. Grace, B. Brauer, and M. S. de Vries, "REMPI Spectroscopy of Jet-Cooled Guanine", *J. Amer. Chem. Soc.* **121**, 4896-4897 (1999).
14. E. Nir, Ch. Janzen, P. Imhof, K. Kleinermanns, and M. S. deVries, "Guanine Tautomerism Revealed by UV-UV and IR-UV Hole Burning Spectroscopy", *J. Chem. Phys.* **115**, 4604-4611 (2001).
15. E. Nir, K. Kleinermanns, and M. S. de Vries, "Pairing of Isolated Nucleic-Acid Bases in the Absence of the DNA Backbone", *Nature* **408**, 949-951 (2000).
16. A. Müller, F. Talbot, and S. Leutwyler, "Hydrogen Bond Vibrations of 2-Aminopyridine · 2-Pyridone, a Watson-Crick Analogue of Adenine-Uracil", *J. Amer. Chem. Soc.* **124**, 14486-14494 (2002).
17. A. Held, B. B. Champagne, and D. W. Pratt, "Inertial Axis Reorientation in the S_1 - S_0 Electronic Transition of 2-Pyridone...", *J. Chem. Phys.* **95**, 8732-8743 (1991).
18. L. D. Hatherly, R. D. Brown, P. D. Godfrey, A. P. Pierlot, W. Caminati, D. Damiani, S. Melandri, and L. B. Favero, "Gas Phase Tautomeric Equilibrium of 2-Pyridone and 2-Hydroxypyridine by Microwave Spectroscopy", *J. Phys. Chem.* **97**, 46-51 (1993).
19. R. A. Kydd and I. M. Mills, "Microwave Spectrum of 2-Aminopyridine", *J. Mol. Spectrosc.* **42**, 320-326 (1972).
20. D. R. Borst, J. R. Roscioli, and D. W. Pratt, "High Resolution Electronic Spectra of 2-Hydroxy and 2-Aminopyridine...", *J. Phys. Chem. A* **106**, 4022-4027 (2002).
21. M. Chao, E. Schempp, and R. D. Rosenstein, "2-Aminopyridine", *Acta Cryst.* **B31**, 2922-2924 (1975).
22. H. W. Yang and B. M. Craven, "Charge Density Study of 2-Pyridone", *Acta Cryst.* **B54**, 912-920 (1998).
23. N. C. Seeman, J. M. Rosenberg, F. L. Suddath, J. J. P. Kim, and A. Rich, "RNA Double Helical Fragment at Atomic Resolution. I. The Crystal and Molecular Structure of Sodium Adenylyl-3', 5'-uridine", *J. Mol. Biol.* **104**, 109-144 (1976).

24. D. R. Borst, J. R. Roscioli, D. W. Pratt, G. M. Florio, T. S. Zwier, A. Müller, and S. Leutwyler, "Hydrogen Bonding and Tunneling in the 2-Pyridone: 2-Hydroxypyridone Dimer...", *Chem. Phys.* **283**, 341-354 (2002), and to be published.
25. F. H. Allen, The Cambridge Structural Database, *Acta Cryst.* **B58**, 380-388 (2002).
26. W. E. Sinclair and D. W. Pratt, "Structure and Vibrational Dynamics of Aniline and Aniline-Ar...", *J. Chem. Phys.* **105**, 7942-7956 (1996).
27. F. Dong and R. E. Miller, "Vibrational Transition Moment Angles in Isolated Biomolecules. A Structural Tool", *Science* **298**, 1227-1230 (2002).
28. P. Hobza and J. Sponer, "Structure, Energetics, and Dynamics of the Nucleic Acid Base Pairs. Nonempirical *Ab Initio* Calculations", *Chem. Rev.* **99**, 3247-3276 (1999).
29. G. A. Jeffrey, *An Introduction to Hydrogen Bonding*, Oxford University Press, Oxford, 1997.
30. Supported by NSF Grant CHE-9987048.

6.0 CONCLUSIONS

Using a high-resolution UV spectrometer, rotationally resolved electronic spectra of several molecules of biological interest have been obtained and interpreted. The structures and electronic distributions of the 2-aminopyridine and 2-hydroxypyridine monomers were found in the gas phase. The active sites in these molecules are identical to the active sites of adenine and *enolated* thymine, respectively. The experimentally determined ground state structures of these molecules are well reproduced by theory, as are the electronic dipole transition moments. Both molecules appear to experience quinoidal excitations similar to aniline and phenol. However, the in-ring nitrogen makes the quinoidal expansion slightly asymmetric, which manifests itself as an excited state axis tilting of roughly 2° in both molecules. The in-ring nitrogen in both molecules causes a significant amount of electron density to be relocated to the amino- or hydroxy-group, which is detected by the tilting of the transition moments by almost 30° from that of aniline and phenol.

The 2-hydroxypyridine/2-pyridone mixed dimer, an analog of the thymine/thymine-*enol* dimer, was also investigated. Its unique double-proton transfer, a motion that may be the source of DNA mutations, was found to only occur in the electronically excited state. With the aid of tunneling theory, the height of the barrier to proton transfer in the excited state was experimentally determined. More recent studies of partially and fully deuterated dimers show a splitting in the 2HP-*d*/2PY dimer, but no others. This indicates that the two stretches (O-H and N-H) do not play identical roles in the transfer, and that one of them, the N-H stretch, plays a larger role in the proton

transfer than the other. In addition, this data indicate that the barrier to the O-H...H transfer is significantly lower than that of the N...H-N transfer.

Finally, the 2-aminopyridine/2-pyridone dimer, a direct analog of the Watson-Crick adenine/thymine dimer, was studied by this method. The results indicate that the dimer is non-planar, because of presence of a non-planar -NH_2 group in the hydrogen bonding scheme. This non-planarity is manifested as an inherent chirality in the dimer, which may play a role in the chirality that the DNA molecule itself chooses. The tilt of the transition dipole moment of the dimer as compared to the 2PY monomer implies that there is a measurable amount of density "leaking" through the hydrogen bonds from 2PY to 2AP. This indicates a covalent character to the hydrogen bonds, which in the ground state is anti-bonding, and in the excited state is bonding. In light of the ground state stability of the dimer, relative to the excited state, this indicates that electrostatic interactions nonetheless dominate the intermolecular bonding.

7.0 Appendix

7.1 Energy level structure theory

A generic energy level structure for a typical molecule is shown in Figure 7.1. The horizontal coordinate is any one of the $3N-6$ vibrational coordinates along which a molecule of N atoms vibrates. The electronic energy levels are formed under Born-Oppenheimer assumptions, with an energetic spacing in the thousands or tens of thousands of cm^{-1} (UV) range. Characteristic to each level is a well that resembles a harmonic oscillator. The force that is felt along this coordinate by the atoms is the classic chemical bond, which vibrates, to a first approximation, as a quantum harmonic oscillator whose energy levels are spaced by $E=h\nu$, where ν is the frequency of the vibration. This energy level spacing is typically in the hundreds of cm^{-1} (IR) energy range. Each vibrational level is associated with a molecule whose vibrationally averaged structure is different from the other levels. Consequently, each level has its own separate rotational energy level manifold built into it. The energy spacing for these levels is usually on the order of a few cm^{-1} , or gigahertz (MW) frequencies. In a high-resolution electronic spectroscopy experiment, a UV laser is roughly tuned to a resonance between two vibrational levels in two different electronic states. The laser is then scanned in energy space, inducing transitions between individual rotational energy levels at different frequencies during the scan.

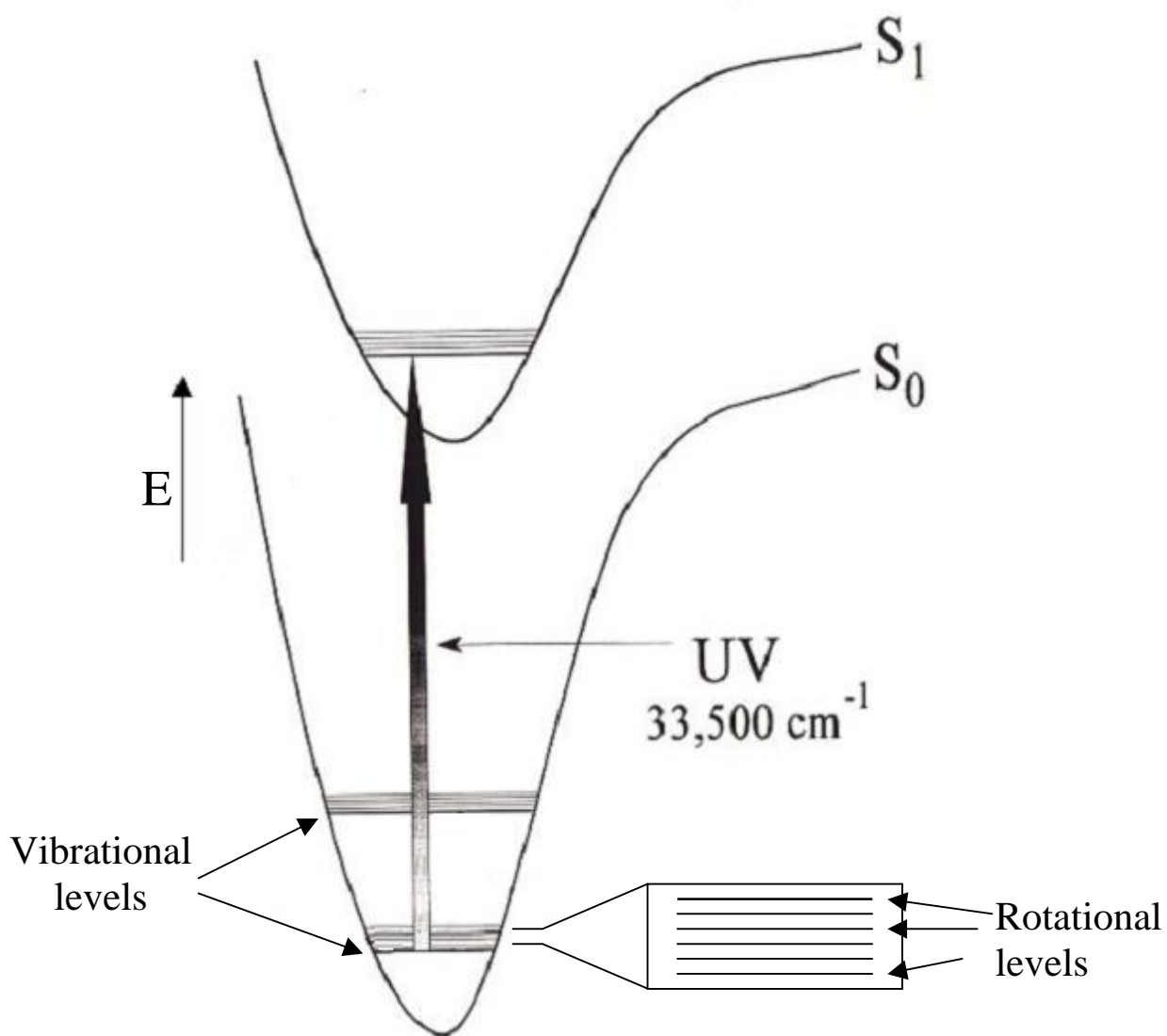


Figure 7.1 Energy level scheme used in high resolution electronic spectroscopy.

In the case of a double-well tunneling splitting, each rotational energy level is split into two distinct levels of opposite parity. The splitting is defined by¹

$$v_t = 4 \frac{\nu}{\pi} \exp \left(\frac{-\sqrt{2} \mu}{\hbar} \int_{-x_1}^{+x_1} (V - E_0)^{\frac{1}{2}} dx \right)$$

There exists no classical analog for the energy difference induced by tunneling splitting.

7.2 Rigid rotor Hamiltonian

The rotational Hamiltonian is described by²

$$\hat{H}_{\text{rot}} = A \hat{P}_a^2 + B \hat{P}_b^2 + C \hat{P}_c^2$$

which is called the rigid rotor Hamiltonian. By rigid, we mean that the eigenfunctions that diagonalize the rigid rotor Hamiltonian matrix are of the form $|J K_a K_c\rangle$, where J is the rotational quantum number, K_a is the projection of the J vector onto the a -axis of the molecule, and K_c is the projection of the J vector onto the c -axis. Applying these to UV spectroscopy, the only allowed transitions are those that increase, decrease, or change the direction of the angular momentum vector. Thus, all rigid rotor transitions will obey selection rules of the form

$$|J K_a K_c\rangle \rightarrow |J+1 K_a K_c\rangle,$$

$$|J K_a K_c\rangle \rightarrow |J K_a+1 K_c\rangle, \text{ or}$$

¹ Harmony, M. D. (1971), *Chem. Phys. Lett.*, **10**, 337

² Walter Gordy, Robert L. Cook, Microwave Molecular Spectra, 1984, p. 232.

$$|J K_a K_c\rangle \hat{a} |J K_a K_c+1\rangle$$

In matrix formalism, this is manifested as a non-diagonal perturbed Hamiltonian in J , in which the only non-zero elements are off-diagonal by order one. A rigid rotor Hamiltonian was used to fit all spectra in this thesis. In cases where a particularly non-rigid molecule is studied, the rigid rotor Hamiltonian must be modified to include Watson's distortion terms², in which there is a modification of the rotational energy associated with centrifugal distortion.

7.3 Experimental Setup

The general experimental setup is shown in figure 7.2. An Ar^+ laser lasing at 514 nm pumps a ring dye laser. The ring dye laser light is double by an intracavity BBO (<630 nm) or LiIO_3 (>620 nm) to create an ultraviolet beam of linewidth $\sim 1\text{MHz}$. The molecular beam is created in a three-chamber quartz source and expanded out of a $150\mu\text{m}$ tip. For experiments with a Doppler-linewidth of 18 MHz, the molecular beam is then skimmed once before probing. The laser beam and molecular beams cross at right angles within a set of 33% efficient collection optics, as shown in figure 7.3. The most efficient region of the optics is a 1mm sphere directly between the two mirrors. A mass spectrometer is in place at the far end of the beam machine to align the molecular beam using argon as the alignment gas, and to test how well the three chambers are being differentially pumped.³

³ W. A. Majewski, D. F. Plusquellic and D. W. Pratt, J. Chem. Phys. **90**, 1362 (1989).

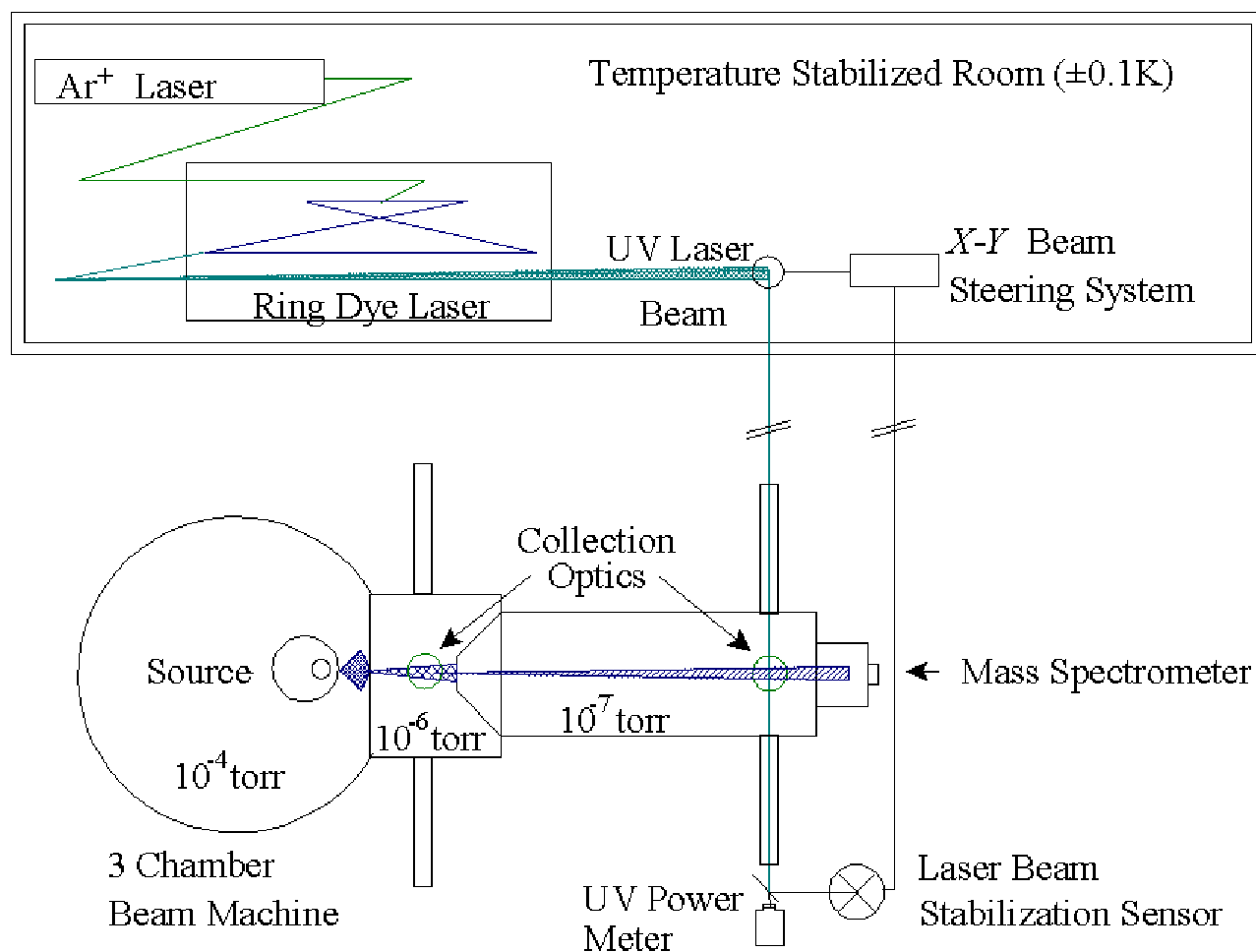


Figure 7.2. The experimental setup of the ultra-high resolution UV spectrometer at the University of Pittsburgh.

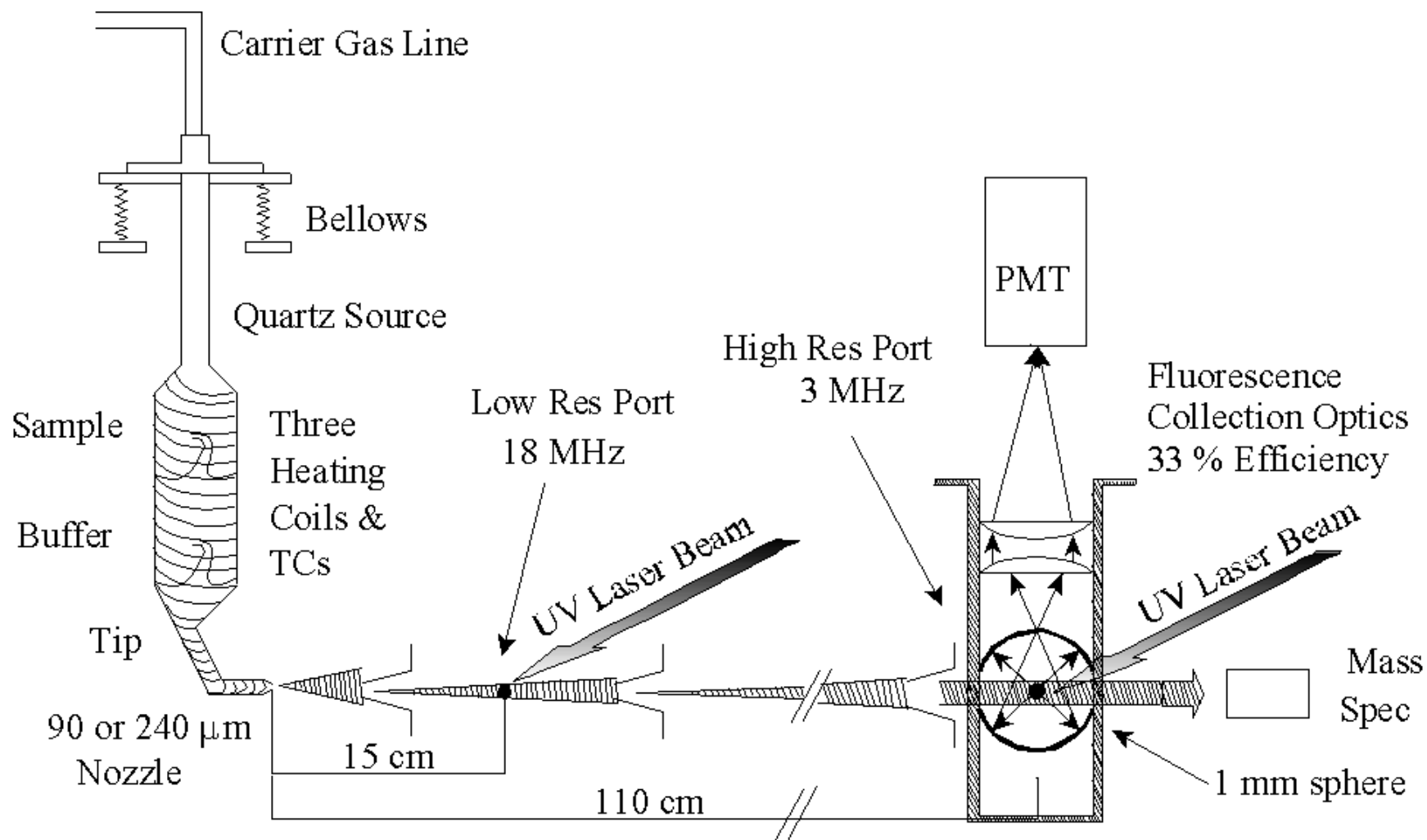


Figure 7.3 Side view of molecular source (on left), set of skimmers (center), and collection optics (right). The molecular beam is aligned by monitoring an argon signal from the molecular source

7.4 Fitting procedure – using JB95

When fitting a high resolution spectrum, one generally begins with either calculated ground state structures or ground state structures derived from microwave studies. Depending upon the system being studied, the starting excited state rotational constants are usually determined by either calculation or comparison to other, already studied molecules. From these beginning structures, a rotationally resolved spectrum is simulated. Such a simulation and its corresponding experimental trace are shown in Figure 7.4 a). Following this, certain simulated transitions are assigned to peaks within the spectrum for which they appear to correspond. The spectrum is then resimulated, while maintaining the assigned lines' positions as well as possible, by adjusting the rotational constants of the ground and excited states and the electronic origin until the best fit has been obtained. It should be noted that the simulation program needs at least 7 assigned lines to begin fitting the spectrum, as there are 7 unknowns (A'' , B'' , C'' , A' , B' , C' , and the electronic origin) that it needs to adjust. The quality of the fit is determined by the OMC (observed-minus-calculated) standard deviation, which is the standard deviation of the distance of assigned lines from their assigned positions. The resimulated spectrum, such as that shown in Figure 7.4 b), begins to show general trends present in the spectrum. The lines associates with these trends are then fit, and the spectrum is recalculated. This process is iteratively continued until the final OMC of the fit is below 10% of the linewidth of the experimental peaks. The resulting rotational constants are generally accurate to within 10% of the OMC (in MHz).

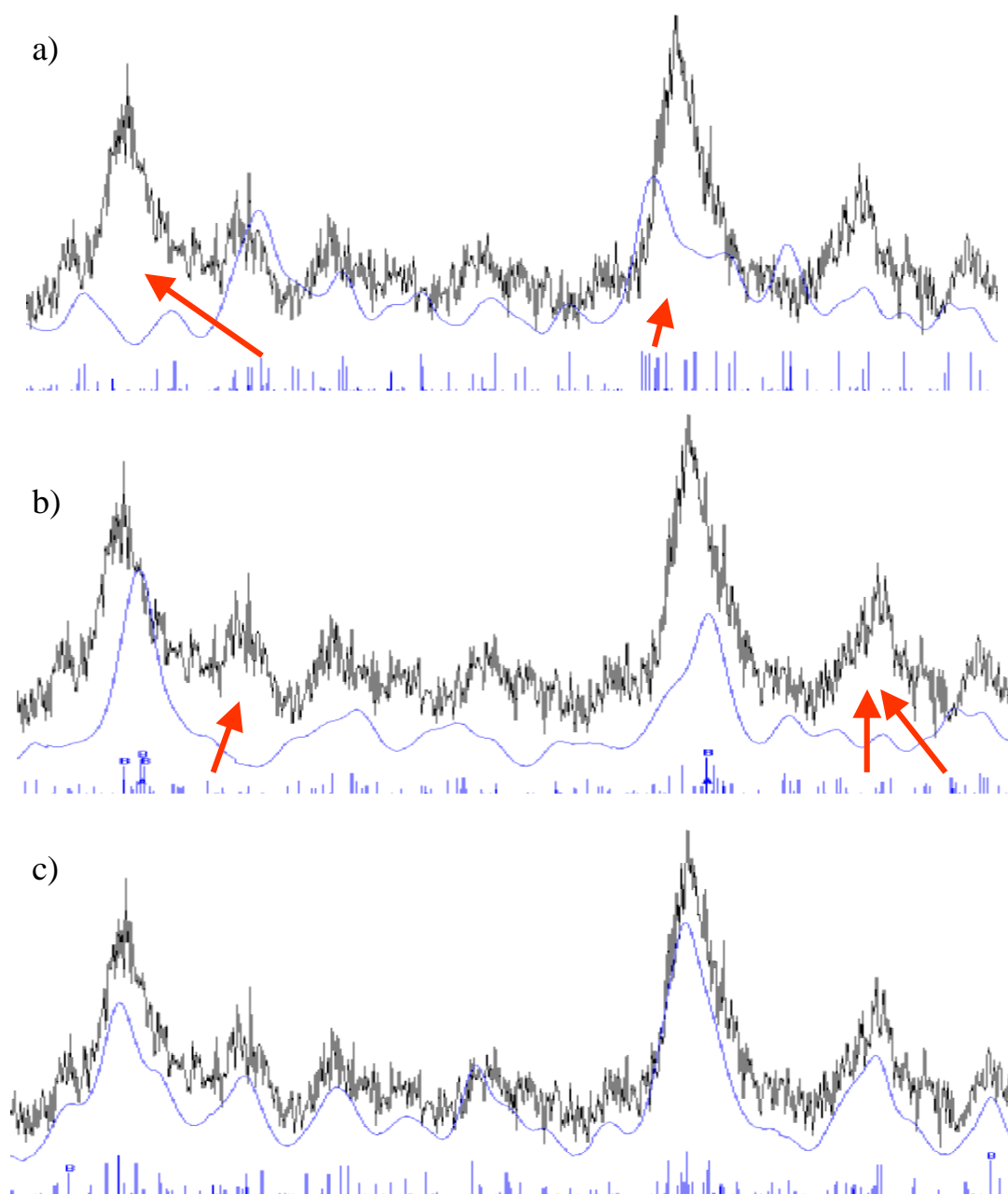


Figure 7.4 The process of fitting a spectrum, a) using the initial rotational constants, the simulated spectrum barely resembles the experimental. b) After fitting several transitions, general trends begin to appear. c) The final fit of the spectrum, after several hundred lines have been fit.

An intensity fit of the spectrum is obtained by adjusting several parameters in the simulation by hand. First, the transition dipole moment affects the spectrum the most, and can be adjusted, while the spectrum is resimulated in real time. Second, the temperature is adjusted, changing the Boltzmann distribution of the occupied levels, thereby making the intensity distribution change in the simulation. Third, various smaller-effect parameters are adjusted, such as axis-tilting terms, non-rigid-rotor coefficients, maximum rotational level calculated (J_{\max}), and spin degeneracy coefficients.